UNIVERSITY OF SOUTHAMPTON

FACULTY OF PHYSICAL SCIENCES AND ENGINEERING

Physics and Astronomy

Holographic Gauged NJL Model and Applications

by

William Clemens

Thesis for the degree of Doctor of Philosophy

August 2019

UNIVERSITY OF SOUTHAMPTON

ABSTRACT

FACULTY OF PHYSICAL SCIENCES AND ENGINEERING

Physics and Astronomy

Thesis for the degree of Doctor of Philosophy

HOLOGRAPHIC GAUGED NJL MODEL AND APPLICATIONS

by William Clemens

There are two models of spontaneous chiral symmetry breaking in strongly coupled gauge theories. The symmetry can be broken when a chiral condensate is formed by the non-abelian gauge interactions in the "natural" QCD vacuum or the condensate can be generated or enhanced by the inclusion of a Nambu-Jona-Lasinio (NJL) term. We study the effect of both of these using AdS/CFT, a strong-weak duality which allows us to transform the gauge theory calculations into a problem of D brane embeddings in an AdS spacetime. This model, termed dynamic AdS/QCD, is then applied to technicolour. Technicolour is a phenomenological theory of electroweak symmetry breaking in which the chiral symmetry breaking mechanism of a new QCD-like sector is exploited to provide the electroweak symmetry breaking mechanism. We first apply the dynamic AdS/QCD theory to studying the physical QCD meson spectrum both with and without four fermion interactions in chapter 4. Next we turn our attention to technicolour. In chapter 5 we discuss extended technicolour using an NJL term to enhance the top mass. While in chapter 6 we discuss ideal walking theories where the theory remains strongly coupled over a large range of scales.

Table of Contents

List of Figures

Declaration of Authorship

I, William Clemens, declare that the thesis entitled *Holographic Gauged NJL Model and Applications* and the work presented in the thesis are both my own, and have been generated by me as the result of my own original research. I confirm that:

- this work was done wholly or mainly while in candidature for a research degree at this University;
- where any part of this thesis has previously been submitted for a degree or any other qualification at this University or any other institution, this has been clearly stated;
- where I have consulted the published work of others, this is always clearly attributed;
- where I have quoted form the work of others, the source is always given. With the exception of such quotations, this thesis is entirely my own work;
- I have acknowledged all main sources of help;
- where the thesis is based on work done by myself jointly with others, I have made clear exactly what was done by others and what I have contributed myself;
- parts of this work have been published as:
  - W. Clemens and N. Evans, "A Holographic Study of the Gauged NJL Model"[1]
  - W. Clemens, N. Evans, M. Scott, "Holograms of a Dynamical Top Quark", [2]
  - K. Bitaghsir Fadafan, W. Clemens, N. Evans, "Holographic Gauged NJL Model: the Conformal Window and Ideal Walking" [3]

Signed: .....

Date: .....

Acknowledgements

Firstly I would like to thank my supervisor, Prof. Nick Evans, without whom I would have been unable to complete this work, his previous student Dr Marc Scott who co authored our first paper and was very helpful as I was finding my feet at the start, as well as Prof. Kazem Bitaghsir Fadafan who worked with us on the final paper while visiting from Iran.

Of course I would like to thank my family for both supporting and tolerating me throughout my PhD and my previous qualifications.

Finally I am extremely grateful to my friends, both at Southampton and at home, for supporting me through the process and helping me both technically and otherwise.

Chapter 1

Introduction

Modern theoretical physics is built upon two foundations:

- Quantum field theory, a quantum description of fundamental particles in terms of fields.
- General relativity, which describes gravity in the language of differential geometry.

Both of these has as their root in Einstein's theory of special relativity [4] first proposed in 1905.

Special Relativity can be stated very simply but has extremely profound consequences. The key idea is that the laws of physics, most importantly the speed of light, are the same for all observers in a reference frame which can be reached by a combination of translations, rotations and boosts [1]. This leads to a number of phenomena, including the famous time dilation and length contraction.

Special relativity, as the name suggests, can be generalised to more broader transformations. General relativity [5] is invariant under diffeomorphisms, or any general coordinate transformation. It turns out that in order to have this invariance general relativity needs to promote spacetime, from the passive background in which events occur, to a dynamical object in its own right and in the process it becomes a theory of gravity as well.

Quantum field theory arises from attempting to reconcile classical field theory with quantum mechanics and special relativity. To understand both of these let us briefly discuss classical mechanics [6]. A physical system's configuration can be described by a number of coordinates, for example a particle in three dimensional space can be described with three coordinates, x, y and z, which are referred to as degrees of freedom. The evolution of the system can be thought of as a path through this configuration space. We can assign a cost to each possible path called an action and then the system will evolve along the path with the lowest action. The action for a classical free point particle

[1] Formally the symmetry group describing this is called the Poincaré group

moving in three spacial dimensions is given by

$$S = \int \mathrm{d}t \mathcal{L} \tag{1.0.1}$$

with

$$\mathcal{L} = \frac{1}{2} m \dot{\boldsymbol{x}}^2 \tag{1.0.2}$$

where the trajectory of the particle is given by the, 3 vector, function $\boldsymbol{x}(t)$ and we have defined the Lagrangian $\mathcal{L}$. The form of $\boldsymbol{x}(t)$ which minimises the action is given by the Euler-Lagrange equation

$$\frac{\mathrm{d}}{\mathrm{d}t} \frac{\partial \mathcal{L}}{\partial \dot{\boldsymbol{x}}} = \frac{\mathrm{d}\mathcal{L}}{\mathrm{d}\boldsymbol{x}}. \tag{1.0.3}$$

Which gives the result

$$\ddot{\boldsymbol{x}} = 0 \tag{1.0.4}$$

So the particle is moving at a constant velocity, the expected result. This is a simplified example but it illustrates the method used to solve more complex problems in classical mechanics. In particular it is easy to add potential energy terms to describe forces on the system.

Now let us generalise to fields [7]. Previously we considered a finite number of degrees of freedom contained within a vector $\boldsymbol{x}(t)$. When we move to field theory we are placing degrees of freedom at every point in spacetime so we now replace our vector with a *field* $\phi(\boldsymbol{x}, t)$ where we have demoted the coordinate x from a dynamical variable to a label for each degree of freedom. We now define the action by integrating this field over all spacetime. For example the action for a massive scalar field, ϕ, is given by:

$$S = \int \mathrm{d}t \int \mathrm{d}^3 x \left(\frac{1}{2} \partial_\mu \phi \partial^\mu \phi - \frac{1}{2} m^2 \phi^2 \right) \tag{1.0.5}$$

where m is the mass and we have combined the spatial and temporal derivatives into ∂^μ. The free scalar field is the simplest case but it is not difficult to include interactions or to describe more complex objects such as vector or even spinor fields.

It is also, conceptually at least, not difficult to move from classical to quantum mechanics. Classically we have assumed that the system only moves along the trajectory which minimises the action however in quantum mechanics we integrate over *all* of the trajectories.

The description of field theory using quantum mechanics is known as Quantum Field Theory [8] A full pedagogical review is beyond the scope of this work so a good working knowledge of quantum field theory will be assumed

Once quantum mechanics and general relativity were settled in the scientific literature people began to think about ways to quantise general relativity. It was realised early on

that quantum mechanics and general relativity were incompatible [9, 10] [2].

A number of theories have been put forward to attempt to resolve this, the most prominent of which is string theory. String theory was originally proposed as "dual resonance theory" [12] to describe hadrons. It was temporarily set aside once Quantum Chromodynamics, a QFT which is our current best model of hadrons, was formulated. However over the course of the 1970s and 80s important features of the model began to be uncovered. In 1974 it was noticed that closed strings could describe the graviton [13, 14].

In the 1980s the so called "First Superstring Revolution" began as people were able to formulate a supersymmetric version of string theory that avoided the instabilities in the bosonic string theory used until that point[3]. A number of different string theories were defined in this period, Type I, Type IIA, Type IIB [15], and Heterotic string theory [16].

In the 1990s in the "Second Superstring Revolution" it was discovered that all of these string theories could be interpreted as different limits of a single theory dubbed "M-Theory" [17].

However the most important progress, for the purposes of this work at least, arrived in 1997 when Maldacena [18] showed that a certain class of QFT's called conformal field thories were equivalent to the low energy limit of a string theory in one more dimension. This equivalence has been named "Holography", "Gauge/Gravity Duality" or "AdS/CFT" and has been applied to an enormous variety of areas in physics. Holographic models, which exploit this AdS/CFT correspondance, have been used to study condensed matter [19], cosmology [20], black holes [21] and QCD [22]. In particular AdS/QCD has had enormous success in correctly predicting the ratio of the shear viscosity to the entropy density of Quark Gluon Plasmas [23], a high energy state of QCD where the confinement of quarks inside hadrons breaks down.

In this thesis I will describe the "dynamic AdS/CFT" model, its background in holography and quantum chromodynamics. We will also discuss technicolour, a QCD-like theory to which we can apply our method.

In the main body of the thesis we will cover some practical calculations. Specifically the masses and couplings of the mesons that are present in these theories.

[2] In technical terminology general relativity is a non-renormalisable theory. It would require an infinite number of counter terms to renormalise. Although there has been some work on asymptotic safety that may casts doubt on this [11].

[3] This will be discussed in detail in section 3.

Chapter 2

Field Theory

Quantum field theory is arguably the most important tool in modern physics being used in particle physics, cosmology and condensed matter physics among other areas. I will not provide an introduction to QFT here but many good introductory texts exist including but not limited to [8, 24].

2.1 Quantum Chromodynamics

Quantum Chromodynamics [25] (or QCD) is one of the most important quantum field theories in modern physics, providing the best available model for the hadron spectrum, their interactions and masses, and of high energy quark interactions. Here we shall briefly introduce QCD and review one method of quantising it. We will also discuss some of it's most important features, confinement, asymptotic freedom and chiral symmetry breaking.

The QCD Lagrangian is made up of two parts: An $SU(3)$ Yang-Mills [26] term describing the dynamics of the gauge field and a piece describing the matter fields including a kinetic term, a minimal coupling to the gauge field and a Dirac mass term:

$$\mathcal{L} = \int \mathrm{d}^4x \left[\mathrm{Tr} G^{\mu\nu} G_{\mu\nu} + i\overline{\Psi}(\not{D} + m)\Psi\right] \tag{2.1.1}$$

where $G^{\mu\nu} = G_a^{\mu\nu} T_a = \partial^\mu A^\nu - \partial^\nu A^\mu - ig\left[A^\mu, A^\nu\right]$ is the Maxwell tensor for the gauge field, Ψ is the quark spinor field, m is a mass matrix incorporating the masses of the different quark states and $\not{D} = \gamma^\mu(\partial_\mu - igA_\mu)$ is the gauge covariant derivative contracted with the gamma matrix (We have suppressed the sum over the colours in the first term and the flavours in the second).

Under a local gauge transformation $\chi(x) \in \mathscr{L}\left[SU(3)\right]$ the fields transform as,

$$\Psi(x) \to \Psi'(x) = e^{i\chi(x)}\Psi(x) \tag{2.1.2}$$

$$A^\mu(x) \to A^{\mu'}(x) = e^{i\chi(x)} A^\mu e^{-i\chi(x)} + \frac{1}{g} e^{i\chi(x)} \partial^\mu e^{-i\chi(x)} \tag{2.1.3}$$

2.1.1 Quantising Yang-Mills

Quantising a non-abelian gauge field is a non trivial task, here we shall discuss a recipe that introduces new non physical fields called Fadeev-Popov ghosts [27].

Recall the change of a, non-abelian, gauge field under an infinitesimal transformation χ^a,

$$\delta A^a_\mu = f^{abc} A_{\mu b} \chi_c - \frac{1}{g}(\partial_\mu \chi^a) \tag{2.1.4}$$

where we have a single latin index running over the adjoint representation of the gauge group since we have separated out the generators for the Lie group. $A^\mu = T^a A^\mu_a$, with $SU(3)$ generators T^a. This gauge redundancy prevents us from simply naively plugging the action into the Feynmann path integral. The Yang-Mills part of the action is

$$\begin{aligned} S &= \int \mathrm{d}^4x \frac{1}{4} G^{\mu\nu}_a G^a_{\mu\nu} \\ &= \int \mathrm{d}^4x \frac{1}{2} A^a_\mu \mathcal{O}^{\mu\nu}_{ab} A^b_\nu, \end{aligned}$$

where

$$\mathcal{O}^{\mu\nu}_{ab} = (g^{\mu\nu}\partial^2 - \partial^\mu\partial^\nu)\delta_{ab}. \tag{2.1.5}$$

The propergator should be given by the inverse of $\mathcal{O}$ however it is singular,

$$\mathcal{O}^{\mu\nu}\partial_\mu \chi(x) = 0, \tag{2.1.6}$$

and so is non invertable, The way to solve this is to fix a gauge $\partial^\mu A_\mu = f(x)$. This is done by adding a functional delta function to the path integral $\delta\left[\partial^\mu A_\mu - f\right]$. Unfortunately we need to introduce a "functional Jacobian" J in order to do this. We can see why by looking at an extremely simple toy example of an integral [24]. Consider an area integral over a square

$$\int_0^L \int_0^L \mathrm{d}x\mathrm{d}y = L^2 \tag{2.1.7}$$

this can be made into a line integral by inserting a delta function

$$\int_0^L \int_0^L \mathrm{d}x\mathrm{d}y\delta(y) = \int_0^L \mathrm{d}x = L. \tag{2.1.8}$$

We can rewrite this in terms of polar coordinates, $r(x,y)$ and $\theta(x,y)$. In order to do this we include a Jacobian,

$$J = \begin{vmatrix} \frac{\partial x}{\partial r} & \frac{\partial y}{\partial r} \\ \frac{\partial x}{\partial \theta} & \frac{\partial y}{\partial \theta} \end{vmatrix} = \begin{vmatrix} \cos\theta & \sin\theta \\ -r\sin\theta & r\cos\theta \end{vmatrix} = r \tag{2.1.9}$$

so

$$\int\int \mathrm{d}x\mathrm{d}y \to \int\int J\mathrm{d}r\mathrm{d}\theta \to \int\int r\mathrm{d}r\mathrm{d}\theta. \tag{2.1.10}$$

Now we can try to repeat the procedure above, insert a delta function in order to reduce the dimension of the integral

$$\int\int \delta(\theta) r \mathrm{d}r\mathrm{d}\theta = \int_0^L r\mathrm{d}r = \frac{L^2}{2}. \tag{2.1.11}$$

Which is obviously incorrect. To correct for this we define a transformation rule for the delta function

$$\delta(y) \to \frac{1}{J}\bigg|_{\theta=\theta_0} \delta(\theta - \theta_0). \tag{2.1.12}$$

So that our integral now reads

$$\int\int \delta(\theta)\ \frac{1}{J}\bigg|_{\theta=0} r\mathrm{d}r\mathrm{d}\theta = L. \tag{2.1.13}$$

Now let us return to gauge theory. Our gauge fixed path integral looks like

$$Z = \int D\left[A_\mu\right] \delta\left[\partial^\mu A_\mu - f\right]\ J|_{\omega=0}\, e^{iS} \tag{2.1.14}$$

where J is the functional Jacobian and is defined in a similar way to the conventional Jacobian, as the determinant of the (functional) matrix of the derivatives describing the basis change. Here our basis change is an infinitesimal transformation of $\partial^\mu A^a_\mu$,

$$\delta(\partial^\mu A^a_\mu) = f^{abc}\partial^\mu A^b_\mu \omega^c - \frac{1}{g}\partial^2\omega^a. \tag{2.1.15}$$

So we can define the functional derivative

$$\frac{\delta(\partial^\mu A^a_\mu)(x)}{\delta\omega^b(y)} = \frac{-1}{g}\delta^4(x-y)\partial^\mu D^{ab}_\mu(x), \tag{2.1.16}$$

where $D^{ab}_\mu = \partial_\mu\delta^{ab} - g f^{abc}A_{c\mu}$. The next step is to calculate the determinant. We can do this by introducing two Grassman valued variables η and $\overline{\eta}$,

$$\mathrm{det}M = \int \mathrm{D}\left[\eta\right]\mathrm{D}\left[\overline{\eta}\right] e^{-\int \mathrm{d}^4x\overline{\eta}M\eta}. \tag{2.1.17}$$

We can see that this is true by expanding η in terms of eigenstates of M, ϕ_n, $\eta = \sum_n c_n\phi_n$ for Grassman valued c_n

$$\begin{aligned}
&\int \mathrm{D}\left[\eta\right]\mathrm{D}\left[\overline{\eta}\right] e^{-\int \mathrm{d}^4x\overline{\eta}M\eta} \\
&= \int \mathrm{d}\overline{c}_n\mathrm{d}c_n e^{-\sum_n \lambda_n\overline{c}_n c_n} \\
&= \prod_n \lambda_n \\
&= \mathrm{det}M.
\end{aligned} \tag{2.1.18}$$

Where λ_n are eigenvalues of M. So inserting J is equivalent to adding a term to the

action

$$\int \mathrm{d}^4x \overline{\eta}^a \partial^\mu D^{ab}_\mu \eta^b, \tag{2.1.19}$$

where we call η and $\overline{\eta}$ the Fadeev-Popov ghosts. These ghosts do not have a kinetic terms and so are auxiliary fields.

We should now fix $f(x)$ however we can take advantage of our functional integration technology to write a Gaussian distribution over $f(x)$. The full partition function now looks like

$$Z = \int \mathrm{D}\left[f\right] e^{i\int \mathrm{d}^4x \frac{1}{2(1-\xi)} f^2(x)} \int \mathrm{D}\left[A_\mu\right] \delta\left[\partial_\mu A^\mu - f\right] J e^{iS}, \tag{2.1.20}$$

where J takes the form described above and ξ parametrises the "width" of the functional Gaussian over $f(x)$. Thanks to the delta function we can do the integral over $f(x)$ giving

$$Z = \int \mathrm{D}\left[A_\mu\right] J e^{iS} e^{i\int \mathrm{d}^4x \frac{1}{2(1-\xi)} (\partial^\mu A_\mu)^2} \tag{2.1.21}$$

The new gauge fixing term can be integrated by parts so the full action takes the form

$$S = i \int \mathrm{d}^4x A^a_\mu \mathcal{O}^{\mu\nu}_{ab} A^b_\nu, \tag{2.1.22}$$

where

$$\mathcal{O}^{\mu\nu}_{ab} = i\delta_{ab}\left(g^{\mu\nu}\partial^2 + \frac{\xi}{1-\xi}\partial^\mu\partial^\nu\right). \tag{2.1.23}$$

This operator does have an inverse

$$-\delta_{ab}\left(g_{\mu\nu} - \xi\frac{k_\mu k_\nu}{k^2}\right)\frac{i}{k^2}, \tag{2.1.24}$$

we can choose ξ to fix the gauge. For example $\xi = 0$ is the Feynman Gauge. Now we have a propagator for the gluons and the theory can be quantised.

The full set of Feynman rules for a gauge theory quantised in this way, in the Feynman gauge, are [24]:

- The ghost propagator,
$$\frac{1}{k^2}\delta^{ab}. \tag{2.1.25}$$
- A ghost-ghost-gluon vertex
$$-gf^{abc}p_\mu. \tag{2.1.26}$$
- The gluon propagator,
$$-\frac{1}{k^2}\left(g_{\mu\nu} + (\alpha-1)\frac{k_\mu k_\nu}{k^2}\right)\delta^{ab}. \tag{2.1.27}$$

- A three gluon vertex

$$-2gf^{abc}\left[(r_\mu - q_\mu)g_{\nu\rho} + (p_\nu - r_\nu)g_{\mu\rho} + (q_\rho - p_\rho)g_{\mu\nu}\right]. \tag{2.1.28}$$

- A four gluon vertex,

$$\begin{aligned} -g^2\Big[&f^{abe}f^{cde}(g_{\mu\rho}g_{\nu\sigma} - g_{\mu\sigma}g_{\nu\rho}) + f^{ace}f^{bed}(g_{\mu\sigma}g_{\rho\nu} - g_{\mu\nu}g_{\rho\sigma}) \\ &+ f^{ade}f^{bce}(g_{\mu\nu}g_{\sigma\rho} - g_{\mu\rho}g_{\sigma\nu})\Big]. \end{aligned} \tag{2.1.29}$$

- The quark propagator,

$$\frac{i\delta_{ab}}{\not{p} - m}. \tag{2.1.30}$$

- A gluon-quark-quark vertex,

$$-ig\gamma_\mu(T^c)_{ab}. \tag{2.1.31}$$

There are a number of features of non-abelian gauge theories that are not immediately clear from looking at the Lagrangian alone. For example the coupling g runs with the renormalisation scale. At low energies QCD is strongly coupled but at high energies $g \to 0$. To understand this we shall briefly and heuristically recap renormalisation.

2.1.2 Renormalisation and Regularisation

Regularisation

Quantum field theories are generally affected by divergences related to either the low energy limit, so called infra red divergences, or the high energy limit, ultra violet divergences [8]. The correct technique for addressing these is to first regularise the theory then perform renormalisation to change our description from one of infinite "bare" parameters to one of finite 'renormalised' parameters which depend on the energy scale.

There are a number of different regularisation techniques one can use. We will review dimensional regularisation here but it is important to note that other valid approaches exist, for example lattice field theory. In dimensional regularisation we move away from $d = 4$ and instead consider $d = 4 - \epsilon$ with small ϵ. At finite ϵ the theory does not exhibit divergences but they reappear as $\epsilon \to 0$. This choice lets us study the divergences in the theory more directly. When we perform this process to the one particle irreducible functionals we find that the divergences take the form of a first order pole in ϵ.

With this in mind we can devise a scheme to remove the divergences from the theory. We add a set of new terms to the Lagrangian called counterterms. These counterterms are chosen so that they create new divergences in the tree level amplitudes which exactly cancel the divergences in the one loop amplitudes.

As an example we shall consider ϕ^4 theory to one loop order. This is a scalar field theory

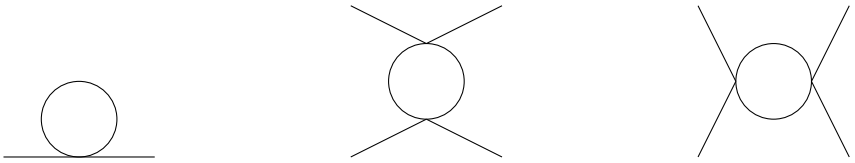

(a) Correction to the propagator. (b) First correction to the four point function. (c) Second correction to the four point function.

Figure 2.1.1: One loop corrections to terms in ϕ^4 theory.

with a quartic term in the Lagrangian

$$\mathcal{L} = \frac{1}{2}\partial^\mu\phi\partial_\mu\phi - \frac{1}{2}m^2\phi^2 - \frac{g}{4!}\phi^4. \tag{2.1.32}$$

The divergent diagrams at one loop are shown in figure 2.1.1. We then find that the required counterterms are

$$\mathcal{L}_{\text{ct}} = \frac{A}{2}\partial^\mu\phi\partial_\mu\phi - \frac{B}{2}\phi^2 - \frac{C}{4!}\phi^4. \tag{2.1.33}$$

where

$$A = 0, B = \frac{gm^2}{16\pi^2\epsilon}, C = \frac{3g^2}{16\pi^2\epsilon}. \tag{2.1.34}$$

Note that there is an ambiguity here, we could also add any constant to A, B or C and the divergences would still be cancelled. We will consider the so called "minimal subtraction" scheme where the divergences are the only contribution to the counterterms.

Renormalisation

We now have a regularised Lagrangian but it is somewhat unsatisfying with infinite bare couplings, defined as $\epsilon \to 0$. Provided that the theory is "renormalisable", that is that it is possible to remove all divergences by adding a finite number of counterterms, we can transform it into a nicer form. This is called renormalisation.

We can define a bare Lagrangian as $\mathcal{L}_{\text{bare}} = \mathcal{L} + \mathcal{L}_{\text{ct}}$ which can be written, in our ϕ^4 example, as

$$\mathcal{L}_{\text{bare}} = -\frac{1}{2}\partial^\mu\phi_0\partial_\mu - \frac{1}{2}m_0^2\phi_0^2 - \frac{1}{4!}g_0\phi_0^4 \tag{2.1.35}$$

where $\phi_0 = Z_\phi^{1/2}\phi$ and $Z_\phi = 1 + A$ with A the same counterterm as before. This can be thought of as the naive Lagrangian for the theory before we consider the effect of renormalisation. The bare parameters of the theory m_0 and g_0 can be expressed, in the minimal subtraction scheme, as:

$$m_0^2 = m^2\left(1 + \frac{g}{16\pi^2\epsilon}\right), \tag{2.1.36}$$

$$g_0 = g\left(1 + \frac{3g}{16\pi^2\epsilon}\right). \tag{2.1.37}$$

However if we are to write down a Lagrangian that is consistent in $4-\epsilon$ dimensions we need a method of keeping the mass dimension of the coupling constant equal to zero. We introduce an arbitrary mass scale μ, called the renormalisation scale, and make the substitution $g \to g\mu^{\epsilon}$. We can now more succinctly write the bare coupling as:

$$g_0 = \mu^{\epsilon}\frac{gZ_g}{Z_\phi^2}. \tag{2.1.38}$$

The parameter μ did not not appear in the bare, unrenormalised, theory but is a new parameter introduced when we regularised the theory.

The Renormalisation Group

We now have a new parameter in the theory, μ, which describes a one dimentional family of theories with different parameters, m and g in our ϕ^4 example. We can define a one dimensional semigroup[1] of finite transformations in μ this is the famed renormalisation group.

Let us consider the vertex functions. We can define bare and renormalised vertex functions in the same way as the fields and parameters above,

$$\Gamma_0^{(n)}(p_1,...,p_n) = Z_\phi^{-n/2}\Gamma^{(n)}(p_1,...,p_n). \tag{2.1.39}$$

Since the left hand side does not depend on μ we can take derivatives to obtain the renormalisation group equation

$$\left(\mu\frac{\partial}{\partial\mu} + \beta\frac{\partial}{\partial g} + m\gamma_m\frac{\partial}{\partial m} - n\gamma\right)\Gamma^{(n)}(p_1,...p_n) = 0 \tag{2.1.40}$$

where we have introduced three new functions

$$\beta = \mu\frac{\partial g}{\partial\mu} \tag{2.1.41}$$

$$\gamma_m = \frac{\mu}{m}\frac{\partial m}{\partial\mu} \tag{2.1.42}$$

$$\gamma = \frac{\mu}{2Z_\phi}\frac{\partial Z_\phi}{\partial\mu} \tag{2.1.43}$$

β and γ_m can be thought of describing how the couplings g and m change or "run" with the renormalisation scale while γ is known as the anomalous dimension of the field and describes how the mass dimension of ϕ^2 runs. These functions are calculated order by order in loops.

We have used ϕ^4 as an illustrative example here but the same story is true for any renormalisable quantum field theory. In particular we will use the two loop formula for the QCD β function, which describes how the coupling g runs, to calculate the running of

[1] A semigroup is defined as a group which lacks an inverse.

parameters throughout this work,

$$\mu\frac{d\alpha}{d\mu} = -b_0\alpha^2 - b_1\alpha^3 \tag{2.1.44}$$

where μ is the renormalisation scale, equivalent to $\log(r)$ in the bulk coordinates that we shall introduce later, $b_0 = \frac{1}{6\pi}(11N_c - 2N_f)$ and $b_1 = \frac{1}{24\pi^2}(34N_c^2 - 10N_cN_f - 3\frac{N_c^2-1}{N_c}N_f)$ and $\alpha = \frac{g^2}{\pi}$. In order to solve this differential equation we choose an intermediate boundary condition, which we will interpret as defining the energy scale we are working at. After two loops the β function becomes dependent on the scheme chosen so we will truncate here for the sake of generality.

In summary couplings can be thought of as describing the amplitudes, after "amputating" the external propagators, for simple diagrams. For example in ϕ^4 theory the interaction term $g\phi^4$ can be thought of as describing the diagram for a 4 point function and the mass term $m^2\phi^2$ describes the 2 point function or propagator. However these diagrams gain corrections due to the effect of higher order loop diagrams so the physical couplings are the "bare" couplings in the Lagrangian plus some contribution from loop corrections. In general these loop corrections will depend on the energy of the interaction, the "renormalisation scale". The effect of this is that the couplings, including the mass, are functions of the energy scale. This is commonly referred to as the "renormalisation group flow".

2.1.3 Asymptotic Freedom and Confinement

From now on we will refer extensively to QCD specifically. We shall define QCD as a gauge theory with $N_c = N_f = 3$ where two of the quarks, up and down, are light and a third, strange, is heavy.

The two features of QCD that make it most fascinating are asymptotic freedom, the fact that QCD is strongly coupled in the IR and flows to a weak coupling in the UV, and confinement, coloured states are not seen in the IR instead particles are arranged into colourless bound states.

In QED photons are not charged under their own $U(1)$ gauge field and so do not self interact [28]. The effect of this is to ensure that the coupling between the photon and the fermions is weak (in the IR at least, in the far UV the coupling becomes very large at what is called the "Landau pole" [29]) and amplitudes can be calculated perturbatively. In QCD, by contrast, the gluons do carry colour charge and so their self interactions create a very strong coupling g in the IR [25, 26] which then flow to a weak coupling in the UV, a feature called "asymptotic freedom", as seen in (2.1.44). This strong coupling is the source of most of the difficulties with working with QCD since the traditional Feynmann diagram loop expansion is no longer helpful. However it is also the source of two related features of QCD at low energies which make it interesting to study: Chiral symmetry breaking and confinement, which we shall briefly review here:

On it's face the QCD Lagrangian has an approximate $U(N_f)_L \times U(N_f)_R$ chiral symmetry[2], if $m = 0$ or an approximate symmetry if $m < \Lambda$, describing a rotation among the fermion fields. Upon quantisation a $U(1)_A$ subgroup of this, referred to as axial symmetry, is broken by the so called axial anomaly. This leaves us with an $SU(N_f)_L \times SU(N_f)_R \times U(1)_B$ symmetry, where $U(1)_B$ is the symmetry associated with the conservation of baryon number. We can see how this anomaly arises by considering the axial charge [30]

$$Q_A \equiv \int \mathrm{d}^3 x \psi^\dagger \gamma_5 \psi, \tag{2.1.45}$$

where ψ is the quark field. This is time independent so axial symmetry is conserved classically. Under this symmetry the fermions transform as $\psi \to e^{i\gamma_5 \theta}\psi$. When we quantise, however, bilinears of the same fermion field at the same spacetime point become ill defined. So Q_A, which depends on a local bilinear of the fermions becomes singular. This singularity can be solved through a renormalisation procedure similar to that described above. However it is not possible to construct a renormalisation procedure that preserves the transformation rules. We have broken the $U(1)$ symmetry. This breaking of a symmetry when we quantise a theory is known as an "anomaly".

Now we are left with a $SU(N_f)_L \times SU(N_f)_R$ symmetry. Since QCD is strongly coupled in the infra red the vacuum is non-perturbative, it does not have vanishing condensates like the naive vacuum, in contrast to QED for example. This can be understood qualitatively by analogy to superconductivity [31]. In the BCS model a weak attraction between electrons leads to a ground state with a $e^- e^-$ condensate. Similarly the very strong interaction between quark antiquark pairs in QCD leads to a ground state with a $\langle \overline{q} q \rangle$ condensate. If we expand out the condensate in terms of the left and right chiral components we obtain $\langle \overline{q}_L q_R + \overline{q}_R q_L \rangle$. The vacuum is then no longer invariant under separate transformations of the left and right hand sectors $U_L \neq U_R$ but only under a subset of these that acts on both sides equally. $U_L = U_R$. What has happened here is that the (approximate) chiral symmetry group has been spontaneously broken $SU(N_f)_L \times SU(N_f)_R \to SU(N_f)$.

Goldstone's theorem [32] tells us that the breaking of a large symmetry group down to a smaller one produces a set of Goldstone bosons. To illustrate this we can return to a ϕ^4 theory [24], this time one that we have constructed to be invariant under some symmetry group G. While this is a toy model it is somewhat relevant to QCD since we can interpret the scalar field as a quark bound state $\phi = \overline{q}_L q_R$.

$$\mathcal{L} = \frac{1}{2}\partial_\mu \phi_i \partial^\mu \phi_i - \frac{m^2}{2}\phi_i \phi_i - \lambda(\phi_i \phi_i)^2 \tag{2.1.46}$$

where ϕ_i now lives in the fundamental representation of G, ie it transforms as

$$\phi_i \to U_i^j \phi_j \tag{2.1.47}$$

[2] Broken only by the mass term

for $u^i_j \in G$ Let us consider the potential,

$$\frac{m^2}{2}\phi_i\phi_i + \lambda(\phi_i\phi_i)^2. \tag{2.1.48}$$

If $m^2 > 0$ the minimum is at zero however if $m^2 < 0$ this becomes a maximum and there is instead a degenerate family of vacua at

$$|\phi_0| = \sqrt{\phi_i\phi_i} = \sqrt{\frac{-m^2}{4\lambda}} = a \tag{2.1.49}$$

The vacuum is not invariant under the full group G but instead only under a subgroup of one fewer dimension which we shall call H. Now let us suppose that our full group is $SU(3)$ so $H = SU(2)$, the theorem is true for any Lie group but this simplifies the analysis. The index i now runs over 1, 2, 3 and we are able to chose ϕ to be the dimension of the group which is broken by the vacuum. We expand around the vacuum in this axis $\phi_3 = \chi + a$. If we write the potential in terms of ϕ_1, ϕ_2 and χ we obtain:

$$V = 4a^2\lambda\chi^2 + 4a\lambda\chi(\phi_1^2 + \phi_2^2 + \chi^2) + \lambda(\phi_1^2 + \phi_2^2 + \chi^2)^2 - \lambda a^4 \tag{2.1.50}$$

we can read off masses for the three fields

$$m_\chi^2 = 8a^2\lambda \tag{2.1.51}$$

$$m_{\phi_1} = m_{\phi_2} = 0 \tag{2.1.52}$$

so after we have broken our symmetry we have obtained one massive boson and two massless bosons. We refer to the massless ones as "Goldstone bosons".

We then obtain a set of light bosons, in $N_f = 3$ we get 8 corresponding to the octet representation of $SU(3)$ for example, which are the lightest set of mesons. This can be seen by considering the group theory representation algebra [33]. A meson consists of a quark and an antiquark which live in the fundamental, $\mathbf{3}$, and antifundamental, $\overline{\mathbf{3}}$ representations of $SU(3)$ so

$$\mathbf{3} \otimes \overline{\mathbf{3}} = \mathbf{8} \oplus \mathbf{1}, \tag{2.1.53}$$

where $\mathbf{8}$ is the octet representation and $\mathbf{1}$ is the singlet. The octet is identified with the observed pions, kaons and η^0 mesons. The singlet is the η' state which would be massless if it were not for the axial anomaly described above. If the chiral symmetry were exact these mesons would be massless however since it is only an approximate symmetry group we get massive, albeit light, pseudo-Goldstone bosons.

A similar analysis produces the possible baryon states. Since baryons consist of three quarks the representations look like

$$\mathbf{3} \otimes \mathbf{3} \otimes \mathbf{3} = \mathbf{1} \oplus \mathbf{8} \oplus \mathbf{8} \oplus \mathbf{10}, \tag{2.1.54}$$

giving us the more complex set of baryons[3].

The other feature of QCD that we will rely on is colour confinement. The quarks and gluons can only exist in bound states with no overall colour. These can either be baryons, with one of each colour represented, or mesons, with a colour or anti colour. There are also structures called glueballs, collections of gluons with no quarks. We will be concerned with mesons in this work. There exists no analytic proof that QCD must exhibit colour confinement, however it is observed both in nature and in lattice simulations of QCD [34]. We can qualitatively understand why confinement occurs by observing that the effective potential between two quarks increases with their separation rather than decreasing as occurs in QED and other weakly coupled theories. If we were to take a meson and attempt to pull the quark and antiquark apart, at some point the potential energy exceeds the energy required to create new quark-antiquark pair. The meson will then split into two and at no point will there be a free quark. This is obviously a very naive example but it illustrates the point that any event energetic enough to separate a meson into it's component quark and antiquark will instead split it into new mesons instead.

Since the bare quarks and gluons never appear outside of bound states when we refer to the "spectrum" of QCD we mean the spectrum of these bound states. The meson and baryon parts of this are well known however the glueballs are more complex. In particular there is no analytic proof of the existence of a mass gap in Yang-Mills although lattice calculations have shown that one must exist [35].

2.1.4 The 't Hooft Limit

A pure Yang-Mills theory, we will not consider matter here, has two parameters. The gauge coupling g and the number of colours N_c. It can be shown [36] that taking the limit $N_c \to \infty$, while keeping $\lambda = g^2 N_c$ fixed, is well defined. This parameter can be understood intuitively by considering the one loop corrections to the gluon propagator. These diagrams pick up a factor of g^2 from the vertices and a factor of N_c from the possible gluons in the loop so the contribution from the whole diagram is proportional to the 't Hooft coupling.

The original motivation for this was to study gauge theories for their own sake and it is used in the original paper to derive some interesting results. In particular it can be shown that non-planar diagrams are suppressed in this limit.

Of interest to us, however, is that the string coupling of the AdS dual is $g_s = \frac{\lambda}{N_c}$ so a QFT in the 't Hooft limit corresponds to a string theory at weak coupling while we are still free to take $\lambda \to \infty$ so we can construct a strong/weak coupling duality.

[3]Note that the full standard model contains three families, each of two quarks, so the full spectrum should be somewhat larger. However these states are much more massive so three flavours is a good approximation for QCD.

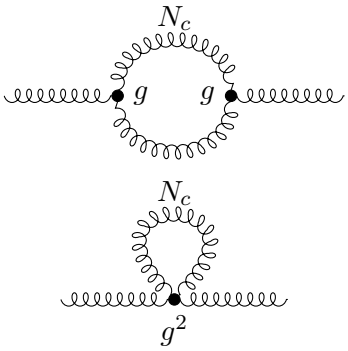

Figure 2.1.2: One loop gluon propagators.

2.2 Nambu-Jona-Lasino Models

The Nambu-Jona-Lasino model is a simple model of mass generation in QCD that can be thought of as the effect of including a gluon mass of Λ. It was first proposed before the introduction of QCD as a theory of nucleons and mesons inspired by BCS superconductivity [37]. The pure theory contains only one field or set of fields, a Dirac fermion ψ, which has a kinetic term and a quartic self interaction. The Lagrangian takes the form:

$$\mathcal{L}_{\text{NJL}} = \overline{\psi} i \partial\!\!\!/ \psi - \frac{1}{2N} \frac{g^2}{\Lambda^2} \left[(\overline{\psi}\psi)^2 + (\overline{\psi} i \gamma_5 \psi)^2 \right]. \tag{2.2.1}$$

Where ψ is an N_f component fermion invariant under some chiral group $SU(N_f)_L \times SU(N_f)_R$. This Lagrangian non-renormalisable but shares the key features we are interested in so we shall consider it here.

At one loop there are two contributions to the effective potential. First the free quark Coleman Weinberg potential [37].

$$V_{\text{eff}} = -\int_0^{\Lambda} \frac{\mathrm{d}^4 k}{(2\pi)^4} \log(k^2 + m^2). \tag{2.2.2}$$

Where we Fourier transformed into momentum space k and Λ is the UV cutoff. In a normal gauge theory this term would be constant since the mass, m, is constant. However as we shall soon see the mass is now a dynamical quantity given by $m = (g^2/\Lambda^2)\langle\overline{\psi}\psi\rangle$. In addition we get a new contribution directly from the four fermion interaction.

$$\Delta V_{\text{eff}} = \frac{\Lambda^2 m^2}{g^2} \tag{2.2.3}$$

With this extra term the effective potential as a function of m is bounded from below with a minimum that depends on g. For small g the NJL term ΔV_{eff} dominates so the minimum is at $m = 0$. As g passes a critical value, 2π, we encounter a phase transition and the minimum becomes nonzero, it's value given by the solution to the famous "gap

equation",

$$1 = \frac{g^2}{4\pi^2}\left(1 - \frac{m^2}{\Lambda^2}\log\left[\frac{\Lambda^2 + m^2}{m^2}\right]\right). \tag{2.2.4}$$

The generation of the mass can be thought of more intuitively by considering the NJL term in terms if left and right hand components of the spinnors, $\overline{\psi}_L\psi_R\overline{\psi}_R\psi + h.c.$ when the QCD chiral condensate forms this can be approximated as $\langle\overline{\psi}_L\psi_R\rangle\,\overline{\psi}_R\psi_L + h.c.$. This can be considered as a mass term with $m \sim \langle\overline{\psi}_L\psi_R\rangle$.

2.3 The Standard Model

Now let us turn our attention to the current best description of nature, the standard model. This section largely follows [38]. The standard model has three sectors:

- A fermion sector consisting of three families of leptons and quarks.
- An $SU(3)_{QCD} \otimes SU(2)_L \otimes U(1)_Y$ gauge sector consisting of the $SU(3)$ strong interaction described above and an electroweak sector, $SU(2)_L \otimes U(1)_Y$.
- A scalar called the Higgs responsible for breaking the electroweak gauge group down to the $U(1)$ electromagnetic and the $SU(2)$ weak interactions as well as to provide masses to the fermions.

2.3.1 Quarks and Leptons

First let us consider the fermionic sector. This neatly decomposes into two halves, the quarks and the leptons. The full particle content of all three families can be written as

$$\begin{aligned}
\text{First} &: \begin{pmatrix}\nu_e\\ e^-\end{pmatrix}_L, e^-_R, \begin{pmatrix}u\\ d\end{pmatrix}_L, u_R, d_R\\
\text{Second} &: \begin{pmatrix}\nu_\mu\\ \mu^-\end{pmatrix}_L, \mu^-_R, \begin{pmatrix}c\\ s\end{pmatrix}_L, c_R, s_R\\
\text{Third} &: \begin{pmatrix}\nu_\tau\\ \tau^-\end{pmatrix}_L, \tau^-_R, \begin{pmatrix}t\\ b\end{pmatrix}_L, t_R, b_R,
\end{aligned}$$

where we have split the fermions into their left and right handed Weyl spinors. This is done to illustrate clearly how the fermions couple to the gauge bosons.

- The $SU(2)$ weak interaction couples only to left handed fermions. With associated quantum number I_3 called isospin.
- The $SU(3)$ strong interaction couples to the quarks.
- The $U(1)$ hypercharge interaction couples to all the matter fields with associated quantum number Y. The Electromagnetic interaction couplings are related to hypercharge and isospin by the formula $Q = I_3 + \frac{1}{2}Y$.

Note that we have only included left handed neutrinos. The standard model does not include right handed, or sterile, neutrinos although they are present in some phenomenological models and there have been searches for them [39].

There is much more that could be elaborated upon here, including the very interesting subject of neutrino oscillation and masses but since that is not relevant to our purposes we will move on to the bosons.

2.3.2 Electroweak Theory and the Higgs Mechanism

The Standard model is sometimes described as a gauge theory of the group $SU(3)_{QCD} \otimes SU(2)_L \otimes U(1)_Y$ although that is not necessarily a helpful description since the fermions do not all transform under this full group, only the quarks transform under $SU(3)_{QCD}$ for example. The QCD sector behaves exactly as described in section 2.1 so we shall move on to the $SU(2)_L \otimes U(1)_Y$ electroweak sector.

The Lagrangian for the electroweak gauge bosons can be written as

$$\mathcal{L}_{\mathcal{EW}} = -\frac{1}{4} W^i_{\mu\nu} W_i^{\mu\nu} - \frac{1}{4} B_{\mu\nu} B^{\mu\nu}, \tag{2.3.1}$$

where W^i and B are the Maxwell tensors corresponding to $SU(2)$ and $U(1)$ gauge groups and we have neglected the gauge fixing and Fadeev-Popov terms. Obviously these are not the observed photons, A_μ, and W and Z gauge bosons, they are all massless and couple to all of the fermions.

In order to resolve this we follow a similar procedure to 2.1.3 introduce a new complex scalar, the Higgs field, that will spontaniously break this symmetry and give us our physical electromagnetic and weak interactions. The Lagrangian for the Higgs takes the form

$$\mathcal{L}_{\text{Higgs}} = (D_\mu \Phi)^\dagger (D^\mu \Phi) + \mu^2 \Phi^\dagger \Phi - \lambda (\Phi^\dagger \Phi)^2, \tag{2.3.2}$$

where Φ is the Higgs field, D_μ is the electroweak covariant derivative, and μ, $\lambda > 0$ parametrise the Higgs potential. The Higgs transforms covariantly under $SU(2)_L \otimes U(1)_Y$ and so can be written as a complex doublet,

$$\begin{pmatrix} \phi^+ \\ \phi_0 \end{pmatrix}. \tag{2.3.3}$$

Depending on the sign of the mass parameter $-\mu^2$ there are two possibilities for the vacuum for the Higgs field:

- $(-\mu^2) > 0$ the minimum is at $\langle 0|\Phi|0\rangle = 0$ and no symmetry breaking occurs.
- $(-\mu^2) < 0$ there is a continuous family of degenerate minima given by

$$|\langle 0|\Phi|0\rangle| = \begin{pmatrix} 0 \\ \frac{v}{\sqrt{2}} \end{pmatrix}, \tag{2.3.4}$$

where the phase, $\arg(\langle 0|\Phi|0\rangle)$, is arbitrary and $v \equiv \sqrt{\frac{\mu^2}{\lambda}}$. This has spontaneously broken the symmetry group down to $U(1)$.

Since we are aiming to break our electroweak symmetry group we will select the second option and for convenience we will choose the phase of the vacuum to be 0.

Let us now consider small excitations around the vacuum,

$$\Phi(x) = e^{\left(i\frac{\xi\cdot\sigma}{v}\right)}\begin{pmatrix}0\\ \frac{v+H(x)}{\sqrt{2}}\end{pmatrix}, \tag{2.3.5}$$

where ξ and H fields that parametrise our excitations. The field ξ is unphysical and can be eliminated by a gauge transformation:

$$\Phi' = U(\xi)\Phi = \begin{pmatrix}0\\ \frac{v+H}{\sqrt{2}}\end{pmatrix}, \tag{2.3.6}$$

$$U(\xi) = e^{\left(-i\frac{\xi\cdot\sigma}{v}\right)}, \tag{2.3.7}$$

$$l'_L = U(\xi)l_L, \tag{2.3.8}$$

$$e'_R = e_R, \tag{2.3.9}$$

$$q'_L = U(\xi)q_L, \tag{2.3.10}$$

$$u'_R = u_R, \tag{2.3.11}$$

$$d'_R = d_R, \tag{2.3.12}$$

$$\left(\frac{\sigma\cdot W'_\mu}{2}\right) = U(\xi)\left(\frac{\sigma\cdot W_\mu}{2}\right)U^{-1}(\xi) - \frac{i}{g}(\partial_\mu U(\xi))U^{-1}(\xi), \tag{2.3.13}$$

$$B'_\mu = B_\mu, \tag{2.3.14}$$

and the same for the other fermion families. The observed boson fields can be seen by rotating the weak eigenstates to mass eigenstates

$$\begin{aligned} W^\pm_\mu &= \frac{{W'}^1_\mu \mp i{W'}^2_\mu}{\sqrt{2}},\\ Z_\mu &= c_w {W'}^3_\mu - s_w {B'}_\mu,\\ A_\mu &= s_w {W'}^3_\mu = +c_w {B'}_\mu, \end{aligned}$$

where the coefficients $c_w = \cos\theta_w$ and $s_w = \sin\theta_w$ are defined in terms of the weak angle

θ_w. It is now easy to read off the masses for the fields by expanding the full Lagrangian,

$$\begin{aligned} M_W &= \frac{gv}{2}, \\ M_Z &= \frac{\sqrt{g^2+g'^2}v}{2}, \\ M_H &= \sqrt{2}\mu, \\ m_e &= \lambda_e \frac{v}{\sqrt{2}}, \\ m_\mu &= \lambda_\mu \frac{v}{\sqrt{2}}, \\ m_\tau &= \lambda_\tau \frac{v}{\sqrt{2}}, \end{aligned}$$

where g and g' are the coupling constants for the W and B fields from the bare Lagrangian respectively and λ_e, λ_μ etc are parameters controlling the charged lepton masses.

It is also simple to obtain the terms corresponding to interactions between the Higgs, H, and the other standard model fields in the same manner but these have been omitted for brevity.

2.4 Technicolour

Technicolour is a proposed alternative to the Higgs mechanism for electroweak symmetry whereby a new QCD like sector couples to the weak interaction [40]. The full gauge group of this theory is

$$SU(N_c) \otimes SU(2)_L \otimes U(1)_Y, \tag{2.4.1}$$

where $SU(N_c)$ is the technicolour part and $SU(2)_L \otimes U(1)_Y$ is the electroweak gauge group. We normally only consider one flavour doublet of (techni-) quarks. These exist in the fundamental representation of $SU(N_c)$:

$$\begin{pmatrix} U \\ D \end{pmatrix}_L = (N_c, 2)\,, \tag{2.4.2}$$

$$U_R = (N_c, 1)\,, \tag{2.4.3}$$

$$D_R = (N_c, 1)\,. \tag{2.4.4}$$

where the first number refers to the technicolour gauge group, the second to $SU(2)_L$.

This sector is confining just like traditional QCD and undergoes spontaneous chiral symmetry breaking below some energy scale Λ_{TC}. The bare theory has the chiral symmetry group $SU(2)_L \otimes SU(2)_R$ which is broken to a single $SU(2)_V$ by the vacuum condensate $\langle \overline{U}_L U_R + \overline{D}_L D_R \rangle$ as discussed earlier.

The associated scalar "pion" then performs the role of the Goldstone boson becoming the longitudinal degrees of freedom for the W and Z bosons.

The other task fulfilled by the Higgs mechanism is to provide effective masses to the

quarks and leptons. A modification of the technicolour model called "Extended Technicolor" can also accomplish this goal. The gauge group is expanded to include the standard model fermions. At some high scale Λ_{ETC}, above Λ_{TC}, this group is broken down to just the section containing the technicolor fermions and the standard model particles emerge as singlets. These singlet states then develop masses through their interaction with the condensate of technifermions or, as we shall see later through the inclusion on NJL terms.

This extended technicolour however struggles to produce sufficiently large masses for the heavy standard model fermions [41]. It is possible to generate larger masses by means of a feature called "walking". In QCD the coupling, g, is asymptotically free so that in the UV it runs with the renormalisation scale, μ as $g(\mu) \propto \frac{1}{\ln(\mu)}$. Since the anomalous dimension γ_m is proportional to g this leads to a correction to the mass proportional to $\ln\left(\frac{\Lambda_{ETC}}{\Lambda_{TC}}\right)^{\gamma_m}$. However if we make the coupling approximately constant we instead obtain a power law relation for the radiative correction: $\left(\frac{\Lambda_{ETC}}{\Lambda_{TC}}\right)^{\gamma_m}$ [40]. This is obviously far larger than the case without walking so we can generate much larger masses. It is sufficient for the coupling to be approximately constant only in the range $\Lambda_{TC} < \mu < \Lambda_{ETC}$.

The discovery of a light Higgs has dampened some interest in alternative phenomenological models of electroweak symmetry breaking [42], however composite Higgs models such as technicolour are still not excluded provided they can predict a sufficiently light boson to explain the observed Higgs. It is our goal here to use the technology of AdS/CFT to study technicolour models in order to check if they are still viable.

Chapter 3

Gravity and Strings

In this chapter we shall first introduce supersymmetry within the context of field theory before generalising to supergravity. We will then discuss string theory before introducing the AdS/CFT correspondence generally and dynamic AdS/QCD specifically.

3.1 Supersymmetry and Supergravity

In order to understand holography we first need a grounding in string theory and its low energy limit, supergravity. This section largely follows [43] and [44].

3.1.1 Supersymmetry

While its actual phenomenological significance is becoming more dubious [45], supersymmetry appears widely across modern theoretical physics most notably in string theory and regardless of whether it is realised in nature can provide important assistance in a number of applications.

The origin of supersymmetry lies in the famous Coleman-Mandula theorem [46], which states that "space-time and internal symmetries cannot be combined in any but a trivial way". Essentially we cannot extend the Poincare group in any nontrivial way. Fortunately there is a loophole here, the authors only considered symmetries with commuting generators and it turns out to be possible to extend the Poincare group using anti-commuting generators.

The Poincare algebra consists of translation generators P_μ and rotation/boost generators $M_{\mu\nu}$. We extend this with the spinor valued generators Q^I_α and $\overline{Q}^I_{\dot{\alpha}}$, Where α and $\dot{\alpha}$ are the two Weyl spinor indices and I runs over the number of supersymmetries $\mathcal{N}$. These generators have the following commutation relations with the Poincare generators

$$\left[P_\mu, Q^I_\alpha\right] = 0, \tag{3.1.1}$$

$$\left[P_\mu, \overline{Q}^I_{\dot{\alpha}}\right] = 0, \tag{3.1.2}$$

$$\left[M_{\mu\nu}, Q^I_\alpha\right] = i(\sigma_{\mu\nu})^\beta_\alpha Q^I_\beta, \tag{3.1.3}$$

$$\left[M_{\mu\nu}, \overline{Q}^I_{\dot{\alpha}}\right] = i\left(\overline{\sigma}_{\mu\nu}\right)^{\dot{\beta}}_{\dot{\alpha}} \overline{Q}^I_{\dot{\beta}}. \tag{3.1.4}$$

Where $(\sigma^{\mu\nu})^{\beta}_{\alpha}$ are the Lorentz generators given by

$$(\sigma^{\mu\nu})^{\beta}_{\alpha} = \frac{1}{4}\left(\sigma^{[\mu}_{\alpha\dot{\gamma}}\overline{\sigma}^{\nu]\dot{\gamma}\beta}\right), \tag{3.1.5}$$

and its Hermitian conjugate, in which σ_μ are the Pauli matrices. The Q's anticommute amongst themselves as

$$\left\{Q^I_\alpha, \overline{Q}^J_{\dot{\beta}}\right\} = 2\sigma^{\mu}_{\alpha\dot{\beta}} P_\mu \delta^{IJ}, \tag{3.1.6}$$

$$\left\{Q^I_\alpha, Q^J_\beta\right\} = \epsilon^{\alpha\beta} Z^{IJ}, \tag{3.1.7}$$

$$\left\{\overline{Q}^I_{\dot{\alpha}}, \overline{Q}^J_{\dot{\beta}}\right\} = \epsilon^{\dot{\alpha}\dot{\beta}}\left(Z^{IJ}\right)^*, \tag{3.1.8}$$

where the antisymmetric matrix Z^{IJ} is the central charge of the supersymmetry. In $\mathcal{N} = 1$ there are obviously no indices I and J and so $Z = 0$. This form of supersymmetry is often called Poincare supersymmetry to distinguish it from the larger superconformal symmetry we shall encounter later.

In order to build up some intuition about what these new generators do, let us consider the commutator of the third component of angular momentum, $J_3 = M_{12}$, $[J_3, Q^I_1] = \frac{1}{2}Q^I_1$ and $J_3 = M_{12}$, $[J_3, Q^I_2] = -\frac{1}{2}Q^I_2$, we get the reverse for its conjugate. Considering these generators as quantum operators, we can conclude that acting Q^I_1 raises the spin of a state by $\frac{1}{2}$ and Q^I_2 lowers it.

A supersymmetric field theory then is one consisting of a number of so called supermultiplets, sets of fields that rotate within themselves under supersymmetric transformations with couplings that are invariant under those transformations. For example $\mathcal{N} = 1$ supersymmetry, without gravity, permits two multiples:

- **The Chiral Multiplet** consists of four degrees of freedom: a complex scalar and a Weyl fermion.
- **The Vector Multiplet** also consists of four degrees of freedom: a Weyl fermion and a gauge boson both of which must be in the adjoint representation of the gauge group.

In $\mathcal{N} > 1$, in $d = 4$ there are more fields in each multiplet since the extra generators make it necessary for the multiplet to permit more "steps" made by interpreting the supersymmetry generators as creation operators acting on the Clifford vacuum. For instance in $\mathcal{N} = 4$ we only have one multiplet consisting of 4 Weyl fermions 3 complex scalars and a gauge boson.

3.1.2 Superspace

Writing down a theory that satisfies supersymmetry is not a trivial affair. Care must be taken to ensure that the number of fermionic and bosonic degrees of freedom match

and to ensure that the interaction terms do not break supersymmetry. We can formulate a much more satisfying language to describe supersymmetric theories by taking inspiration from Lorentz symmetry.

The technique of using Einstein notation to sum over spacetime indices ensures that any term we write down automatically satisfies Lorentz symmetry by absorbing the different degrees of freedom in, for example, a vector or spinor into one field. In this spirit we shall try and absorb all fields in a supermultiplet into one "superfield". To illustrate this approach we will restrict to $\mathcal{N} = 1$ it is possible to generalise to extended supersymmetry but this makes the notation much less simple.

We will extend the spacetime coordinates x^μ with two new constant spinor valued coordinates θ_α and $\overline{\theta}_{\dot{\alpha}}$. These anticommute amongst themselves and have derivatives and integrals defined in the usual manner for Grassmann variables

$$\frac{\partial}{\partial\theta^\alpha}\theta^\beta = \delta^\beta_\alpha, \tag{3.1.9}$$

$$\frac{\partial}{\partial\overline{\theta}^{\dot{\alpha}}}\overline{\theta}^{\dot{\beta}} = \delta^{\dot{\beta}}_{\dot{\alpha}}, \tag{3.1.10}$$

$$\int \mathrm{d}^2\theta\theta\theta = \int \mathrm{d}^2\overline{\theta}\,\overline{\theta}\,\overline{\theta} = 1 \tag{3.1.11}$$

where we have defined the dot product $\theta^\alpha\theta_\alpha = 2\theta_1\theta_2$ and likewise for $\overline{\theta}$. One of most the interesting properties of Grassmann variables is that the Taylor series of any function truncates. For our case we can write down any general scalar function of x, θ, $\overline{\theta}$.

$$\begin{aligned} F(x,\theta,\overline{\theta}) = f(x) + \theta\psi(x) + \overline{\theta}\overline{\chi}(x) + \theta\theta m(x) + \overline{\theta\theta}n(x) \\ + \theta\sigma^\mu\overline{\theta}v_\mu(x) + \theta\theta\overline{\theta}\overline{\lambda}(x) + \overline{\theta\theta}\theta\rho(x) + \theta\theta\overline{\theta\theta}d(x), \end{aligned} \tag{3.1.12}$$

where we have introduced scalar functions of x alone: f, m, n and d, Weyl spinors: ψ, χ, λ and ρ and a vector v_μ.

So we now have the language to write down a field in this new superspace language. The next step is to return to the generators of the superalgebra and write them down in terms of our supercoordinates. By requiring that our superfield transforms covariantly under supersymmetry transformations we obtain formulae for the supercharges:

$$Q_\alpha = -i\frac{\partial}{\partial\theta^\alpha} - \sigma^\mu_{\alpha\dot{\beta}}\overline{\theta}^{\dot{\beta}}\partial_\mu \tag{3.1.13}$$

$$\overline{Q}_{\dot{\alpha}} = i\frac{\partial}{\partial\overline{\theta}^{\dot{\alpha}}} + \theta^\beta\sigma^\mu_{\beta\dot{\alpha}}\partial_\mu \tag{3.1.14}$$

and the infinitesimal supersymmetry transform is given by

$$\delta_{\epsilon,\overline{\epsilon}}F = i(\epsilon Q + \overline{\epsilon}\overline{Q})F \tag{3.1.15}$$

for infinitesimal spinors ϵ and $\overline{\epsilon}$. Now we are well on our way to building the technology

necessary to express a quantum field theory in superspace. Next we need superderivatives these are defined rather intuitively as

$$D_\alpha \equiv \frac{\partial}{\partial\theta^\alpha} + i\sigma^\mu_{\alpha\dot{\alpha}}\overline{\theta}^{\dot{\alpha}}\partial_\mu \tag{3.1.16}$$

$$\overline{D}_{\dot{\alpha}} \equiv -\frac{\partial}{\partial\overline{\theta}^{\dot{\alpha}}} - i\theta^\alpha\sigma^\mu_{\alpha\dot{\alpha}}\partial_\mu. \tag{3.1.17}$$

Our general superfield F has too many degrees of freedom to describe either of the supermultiplets in $\mathcal{N}=1$ supersymmetry. Fortunately we can impose conditions on the superfield to ensure it describes one of the two multiplets.

- The chiral superfield can be described by requiring the condition $\overline{D}_{\dot{\alpha}}\Phi = 0$.
- The vector superfield is given by $V = V^\dagger$.

3.1.3 $\mathcal{N}=4$ Super Yang-Mills

Moving away from superspace for now let's discuss what is probably the most important single supersymmetric theory in modern physics, $\mathcal{N}=4$ super Yang-Mills in $d=4$. The Lagrangian for this theory is

$$\begin{aligned}\mathcal{L} = \mathrm{Tr}\Big\{ &-\frac{1}{2g^2}F_{\mu\nu}F^{\mu\nu} + \frac{\theta_I}{8\pi^2}F_{\mu\nu}\overline{F}^{\mu\nu} - \overline{\lambda}^a\overline{\sigma}^\mu D_\mu\lambda_a - D_\mu X^i D^\mu X^i \\ &+ gC_i^{ab}\lambda_a\left[X^i,\lambda_b\right] + g\overline{C}_{iab}\overline{\lambda}^a\left[X^i,\overline{\lambda}^b\right] + \frac{g^2}{2}\left[X^i,X^j\right]^2\Big\}.\end{aligned} \tag{3.1.18}$$

where $F_{\mu\nu}$ is the Maxwell tensor for the gauge field, λ_a are a set of 4 Weyl fermions in the adjoint representation of the gauge group, X^i are a set of 6 scalars again in the adjoint representation. D_μ is the gauge coveriant derivative *not* the superderivative $D_{\alpha\dot{\alpha}}$, g is the gauge coupling, σ^μ are the Pauli matrices and C_i^{ab} and θ_I are constants. C_i^{ab} arise from the Clifford Dirac matrices and θ_I is a parameter known as the real instanton angle.

By construction this theory is invariant under supersymmetry and gauge transformations however it is also invariant under scale transformations. In order to see this at the classical level we assign the fields their usual mass dimensions

$$[A_\mu] = \left[X^I\right] = 1 \tag{3.1.19}$$

$$[\lambda_a] = \frac{3}{2}. \tag{3.1.20}$$

Requiring that the Lagrangian has mass dimension 4 then leads us to find that the coupling constants are dimensionless,

$$[g] = [\theta_I] = 0, \tag{3.1.21}$$

which is the definition of a scale invariant theory. When we combine scale invariance and Poincare supersymmetry we get the full superconformal symmetry $SU(2,2|4)$. The

generators of this new symmetry include those we have already met: The Poincare generators $M^{\mu\nu}$ and P^{μ}, the Poincare supersymmetry generators Q^I_α and $\overline{Q}^I_{\dot{\alpha}}$. We also have the additional generators of conformal symmetry:

- $D \equiv -ix_\mu \partial^\mu$, Dilations. These can be thought of as local scale transformations.
- $K_\mu \equiv i(x^2\partial_\mu - 2x_\mu x_\nu \partial^\nu)$, Special Conformal Symmetries. These have a more subtle interpretation as first an inversion, $x^\mu \to \frac{x^\mu}{x^2}$, then a translation, $x^\mu \to x^\mu - b^\mu$, and finally another inversion.

In addition to these we also have the 15 generators of $SU(4)$ R-symmetry T^A and two new superconformal supersymmerties S^I_α and $\overline{S}^I_{\dot{\alpha}}$ which arise from the commutators of the Poincare supersymmetries with the conformal symmetry generators.

It is important to note that this conformal symmetry group is preserved by the loop corrections to the theory.

3.1.4 Motivating Supergravity

In the section above we have considered global or rigid supersymmetry where we act with a constant transformation across the whole of spacetime. Now we will allow spacetime dependent supersymmetry transformations and we will discover that this inevitably leads us to include gravity.

Recall that supersymmetry transformations are generated by the supercharges Q^I_α and $\overline{Q}^I_{\dot{\alpha}}$ which anticommute with themselves and have the cross-anticommutor.

$$\left\{Q^I_\alpha, \overline{Q}^J_{\dot{\beta}}\right\} = 2\sigma^\mu_{\alpha\dot{\beta}} P_\mu \delta^{IJ}. \tag{3.1.22}$$

Since this includes P_μ, the generator of translations, the supersymmetry algebra requires the inclusion of translations in order to be closed. This is not usually a concern, it is very rare that we are interested in a Lorentz violating supersymmetric theory.

When we move to local supersymmetry we find that the anticommutator of two local supersymmetry generators is the generator of diffeomorphisms. This means that in order to have a closed local supersymmetry algebra we necessarily need to make our theory invariant under general diffeomorphisms, i.e. we need to include gravity.

3.1.5 Spinors and Supersymmetry in Higher Dimensions

We will normally be working in higher dimensions when we discuss supergravity, in particular for superstring theory and the AdS/CFT correspondence we will need $d = 10$, let's discuss how we go about working with spinors in higher dimensions. First let us recap where spinors come from.

Origin of Fermions

The Poincare group is not simply connected i.e.

$$U(\Lambda_1)U(\Lambda_2) = e^{i\varphi(\Lambda_1,\Lambda_2)}U(\Lambda_1\Lambda_2) \tag{3.1.23}$$

where $U(\Lambda)$ is the unitary operator corresponding to the Poincare transformation Λ and φ is called the projective phase. This may seem an arcane mathematical point but it can be understood relatively easily by considering the effect of Lorentz transformations. It is intuitive for example that rotations and boosts do not generally commute.

It turns out that the Lorentz group has genus one so it is possible to pick a unitary representation such that $e^{i\varphi(\Lambda_1,\Lambda_2)} = \pm 1$. We can go further and extend the Lorentz group to $SL(2,C) \cong SO(3,1) \times Z_2$ such that the group is doubly covered. Finally we can decompose $SL(2,C) \cong SU(2) \times SU(2)$.

It is possible to categorise the physical states permitted by the Lorentz group by the irreducible representations (irreps) of this group. Note that we are not claiming that the Lorentz group is isomorphic to $SU(2) \times SU(2)$ just that their Lie algebras are the same.

Now irreps of $SU(2)$ are labelled by (half) integers which we shall call m and can be described by vectors $|s\rangle$ given by:

$$|s\rangle = \begin{pmatrix} s_1 \\ \vdots \\ s_{2m+1} \end{pmatrix} \tag{3.1.24}$$

$$C|s\rangle = -m(m+1)|s\rangle. \tag{3.1.25}$$

where C is the $SU(2)$ Casimir operator. Knowing this we label irreps of $SU(2) \times SU(2)$ with tuples (m_1, m_2). Finally by identifying the Casmimir operator of the combined group with the spin operator so that

$$C^2|s,s'\rangle = -(m_1+m_2+1)(m_1+m_2)|s\rangle = S(S+1)|s,s'\rangle. \tag{3.1.26}$$

Where C^2 is the Casimir of $SU(2) \times SU(2)$, $|s,s'\rangle$ is a particular state and S is interpreted as the spin of the particle. Since both m_1 and m_2 are can take either integer or half integer values we can have both fermionic and bosonic representations.

Clifford Algebra and Dirac Spinors

Now that we have shown where spin comes from let's review what spinors are. The simplest possible definition of a Dirac spinor is done in terms of the generators of Lorentz symmetry.

The Lorentz algebra $M_{\mu\nu}$ is made up of both boosts and rotations $J_{\mu\nu}$. The Clifford algebra is defined as:

$$J_{\mu\nu} = \frac{i}{4}\left[\Gamma_\mu, \Gamma_\nu\right] \tag{3.1.27}$$

$$\{\Gamma_\mu, \Gamma_\nu\} = 2\eta_{\mu\nu}. \tag{3.1.28}$$

where Γ are a set of $2^{[d/2]} \times 2^{[d/2]}$ matrices with $[d/2]$ being the integer obtained by rounding down. If the generators $J_{\mu\nu}$ built out of Clifford matrices are to form a representation of the rotation group they need some $2^{[d/2]}$ vectors to act on. These will be our Dirac spinors ψ.

Weyl Spinors

The discussion above is completely agnostic as to the number of dimensions. Here, however, we will discuss some additional structure that only appears in d even. The Dirac spinor can be decomposed into two Weyl spinors. To see this notice that we can construct a chirality matrix

$$\overline{\Gamma} \equiv i^{\frac{1}{2}d(d-1)+1}\Gamma_0\Gamma_1\ldots\Gamma_{d-1} \tag{3.1.29}$$

which anti-commutes with all Γ_μ and therefore commutes with all $J_{\mu\nu}$. This implies that the Clifford algebra is reducible and so the Dirac spinor can be considered the direct product of left and right handed Weyl spinnors

$$S_D = S_+ \oplus S_- \tag{3.1.30}$$

The spacetime dimension determines the reality properties of Weyl spinors:

$$d = 0, 4 (\text{mod } 8): \qquad S_- = S_+^* \tag{3.1.31}$$

$$d = 2, 6 (\text{mod } 8): \qquad S_+ = S_+^* S_- = S_-^*. \tag{3.1.32}$$

An example of Weyl spinors in 4 dimensions are the left and right handed components of the standard model fermions which are differentiated by the weak interaction as discussed in the previous chapter.

Higher Dimensional Supersymmetry

So we now understand the idea of spinors in general dimensions we can start to consider supersymmetry in higher dimensions.

Recall that supersymmetry is generated by spinor supercharges Q_α^I where I runs over the number of supersymmetries $\mathcal{N}$ and α is the spinoral index. Q can be either a Dirac or a Weyl spinor in general however in order to ensure that our discussion is valid for both odd and even dimensions we shall only use Dirac spinors here. We shall also not consider supersymmetry representations with a nonzero central charge since these theories do not permit a massless graviton and we are building towards supergravity.

Now let us put some limits on the viable sumpersymmetry algebras. The anti-commutators for the supercharges are given by

$$\left\{Q_\alpha^I, \left(Q_\beta^J\right)^\dagger\right\} = 2\delta_J^I \left(\Gamma_\mu\right)_\alpha^\beta R^\mu \tag{3.1.33}$$

$$\left\{Q^I_\alpha, Q^J_\beta\right\} = 0. \tag{3.1.34}$$

Now let us consider a massless representation such that $P^\mu = (E, 0, \ldots, 0, E)$. The anti-commutator now becomes

$$\left\{Q^I_\alpha, \left(Q^J_\beta\right)^\dagger\right\} = 2\delta^I_J \begin{pmatrix} 4E & 0 \\ 0 & 0 \end{pmatrix}_{\beta\alpha}, \tag{3.1.35}$$

so half of our supercharges have vanished immediately and we are left only with those with $\alpha \leq \frac{1}{2}\mathrm{dim}S$. We must interpret half of these as raising operators and half as lowering operators, so we have $\frac{1}{4}\mathcal{N}\mathrm{dim}_{\mathbf{R}}S$ raising operators where $\mathrm{dim}_{\mathbf{R}}$ is the number of real dimensions. We have established that spin can only range between -2 and $+2$ so we are only allowed a total of 8 raising operators. This implies that

$$\mathcal{N}\mathrm{dim}_{\mathbf{R}}S \leq 32, \tag{3.1.36}$$

so that there can only ever be a maximum of 32 Poincare supercharges.

For example the largest supergravity theory permitted is $d = 11$, $\mathcal{N} = 1$. In $d = 10$ supergravity, which is of interest to us as the low energy limit of superstring theory, we are allowed $\mathcal{N} = 2$.

3.1.6 Supergravity

Kaluza-Klein Compactification

It is interesting to note that we can obtain a $d = 10$, $\mathcal{N} = 2$ supergravity by Kaluza-Klein compactification of the full $d = 11$, $\mathcal{N} = 1$ theory. Intuition about Kaluza-Klein compactification will also be useful when we consider $\mathrm{AdS}^{4+1}\times\mathrm{S}^5$ spacetime with an internal space so we shall briefly discuss it here.

Consider a spacetime with topology $\mathbb{R}^{d-1} \times S^1$. We will label the extended coordinates as x^μ and the coordinate on the S^1 that we will compactify as y. Kaluza-Klein compactification consists of taking the limit where the radius of the coordinate y goes to zero in order to construct a theory in one fewer dimensions.

To illustrate this process we will discuss a scalar field θ. It is helpful to perform a Fourier series expansion on y

$$\theta(x^\mu, y) = \sum_n \theta_n(x^\mu) e^{\frac{2\pi i n y}{R}}, \tag{3.1.37}$$

where μ runs over the $d-1$ extended dimensions, n runs over the natural numbers, θ_n are the Fourier modes of θ and R is the radius of the y circle. The action for a massive scalar becomes:

$$\int \mathrm{d}^d x\theta \left(-\Box_d + m^2\right)\theta = \sum_n 2\pi R \int \mathrm{d}^{d-1}x\theta_n \left(-\Box_{d-1} + m^2 + \frac{4\pi^2 n^2}{R^2}\right)\theta_n, \tag{3.1.38}$$

where $\Box_d$ is the d dimensional d'Alembertian. So our single scalar of mass m has become

an infinite tower of states with masses $\sqrt{m^2 + \frac{4\pi^2 n^2}{R^2}}$. If we were to take the limit of $R \to 0$ then the masses of all states other than the lightest go to infinity and can be neglected.

Things become more complex for multi component fields. For bosons, which have tensorial indices, we must separate out the y components and treat them separately resulting in a family of fields. For example the Graviton becomes three separate fields:

- $G_{\mu\nu}$ the $d-1$ dimensional metric.
- $G_{\mu y}$ a vector field, referred to as the graviphoton, that transforms under a new $U(1)$ symmetry corresponding to rotations of the S^1 internal space.
- G_{yy} a new scalar that mixes with the dilaton.

A fermion by contrast decomposes into the direct sum of lower dimensional fermions.

$d = 11$ and $d = 10$ Supergravity

The $d = 11$, $\mathcal{N} = 1$ supergravity theory that we introduced above has the following fields:

- A metric $G_{\mu\nu}$, containing 44 bosonic degrees of freedom.
- An antisymmetric rank 3 tensor containing 84 further bosonic degrees of freedom.
- A Majorana gravitino containing 128 fermionic degrees of freedom.

There are two ways to write down a $d = 10$, $\mathcal{N} = 2$ theory, first by compactifying the full $d = 11$ theory on a circle, as described above, to obtain so called type IIA supergravity and a second theory called type IIB which will end up being more relevent for our purposes later. This gives the field content, we shall label the number of degrees of freedom with an integer subscriped by either a B or an F to label bosons and fermions.

- $G_{\mu\nu}$ the 10 dimensional metric, containing 25_B degrees of freedom.
- Φ the dilaton, a scalar with 1_B degree of freedom.
- $B_{\mu\nu}$ an antisymmetric rank 2 tensor with 28_B degrees of freedom
- $A_{3\mu\nu\rho}$ a totally antisymmetric rank 3 tensor carrying 56_B degrees of freedom.
- $A_{1\mu}$ the graviphoton mentioned above carrying 8_B degrees of freedom
- $\psi^{\pm}_{\mu\alpha}$ Majorana-Weyl gravitionos carrying 112_F degrees of freedom.
- $\lambda^{\pm}_{\alpha}$ Majorana-Weyl dilatinos with 16_F degrees of freedom.

This theory preserves chiral symmetry since there are two gravitinos and two dilatinos with opposite chirality, labelled by $\pm$.

The type IIB theory has the content:

- The metric $G_{\mu\nu}$ as before with 35_B degrees of freedom.
- $C + i\Phi$ an axion and dilaton with 2_B.
- $B_{\mu\nu} + iA_{2\mu\nu}$ a rank 2 antisymmetric tensor with 56_B
- $A^+_{4\mu\nu\rho\sigma}$ a rank 4 antisymmetric tensor with 35_B
- $\phi^I_{\mu\alpha}$ gravitinos labeled by $I = 1, 2$ with 112_F.
- λ^I_α dilatinos with 16_F.

This theory, by contrast to type IIA, breaks chiral symmetry since both gravitinos have the same chirality, but opposite to the dilatinos.

It is important to remember that supergravity is still at its heart a gravity theory and so is non-renormalisable [1]. Fortunately we shall only consider classical supergravity in the main body of this work.

3.2 String Theory

String theory has been possibly the most important development in theoretical physics in the last half century. Not just for it's potential to be the correct theory of quantum gravity in nature but also for the "spin off" fields it has created, such as the topic of this thesis, AdS/CFT. In this section we shall briefly introduce string theory and show that certain supergravity theories can be thought of as the low energy limit of certain string theories. This section largely follows [48].

3.2.1 Point Particles and Classical Strings

In order to build up intuition about how we describe strings mathematically let us first consider a relativistic point particle. We will describe this particle with a four vector X^μ which is a function of an affine parameter τ. As we change τ X^μ traces out a path through spacetime that we refer to as a worldline.

The dynamics of a massive particle are captured by the action

$$S = -m \int \mathrm{d}\tau \sqrt{-\dot{X}^\mu \dot{X}^\nu \eta_{\mu\nu}}. \tag{3.2.1}$$

We can rewrite this in terms of an auxiliary field e,

$$S = \frac{1}{2} \int \mathrm{d}\tau \left(e^{-1} \dot{X}^2 - e m^2 \right), \tag{3.2.2}$$

this is equivalent to 3.2.1 for massive particles but has the advantage of also being valid for $m = 0$.

[1] Although there is some speculation that $\mathcal{N} = 8$, $d = 4$ supergravity may be renormalisable. It is known to be finite to 7 loops [47].

Now we can think about how to represent strings in this language. Instead of a $0+1$ dimensional worldline we now have a $1+1$ worldsheet that we parameterise by σ and τ. We will consider closed strings here so $\sigma \in [0, 2\pi)$. We will combine these two coordinates together $\sigma^\alpha = (\tau, \sigma)$ where α runs over 0 and 1. We describe the embedding of the string in spacetime with a set of worldsheet fields $X^\mu(\sigma, \tau)$.

When considered from the spacetime, sometimes called "target space", point of view X^μ is a vector of coordinates however when looked at from the worldsheet it is a set of scalars.

The worldsheet metric can be described by the pull-back of the spacetime metric onto the worldsheet,

$$\gamma_{\alpha\beta} = \frac{\partial X^\mu}{\partial \sigma^\alpha} \frac{\partial X^\nu}{\partial \sigma^\beta} \eta_{\mu\nu}. \tag{3.2.3}$$

The volume element of a spacetime is given by the square root of the determinant of the metric. The dynamics of the string will be given by minimising the area of the string worldsheet so we can write down a string action

$$S = -T \int \mathrm{d}^2\sigma \sqrt{-\mathrm{det}\gamma} \tag{3.2.4}$$

where T is the a constant referred to as the string tension. This can be written in terms of X directly

$$S = -T \int \mathrm{d}^2\sigma \sqrt{-(\dot{X})^2 (X')^2 + (\dot{X} \cdot X')^2} \tag{3.2.5}$$

where $\dot{X} = \frac{\partial X}{\partial \tau}$ and $X' = \frac{\partial X}{\partial \sigma}$. This is refered to as the Nambu-Goto action and has equations of motion:

$$\partial_\alpha (\sqrt{-\mathrm{det}\gamma} \gamma^{\alpha\beta} \partial_\beta X^\mu) = 0. \tag{3.2.6}$$

The square root makes this action somewhat difficult to work with in the same way as our first particle action. Fortunately we can rewrite it by analogy to the second particle action,

$$S = -T \int \mathrm{d}^2\sigma \sqrt{-g} g^{\alpha\beta} \partial_\alpha X^\mu \partial_\beta X^\nu \eta_{\mu\nu} \tag{3.2.7}$$

where we $g^{\alpha\beta}$ is a dynamical worldsheet metric with it's own equations of motion, as opposed to the pull back metric γ and $g = \mathrm{det} g$. It is possible to pick coordintates such that the worldsheet metric is flat giving us the action

$$S = \frac{1}{4\pi\alpha'} \int \mathrm{d}^2\sigma \partial_\alpha X \cdot \partial^\alpha X, \tag{3.2.8}$$

where we have rewritten the tension in terms of the "universal Regge slope" α'. This gets it's name from the original form of string theory as an alternative to QCD. We will see the connection of this parameter to QCD Regge slopes when we quantise the theory shortly.

The equation of motion for X is now, simply,

$$\partial_\alpha \partial^\alpha X^\mu = 0. \tag{3.2.9}$$

The stress energy tensor, $T_{\alpha\beta}$, can be written down as for any scalar,

$$T_{\alpha\beta} = \partial_\alpha X \cdot \partial_\beta X - \frac{1}{2}\eta_{\alpha\beta}\eta^{\rho\sigma}\partial_\rho X \cdot \partial_\sigma X. \tag{3.2.10}$$

It will be helpful to expand the field X in its Fourier modes. First we will move to world-sheet lightcone coordinates $\sigma^\pm = \tau \pm \sigma$ so the equation of motion becomes separable $\partial_+\partial_- X^\mu = 0$ with a general solution made up of left and right handed waves,

$$X^\mu(\sigma^\pm) = X^\mu_L(\sigma^+) + X^\mu_R(\sigma^-). \tag{3.2.11}$$

These can then be expanded in Fourier modes,

$$X^\mu_L(\sigma^+) = \frac{1}{2}x^\mu + \frac{1}{2}\alpha' p^\mu \sigma^+ + i\sqrt{\frac{\alpha'}{2}}\sum_{n\neq 0}\frac{1}{n}\tilde{\alpha}^\mu_n e^{-in\sigma^+}, \tag{3.2.12}$$

$$X^\mu_R(\sigma^-) = \frac{1}{2}x^\mu + \frac{1}{2}\alpha' p^\mu \sigma^- + i\sqrt{\frac{\alpha'}{2}}\sum_{n\neq 0}\frac{1}{n}\alpha^\mu_n e^{-in\sigma^-}, \tag{3.2.13}$$

where α^μ_n and $\tilde{\alpha}^\mu_n$ are the Fourier modes which obey

$$\alpha^\mu_n = \left(\alpha^\mu_{-n}\right)^*, \tag{3.2.14}$$

$$\tilde{\alpha}^\mu_n = \left(\tilde{\alpha}^\mu_{-n}\right)^* \tag{3.2.15}$$

and p^μ is the aggregate momentum of the string state.

3.2.2 Quantisation

Setting our metric to be flat has not used all of our gauge freedom, we still have a Weyl invariance:

$$\eta_{\alpha\beta} \to \Omega^2(\sigma)\eta_{\alpha\beta} \tag{3.2.16}$$

for any local scalar function Ω. We fix this with the "lightcone gauge".

First let us introduce lightcone coordinates for spacetime

$$X^\pm = \sqrt{\frac{1}{2}}(X^0 \pm X^{d-1}), \tag{3.2.17}$$

the remaining $d-2$ coordinates are unchanged and labelled as X^i. We now fix the gauge in such a way that the $+$ components of the two waves are

$$X^+_L = \frac{1}{2}x^+ + \frac{1}{2}\alpha' p^+ \sigma^+, \tag{3.2.18}$$

$$X_R^+ = \frac{1}{2}x^+ + \frac{1}{2}\alpha' p^+ \sigma^-, \tag{3.2.19}$$

or we can combine the two into

$$X^+ = x^+ + \alpha' p^+ \tau \tag{3.2.20}$$

where x^+ is a parameter describing the initial position of the string. So we have eliminated α_n^+. We can also eliminate α_n^- by solving the equation of motion for X^- giving:

$$\alpha_n^- = \sqrt{\frac{1}{2\alpha'}}\frac{1}{p^+}\sum_{m=-\infty}^{+\infty}\sum_{i=1}^{d-2}\alpha_{m-n}^i\alpha_m^i. \tag{3.2.21}$$

So we now know that the physical degrees of freedom are; The overall string position and momentum x and p, and the string modes α_n^i and $\tilde{\alpha}_n^i$. In order to quantise we promote these to operators and equip them with commutation relations:

$$\left[x^i, p^j\right] = i\delta^{ij}, \tag{3.2.22}$$

$$\left[x^+, p^-\right] = -i, \tag{3.2.23}$$

$$\left[x^-, p^+\right] = -i, \tag{3.2.24}$$

$$\left[\alpha_n^i, \alpha_m^j\right] = \left[\tilde{\alpha}_n^i, \tilde{\alpha}_m^j\right] = n\delta^{ij}\delta_{n+m,0}. \tag{3.2.25}$$

We can now define the Hilbert space, starting with a vacuum $|0;p\rangle$ such that

$$p^\mu|0;p\rangle = p^\mu|0;p\rangle, \tag{3.2.26}$$

$$\alpha_n^i|0;p\rangle = \tilde{\alpha}_n^i|0;p\rangle = 0, \tag{3.2.27}$$

for $n > 0$. We then build the excited states by interpreting α_{-n}^i and $\tilde{\alpha}_{-n}^i$ as creation operators.

We want to interpret states in this Hilbert space as physical states and so we need to be able to read off masses. We do this first by defining the number operators

$$N = \sum_{i=1}^{d-2}\alpha_{-n}^i\alpha_n^i, \tag{3.2.28}$$

and

$$\tilde{N} = \sum_{i=1}^{d-2}\tilde{\alpha}_{-n}^i\tilde{\alpha}_n^i, \tag{3.2.29}$$

and noting that the number of left handed and right handed modes must match, $N = \tilde{N}$. We can then write down the mass as

$$M^2 = \frac{4}{\alpha'}(N-a) = \frac{4}{\alpha'}(\tilde{N}-a) \tag{3.2.30}$$

with a a constant arising from the ordering ambiguity. a can be computed by noting that N is the Casimir energy and using either Ramanujan summation or zeta-function regularisation to obtain,

$$a = \frac{d-1}{24}. \tag{3.2.31}$$

3.2.3 Bosonic String Theory

Now we shall consider the masses of the states in our Hilbert space. First the ground state,

$$M^2 = -\frac{1}{\alpha'}\frac{d-2}{6}, \tag{3.2.32}$$

the ground state is a tachyon so we are expanding around an unstable point. Nevertheless we shall press on and write down the first excited state. With the conditon that $\tilde{N} = N$ the next lightest state is a set of $(d-2)^2$ states,

$$\tilde{\alpha}^i_{-1}\alpha^i_{-1}|0;p\rangle, \tag{3.2.33}$$

which has mass

$$M^2 = \frac{4}{\alpha'}\left(1 - \frac{d-1}{24}\right). \tag{3.2.34}$$

There are $(d-2)^2$ degrees of freedom here but each of the operators. α and $\tilde{\alpha}$ transform under the little group $SO(d-2)$. The only way to square these two requirements is for the state to be massless which occurs at the critical dimension of $d = 26$.

Bosonic string theory, then, has a number of limitations:

- It is unstable due to the presence of a tachyon.
- It is only valid in 26 dimensions
- There are no fermions

Fortunately we can mostly fix this by moving to superstring theory.

3.2.4 Superstring Theory

We can make string theory supersymmetric by including a set of Dirac fermions Ψ^M. The Nambu-Goto action then becomes

$$S = -\frac{1}{4\pi\alpha'}\int \mathrm{d}^2\sigma\eta^{\alpha\beta}\left(\partial_\alpha X^M\partial_\beta X^N + i\overline{\Psi}^M\Gamma_\alpha\partial_\beta\Psi^N\right)g_{MN}\left(X\right), \tag{3.2.35}$$

In the worldsheet lightcone gauge, in even dimensions, we can write the Dirac spinor as two Majorana spinors, $\Psi^M = \left(\psi^M_+, \psi^M_-\right)$ and so the fermionic part of the action becomes

$$S_f = \frac{i}{2\pi\alpha'}\int \mathrm{d}^2\sigma\left(\psi^M_-\partial_+\psi_{-M} + \psi^M_+\partial_-\psi_{+M}\right), \tag{3.2.36}$$

$\psi_\pm$ describe left and right moving excitations just like our scalars above. There are two possible ways to fill the boundary conditions. This gives rise to two possible "sectors" of

solutions:

- The Ramond sector $\psi_+^M(\tau,\pi) = +\psi_-^M(\tau,\pi)$.
- The Neveu-Schwarz sector $\psi_+^M(\tau,\pi) = -\psi_-^M(\tau,\pi)$.

We can expand these in Fourier modes similarly to how we handled the bosons. The R sector is expanded as

$$\psi_\pm^M(\tau,\pi) = \frac{1}{\sqrt{2\pi}}\sum_n d_n^M e^{-in\sigma_\pm}, \tag{3.2.37}$$

where n runs over the natural numbers, and the NS

$$\psi_\pm^M(\tau,\pi) = \frac{1}{\sqrt{2\pi}}\sum_r b_r^M e^{-ir\sigma_\pm} \tag{3.2.38}$$

where r runs over the half integers $\mathbb{Z}-\frac{1}{2}$. In the open string case the left and right movers mix and so a state of an open string exists only in one of the two sectors. However in the closed string case the left and right movers are disconnected so they can each, independently, exist in either the NS or R sectors.

There are four consistent superstring theories one can write down[2] [49]:

- Type I: Which has unorientable strings.
- Type IIA: With oriented but chirally symmetric strings.
- Type IIB: With chiral strings.
- Heterotic String theory: This is somewhat stranger with only closed strings and the left movers being bosonic and the right movers being supersymmetric.

If one follows the same quantisation procedure as described above for the bosonic string with the type IIA or IIB theories then take the low energy limit, i.e. throw away all but the zero mass states, we obtain type IIA or IIB supergravity hence the name.

The difference between type IIA and type IIB superstring theory lies in the method used to eliminate tachyons, known as the GSO projection [50]. If we naively write down a superstring theory we will still have a tachyon in the NS sector. The procedure to eliminate these is fairly simple[3]. First we introduce the G-parity operator for the NS sector,

$$G_{NS} = (-1)^{F_{NS}+1} \tag{3.2.39}$$

where F_{NS} is the NS fermion number, and the R sector,

$$G_R = \Gamma_{11}(-1)^{F_R} \tag{3.2.40}$$

[2] There is also a poorly understood 11 dimensional theory called M theory which has 11 dimensional supergravity as it's low energy limit.

[3] This section largely follows the corresponding section in [49]

where F_R is the R fermion number and $\Gamma_{11} = \Gamma_0\Gamma_1...\Gamma_9$ is the 10 dimensional equivalent of the γ_5 matrix. Using Γ_{11} we can define positive and negative chirality Weyl spinors as those that satisfy

$$\Gamma_{11}\psi = \pm\psi \tag{3.2.41}$$

and the chirality projection operator

$$P_\pm = \frac{1}{2}(1 \pm \Gamma_{11}), \tag{3.2.42}$$

just as we are used to in QFT. The GSO projection consists simply of removing all NS states with negative G-parity. This immediately eliminates the tachyon since it is easy to see that

$$G|0\rangle_{NS} = -|0\rangle_{NS}. \tag{3.2.43}$$

The GSO projection may seem a somewhat artificial imposition but it turns out to not only produce a viable theory but also preserve supersymmetry.

Since we have removed half of the NS sector states we must also remove half of the R states in order to have a consistent theory. There are two choices here. Keep the positive G-parity states or keep the negative G-parity states. This leads to two possible theories:

- Left and right moving R sectors have the opposite G-parity. This is type IIA theory.
- Left and right moving R sectors have the same G-parity. Type IIB theory.

In the above we have only discussed closed strings, however open strings can also exist. The analysis for open strings is largely the same as above except that now modes are reflected at the end points so we no longer have separate left and right movers. The subtleties regarding the boundary conditions of these open strings will be discussed in the following section.

3.2.5 D Branes

String theory is an enormously rich topic which could fill many more pages by itself, however we must focus on introducing the concepts necessary for our work. The next of these are D branes.

The dynamics of an open string are described by second order differential equations which permit two kinds of boundary conditions:

- Neumann boundary conditions where the velocity at the end point is fixed.
- Dirichlet boundary conditions where the position at the end point is fixed.

Since we describe the string's location in different dimensions by different scalar fields our strings may have Neumann boundary conditions in some dimensions and Dirichlet boundary conditions in others.

It is helpful to consider what happens to momentum at a string end obeying these boundary conditions. In Neumann boundary conditions waves are reflected and so momentum is conserved. In Dirichlet boundary conditions, by contrast, momentum is not conserved and waves can propagate off the end of the string.

Naively we cannot equip a string with Dirichlet boundary conditions without violating the conservation of momentum, however there is a work around here. We can attach the string to another dynamical object, a Dp brane. This is a $p+1$ dimensional object, the p refers to the number of Dirichlet boundary conditions that a string ending on it has[4].

By analogy to the string we can write down an effective action describing the embedding of a Dp brane in spacetime

$$S_{DBI} = \tau_p \int \mathrm{d}^{p+1}\xi e^{-\phi}\sqrt{-\mathrm{del}\left(P[g]_{ab} + P[B]_{ab} + 2\pi\alpha' F_{ab}\right)}, \tag{3.2.44}$$

where ξ refers to the coordinates on the brane, the constant $\tau_p = (2\pi)^{-p}\alpha'^{-(p+1)/2}$, ϕ is the dilaton, $P[\cdot]$ refers to the pull back of a spacetime field onto the brane, g is the spacetime metric, B is the spacetime antisymmetric tensor and F is the Maxwell tensor for a $U(1)$ gauge field living on the brane.

A full quantum mechanical description of D branes is extremely non-trivial and far beyond the scope of this work. In practice finding classical, static solutions will be sufficient for our work.

Now that we, loosely, understand the behaviour of branes themselves we shall turn on dynamical gravity and consider the effect they have on the surrounding spacetime.

3.3 Holography

Now we shall move on to introduce the most important piece of background for this thesis, the AdS/CFT correspondance which shall be used throughout the bulk of this work.

The gauge/gravity correspondence is a conjectured duality that states that a quantum field theory in d dimensions is dynamically equivalent to a string theory in $d+1$ dimensions [51]. Our model is based upon the most commonly used case of this: the AdS/CFT correspondence.

The AdS/CFT correspondence relates an $N = 4$ super-Yang-Mills theory to type IIB string theory living in an asymptotically anti-de-Sitter spacetime. AdS space has a spacelike boundary and the field theory can be thought of as living on that. This was originally proposed by considering the symmetry group of the spacetime generated by a stack of D3 branes in a certain limit this will be made formal shortly.

We can perform a quick sanity check by comparing the global symmetry group of $N = 4$ SYM to that of $\mathrm{AdS}_5 \times S^5$.

[4] Note that this is not the original path by which D branes were discovered. They were originally found as soliton solutions of supergravity.

First the CFT side: The conformal group is $SO(4,2)$. In addition we have 16 Poincaré supercharges and 16 superconformal supercharges. Together these generate the supergroup $PSU(2,2|4)$ which is the full symmetry group of $N=4$ SYM.

Then the AdS side. The isometry groups of AdS_5 and S^5 are $SO(4,2)$ and $SO(6)$ which coincides with the bosonic subgroup of $PSU(2,2|4)$. Now let us turn our attention to the fermionic part. Type IIB string theory in 10 dimensions has 32 Poincaré supercharges [44]. The presence of the $D3$ branes required to generate the $AdS_5 \times S^5$ spacetime breaks 16 of the Poincaré supercharges but provides an extra 16 superconformal supercharges. So the total global symmetry group is $PSU(2,2|4)$, the same as for $N=4$ SYM.

3.3.1 The Maldacena Limit

The metric for the spacetime generated by a stack of N_c D3 branes is given by [18]

$$\overline{G}_{MN}(x;L)\mathrm{d}x^M\mathrm{d}x^N = \left(1+\frac{L^4}{u^4}\right)^{\frac{1}{2}}\left(\frac{\mathrm{d}u^2}{u^2}+\mathrm{d}\Omega_5^2\right)+\left(1+\frac{L^4}{u^4}\right)^{-\frac{1}{2}}\frac{1}{u^2}\mathrm{d}x^2, \tag{3.3.1}$$

where $u=\frac{1}{z}$ and the brane radius L is given by $L^4=4\pi gN(\alpha')^2$ with α' the string coupling constant. We can substitute this into the nonlinear sigma model for string theory[5] to obtain the action

$$S=\frac{L^2}{4\pi\alpha'}\int \mathrm{d}^{10}x\sqrt{\gamma}\gamma^{mn}\overline{G}_{MN}(x;L)\partial_m X^M\partial_n X^N, \tag{3.3.2}$$

where γ is the worldsheet metric, X^M are the worldsheet scalars describing the string embedding into the target space and lower case m and n run over worldsheet coordinates.

The coupling for this nonlinear sigma model can be read off as

$$\frac{L^2}{4\pi\alpha'}=\sqrt{\frac{\lambda}{4\pi}} \tag{3.3.3}$$

where $\lambda\equiv gN$. The Maldacena limit then consists of taking $\alpha'\to\infty$ while keeping g and N fixed [18]. This implies that when $L\to 0$ The action then becomes

$$S=\sqrt{\frac{\lambda}{4\pi}}\int \mathrm{d}^{10}x\sqrt{\gamma}\gamma^{mn}\overline{G}_{MN}(x;0)\partial_m X^M\partial_n X^N, \tag{3.3.4}$$

and the metric $\overline{G}_{MN}(x;0)$ is now the metric of pure $AdS_5\times S^5$ with unit radius for both parts. The coupling constant α' has been replaced with $\frac{1}{\sqrt{\lambda}}$. We make the identification that $g_{\text{string}}=g^2_{\text{Yang}-\text{Mills}}$. Note that we are still free to take the 't Hooft limit, $N_c\to\infty$ while λ is kept fixed. This results in $g_{\text{string}}\to 0$ while λ can be arbitrarily large.

This is a very important result. In the large N_c limit a field theory on the boundary corresponds to a *weakly coupled* string theory in the bulk.

[5] We will only consider the bosonic part here.

3.3.2 Field Operator Map

The relationship between the two theories can be understood by looking at the partition function for the boundary theory [51, 44],

$$Z = \int \mathrm{D}\left[\phi\right] e^{-i\int \mathrm{d}^d x \mathcal{L}[\phi]} \tag{3.3.5}$$

where ϕ runs over the space of fields in the theory and $\mathcal{L}$ is the Lagrangian for the theory.

The Lagrangian can be thought of as a series of terms which look like sources. For example consider the scalar mass term, $m^2\phi^2$, this looks very much like the kind of source term you would add to the path integral to compute the one point function of ϕ^2, you would differentiate the partition function by m^2 then evaluate it at $m^2 = 0$. We can define a generating functional $W\left[\phi_{(0)}\right]$ by $Z\left[\phi_{(0)}\right] = e^{-W\left[\phi_{(0)}\right]} = \left\langle e^{\int \mathrm{d}^d x \phi_{(0)}(x)\mathcal{O}(x)} \right\rangle$ where $\mathcal{O}$ is the space of operators corresponding to the source fields $\phi_{(0)}$.

The AdS/CFT correspondence can be formulated as a relationship between this generating function and the supergravity action

$$W\left[\phi_0\right] = \mathcal{S}_{\mathrm{SUGRA}}\left[\phi_{(0)}\right]\big|_{\lim_{z\to 0}(\phi(z,x)z^{\Delta-d})=\phi_{(0)}(x)} \tag{3.3.6}$$

where $\mathcal{S}_{\mathrm{SUGRA}}\left[\phi\right]$ is the supergravity action over the bulk fields ϕ, to be distinguished from the boundary source fields $\phi_{(0)}$, z is the AdS radial direction and Δ is the conformal dimension of $\mathcal{O}$ the operator corresponding to the source $\phi_{(0)}$. Essentially every operator in the boundary action has a corresponding field in the bulk theory. For example the bulk graviton $h^{\mu\nu}$ corresponds the the boundary stress energy tensor $T_{\mu\nu}$ and the bulk vector A^μ corresponds to the boundary charge current J_μ.

The AdS radial direction $r = \frac{1}{z}$ corresponds to the renormalisation scale with the center of AdS being the IR and the boundary at the UV.

Strictly speaking we should be working with the full string theory action. However we shall be working in the probe brane limit where we can ignore gravitational back reaction and so we can work only with the massless modes in the SUGRA limit.

3.3.3 BF Bound

There are a great many subtleties when studying field theories in AdS space. Here we will discuss one of the most important: the Breitenlohner-Freedman bound [52].

In flat space it is well known that a theory becomes unstable if it contains fields with $m^2 < 0$ however in AdS$_{d+1}$ this limit is lower, $m^2 < -\frac{d^2}{4}$. To illustrate this we will derive the bound for a scalar field in $d+1$ dimensions.

Our metric takes the form:

$$ds^2 = \frac{1}{z^2}(dz^2 + \eta_{\mu\nu}dx^\mu dx^\nu), \tag{3.3.7}$$

where z is the AdS radial coordinate and $\eta^{\mu\nu}$ is the d dimensional Minkowski metric.

The equation of motion for a scalar field is:

$$(\Box - m^2)\phi(z,x) = 0, \tag{3.3.8}$$

where m is the mass, ϕ is the scalar field and $\Box$ is the Laplacian given by:

$$\Box = \frac{1}{\sqrt{-g}}\partial_a\sqrt{-g}g^{ab}\partial_b, \tag{3.3.9}$$

for some metric g. Plugging in the AdS metric we get the equation of motion.

$$\partial_z^2\phi(z,x) - \frac{d-1}{z}\partial_z\phi(z,x) + z^2\eta^{\mu\nu}\partial_\mu\partial_\nu\phi(z,x) - \frac{m^2}{z^2}\phi(z,x) = 0. \tag{3.3.10}$$

Separating out the x dependence and performing a Fourier transform we obtain

$$\partial_z^2\varphi(z) - \frac{d-1}{z}\partial_z\varphi(z) - k^2\varphi(z) - \frac{m^2}{z^2}\varphi(z) = 0, \tag{3.3.11}$$

we can greatly simplify this through the transformation $\varphi(z) \to z^{\frac{1-d}{x}}\varphi(z)$ giving

$$(-\partial_z^2 + V(z))\varphi(z) = \omega^2\varphi(z), \tag{3.3.12}$$

where ω is temporal component of k and the effective potential V is given by

$$V(z) = \vec{k}^2 + \frac{1}{z^2}\left(m^2 + \frac{d^2-1}{4}\right). \tag{3.3.13}$$

We now have a one dimensional Schroedinger equation defined for positive z with an inverse square potential of strength $\kappa = -m^2 - \frac{d^2-1}{4}$ and energy ω^2. The solutions of this equation are only stable if $\kappa > \frac{1}{4}$ so we can conclude that in order to have a stable solution we need $m^2 > -\frac{d}{4}$. This is the BF bound.

3.3.4 Bulk Radial Coordinate, Boundary Energy Scale and Conformal Scaling

Now let us turn our attention to a specific relationship between a boundary quantity, the renormalisation scale, and a bulk quantity, the radial coordinate, which will be particularly useful in this work.

If we, temporarily, forget about the S^5 internal space of the bulk we can write the metric of AdS_5 as

$$\mathrm{d}s^2 = \frac{\mathrm{d}x^2 + \mathrm{d}z^2}{z^2} \tag{3.3.14}$$

where z is the AdS radial coordinate and x^μ are the coordinates perpendicular to z and, at $z = 0$, correspond to the Cartesian coordinates on the boundary.

Recall that the global symmetry group of AdS_5 is $SO(4,2)$ the same as the four dimensional conformal group. In particular it is important to note that the generator of dilations on the boundary $x^\mu \to \lambda x^\mu$ corresponds to the generator of dilations of the z

coordinate $z \to \lambda z$ [53]. We can therefore make an identification $\mu = \frac{1}{z}$ where μ is the boundary log energy scale.

Now let us consider a bulk scalar $\phi(z, x^\mu)$. The action is

$$S = \int \mathrm{d}z\mathrm{d}x \frac{1}{z^5}(z^2(\partial_z\phi)^2 + z^2(\partial_\mu\phi)^2 - m^2\phi^2). \tag{3.3.15}$$

The equation of motion for this field is[6]

$$\partial_z\left(\frac{1}{z^3}\partial_z\phi\right) + \partial_\mu\left(\frac{1}{z^3}\partial_\mu\phi\right) = \frac{2}{z^5}m^2\phi. \tag{3.3.16}$$

If we only consider radial modes, $\partial^\mu\phi = 0$, as are expected close to the vacuum we get the much simplified equation

$$z^5\partial_z(z^{-3}\partial_z\phi) = m^2\phi \tag{3.3.17}$$

The solution to this equation is a power law $\phi \sim z^\Delta$ with scaling dimension Δ given by

$$m^2 = \Delta(\Delta - 4). \tag{3.3.18}$$

As we discussed above dilations of the AdS radial coordinate z correspond to dilations in the boundary theory. So we can identify Δ as the conformal dimension of the boundary operator $\mathcal{O}$. This is a very important result and similar analysis can produce relations between bulk masses and boundary conformal dimensions for different field/operator pairs. Some examples are shown in 3.3.1.

Type of Field	**Relation between m and Δ**
Scalar	$m^2 = \Delta(\Delta - 4)$
Spin 2	$m^2 = \Delta(\Delta - 4)$
p-form	$m^2 = (\Delta - p)(\Delta + p - d)$
Spin $\frac{1}{2}$	$\lvert m\rvert = \Delta - 2$
Spin $\frac{3}{2}$	$\lvert m\rvert = \Delta - 2$
Rank s symmetric traceless tensor	$m^2 = (\Delta + s - 2)(\Delta - s - 2)$

Figure 3.3.1: A table of the relations between conformal dimensions and mass for different field types.

3.4 Quarks in AdS/QCD

Strongly coupled models are very difficult to make progress in since they cannot be studied perturbatively. Holography allows us to skirt this problem by transforming the task of finding the spectrum and vacuum expectation values in the strongly coupled quantum field theory to a problem of brane embeddings in AdS space in weakly coupled gravity.

[6] We have set the AdS radius to 1 here.

On the QFT side we have a 3+1 dimensional Minkowski space with our QCD-like theory living on it. The gravity side is more complex. We have a stack of N_c massive D3 branes at the origin of the spacetime which generate an AdS space and a stack of N_f D7 probe branes extending in from the AdS boundary. As we shall discuss below, this brane configuration leads to a set of states which match those which appear in QCD.

The D7 branes are included in order to generate the quark fields [54]. Since we are in type IIB string theory open strings are oriented and must end on branes. There are three possible configurations (plus configurations of opposite orientation which are interpreted as antiparticles):

- A string can stretch between the D3 branes and the D7 branes. This state has quantum numbers from two groups, an $SU(N_c)$ corresponding to the connection to the D3 branes, which we interpret as colour charge, and an $SU(N_f)$ from the D7 branes which we interpret as flavour. With this in mind we conclude that this state represents a free quark.
- A string can also have both ends on the D7 branes. In this case it carries flavour and anti-flavour so we interpret this as a meson.
- Finally a string can have both ends on the D3 branes. This state carries colour and anti-colour and so is a gluon.

These configurations are illustrated in 3.4.1.

Note that we do not consider baryons here. There are many techniques to include baryons into AdS/QCD most prominently by introducing bulk spinors or by interpreting baryons as instantons [55] however we will not consider them here. There are also closed strings describing the graviton supermultiplet but since we are in the probe brane limit we will again not discuss them here except to note that they are generating our AdS metric.

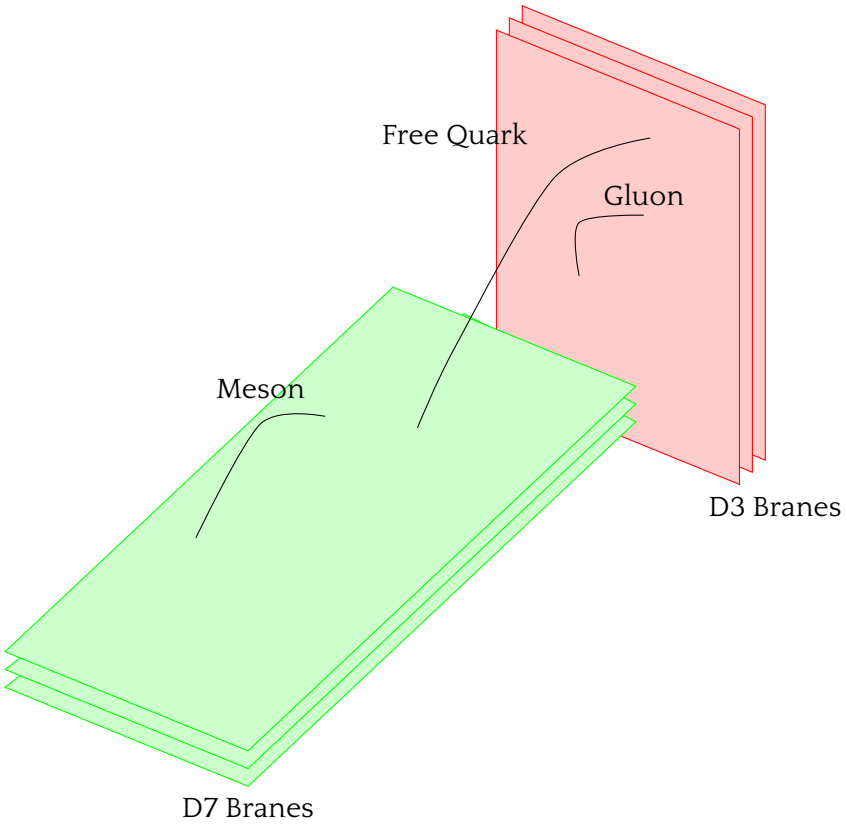

Figure 3.4.1: The different string configurations possible in our system. Strings which end on the D3 branes carry (anti)colour and strings which end on the D7 branes carry (anti)flavour. As a result there are three possible states: free quarks, mesons and gluons.

The result of all this is that we have an $AdS_5 \times S^5$ spacetime. The AdS radius is labelled r and the $3+1$ directions perpendicular to that are labelled by the Cartesian coordinates x^μ since they correspond to the boundary coordinates in the deep UV. We make one change to this coordinate system. We take the AdS radius r and one of the angles that parameterise the internal space S^5, which we will call ϕ, as describing a 2D space by polar coordinates and so re-label them as $\rho = r\cos\phi$ and $L = r\sin\phi$. We do this because, when we express the embeddings of the D7 branes in terms of a function $L(\rho)$, L corresponds to the quark mass at an energy scale related to the parameter ρ. The full metric is given by:

$$ds^2 = r^2 dx^2_{3+1} + \frac{1}{r^2}(d\rho^2 + \rho^2 d\Omega_3^2 + |dX|^2). \tag{3.4.1}$$

Where Ω_3^2 describes rotations in the transverse space of $AdS_5 \times S^5$ and $X = Le^{i\theta}$ is a complex number with magnitude L and exponent, θ, describing rotations into the internal space. For most of this work ρ and L will be the most important coordinates to consider however when we consider the meson spectrum it will be helpful to formulate the system in terms of X.

We can describe the dimensions in which the branes, initially, lie in the following table: Where a ·denotes dimensions in which the branes lie.

	0	1	2	3	4	5	6	7	8	9
D3	·	·	·	·						
D7	·	·	·	·	·	·	·	·		

The exact embedding of the D7 branes is found by pulling back the AdS metric onto the branes and writing L as a function of ρ. We can then plug this into the DBI action:

$$S_{D7} = -T_7 \int d^8\xi e^{\phi} \sqrt{-\det(G_{ab} + F_{ab})}. \tag{3.4.2}$$

where ξ runs over the surface of the brane, G_{ab} is the induced metric on the brane and F_{ab} is a gauge field.

The dilaton factor ϕ is constant in pure AdS.

3.5 Dynamic AdS/QCD

Now that we have the language needed to describe QCD holograpically we will introduce the specific AdS/QCD model that will be the primary topic of this thesis, dynamic AdS/QCD.

After we substitute our pulled back metric and expand in small L we can obtain an action for the 5D theory. We will not, however, use a theory obtained as the formal low energy limit of a string theory. Instead we write down a phenomenological theory inspired by this technique that provides a sensible boundary theory.

The normal procedure for introducing mass, and breaking conformal invariance, to a holographic model is to introduce a bulk dilation to provide an energy scale. The action for this looks like

$$S = \int \mathrm{d}\rho e^{\phi} \rho^3 \sqrt{1 + L'^2}, \tag{3.5.1}$$

with a dilation e^{ϕ}. We can imagine a range of theories with an effective external dilaton who's form can be chosen to get the behaviour we desire. For example by including a magnetic field B associated with the $U(1)$ baryon number [**?**]

$$e^{\phi} = \left(1 + \frac{B^2}{(\rho^2 + L^2)^2}\right)^{\frac{3}{2}}. \tag{3.5.2}$$

In our case we will artificially insert a field $\lambda = e^{\phi}$ which couples to the D7 branes in the usual way.

The action for the D7 branes can now be written as

$$S_{D7} = -T \int \mathrm{d}\rho \rho^3 \lambda(r) \sqrt{1 + (\partial_\rho L)^2}. \tag{3.5.3}$$

We then expand this in terms of small L to get

$$S = \int \mathrm{d}\rho \left(\frac{1}{2}\, \lambda(r)|_{L=0}\, \rho^3 L'^2 + \rho^3 \frac{\mathrm{d}\lambda}{\mathrm{d}L^2}\bigg|_{L=0} L^2 \right). \tag{3.5.4}$$

We can then make a coordinate transformation

$$\lambda(\rho)\rho^3 \frac{\mathrm{d}}{\mathrm{d}\rho} = \tilde{\rho}^3 \frac{\mathrm{d}}{\mathrm{d}\tilde{\rho}} \tag{3.5.5}$$

$$\tilde{\rho} = \sqrt{\frac{1}{2} \frac{1}{\int_{\rho_0}^{\infty} \rho \frac{\mathrm{d}\rho'}{\lambda \rho'^3}}}, \tag{3.5.6}$$

to simplify to

$$S = \int \mathrm{d}\tilde{\rho} \frac{1}{2} \left(\tilde{\rho}^5 \phi'^2 - 3\tilde{\rho}^3 \phi^2 \right) + \frac{1}{2} \lambda \frac{\rho^5}{\tilde{\rho}} \frac{\mathrm{d}\lambda}{\mathrm{d}\rho} \phi^2. \tag{3.5.7}$$

This is just the action of a scalar in AdS with $m^2 = -3$ plus an additional λ dependent correction.

Our goal is to describe QCD like theories so we will re-label $\Delta m^2 = \frac{\mathrm{d}\lambda}{\mathrm{d}L}$ in order to encode the QCD running. We can now write down our dynamic AdS/QCD action

$$S = -\int d^4x d\rho \mathrm{Tr} \rho^3 \left[\frac{1}{r^2} |DX|^2 + \frac{\Delta m^2(r)}{\rho^2} |X|^2 + \frac{1}{2\kappa^2} (F_V^2 + F_A^2) \right], \tag{3.5.8}$$

where F_V and F_A are the Maxwell tensors for vector and axial gauge fields, D is the gauge covariant derivative for $SU(N_c)$ with minimal coupling.

There are a number of subtleties here that should be explained before we move on:

- This action is to leading order in X and as such the two factors of r should naively be replaced by ρ. However this may prevent us from finding stable solutions for the embedding if this term causes us to cross the BF bound. This may be understood by remembering that, in our coordinate system, the mass of a, boundary, bare quark is given by the position of the D7 brane in the L coordinate. In this language the BF bound is framed as a surface $L = \rho$ below which the brane does not pass. If we use L instead of r then for small ρ we risk "tripping" over the BF bound and the theory becoming unstable.

- We have artificially inserted the axial gauge field symmetrically with the vector field. If we were to formally take the low energy limit of the string theory there would be a more complex set of terms describing this state.

- Supersymmetry has been broken through the introduction of a parameter κ which we will fit phenomenologically.

There are two free objects in our theory: the coupling κ and the function $\Delta m^2(r)$. κ will map to a coupling in the boundary theory so we will ignore that for now. For Δm^2 we

need to choose a functional form. We choose the two loop beta function discussed in 2.1.2 with the identification:

$$\Delta m^2 = -2\gamma = -\frac{3(N_c^2-1)}{2N_c\pi}\alpha. \tag{3.5.9}$$

We now have all the technology in place to begin calculating the embeddings of our probe branes. We are working in the probe brane limit so we will forget about all the other fields and simply write down the equation of motion for L

$$\partial_\rho(\rho^3\partial_\rho L) - \rho\Delta m^2 L = 0. \tag{3.5.10}$$

The boundary conditions are obtained from the requirements that $L(\Lambda_{\rm UV}) = m_{\rm UV} + \frac{c}{\Lambda^2_{\rm UV}}$ so that the brane is orthogonal to the boundary where they meet in the UV, this is a requirement to ensure regular solutions. The other condition is that in the IR $L(r_{\rm min}) = r_{\rm min}$ and $L'(r_{\rm min}) = 0$ to enforce the BF bound for the quarks.

3.5.1 Calculations in Dynamic AdS/QCD

Once we have the embedding we can then calculate a number of other useful results. In the UV the embedding takes the form

$$L(\rho) = m_{\rm UV} + \frac{c}{\rho^2} \tag{3.5.11}$$

with $m_{\rm UV}$, the UV quark mass, and c, the $q\bar{q}$ condensate, as constants. We can easily obtain these by fitting to the form of our embedding.

In AdS/QCD models the attractive force between a quark and an antiquark can be understood by interpreting the two quarks on the boundary as the end points of a string that extends into the bulk. The energy of the bound state is related to the length of the string. Due to the warped metric of AdS space the string length is actually reduced if the string can extend further into the bulk. Because of this configurations have less energy the greater the separation. Obviously this does not exhibit confinement. In order to solve this a "wall" is normally introduced in the AdS spacetime preventing the string from extending beyond a certain distance into the bulk. This means that, once the string has reached the wall, the string length increases linearly with the separation and confinement occurs. The wall can either be a "hard wall" where there is a sudden stoppage of the spacetime or a "soft wall" where the spacetime closes off smoothly. We do not explicitly probe the far IR in our theory to check that confinement exists however it is reasonable to expect that we see a hard wall since the theory becomes pure glue below the quark mass $\rho = m_{IR}$ and it is known that the gauge coupling of a pure glue theory goes to infinity in the IR, thus providing a hard wall.

The masses and decay constants of the quark bound states can be found by putting scalar, vector and axial vector fields on the branes. By solving the Schrödinger equations

for these fields we find a tower of states for these with quantised masses corresponding to the higher excited states of mesons. We record the lowest masses here as the mass of the state in question. The decay constants can be found by substituting these solutions back into the action and coupling to external massless fields. These procedures were laid out in [56].

For the scalar we first write down an equation of motion for small excitations around the vacuum embedding, δ,

$$\partial_\rho\left(\rho^3\delta'\right) - \Delta m^2\rho\delta - \left(\rho L_0\delta\frac{\partial\Delta m^2}{\partial L}\right)\Big|_{L_0} + M^2\frac{\rho^3}{\left(L_0^2+\rho^2\right)^2}\delta = 0 \tag{3.5.12}$$

where M is the mass of the excitation, analogous to the energy in a Schrödinger equation. We look for solutions where $\delta(\Lambda_{\rm UV}) = 0$. There is a tower of modes of increasing M. We associate these solutions with the excited meson states.

The scalar decay constant f_S is calculated by substituting into the action with an external scalar to obtain the formula

$$f_S^2 = \int \mathrm{d}\rho\partial_\rho(-\rho^3\partial_\rho\delta)K_S(q^2=0) \tag{3.5.13}$$

where $K_S(q^2=0)$ is an external scalar (equivalent to the solution to the scalar equation of motion with $M = 0$ and boundary conditions such that it is finite at the boundary rather than at the closing of point of the $D7$ branes.

A similar process is used to calculate the vector and axial vector masses and decay constants. The equation of motion for the vector is

$$\partial_\rho\left(\rho^3\partial_\rho V\right) + \frac{\rho^3M^3}{(L_0^2+\rho^2)^2}V = 0 \tag{3.5.14}$$

where once again M is the mass of the state. We can then calculate the decay constant by substituting back into the action to derive the formula

$$f_V^2 = \int \mathrm{d}\rho\partial_\rho\left(-\rho^3\partial_\rho V\right)K_V(q^2=0) \tag{3.5.15}$$

where the external vector, $K_V(q^2=0)$, is the massless solution to the equation of motion above with a finite value in the UV. The axial vector equation of motion has a additional term

$$\partial_\rho\left(\rho^3\partial_\rho A\right) - \kappa^2\frac{L_0^2\rho^3}{(L_0^2+\rho^2)^2}A + \frac{\rho^3M^3}{(L_0^2+\rho^2)^2}A = 0 \tag{3.5.16}$$

however the formula for the decay constant f_A is the same as that for the vector with A substituted for V.

In addition we can calculate the pion decay constant f_π with the formula

$$f_\pi^2 = \int \mathrm{d}\rho \frac{1}{\kappa^2} \left[\rho^3 \partial_\rho K_A(q^2=0)\right] K_A(q^2=0). \tag{3.5.17}$$

3.5.2 NJL Interactions in Dynamic AdS/QCD

In order to include four fermion interactions we will return to the boundary theory for the moment. We can add an NJL term $\frac{g^2}{\Lambda^2}\overline{q_L}q_R\overline{q_R}q_L$ to the boundary action.

As discussed in 2.2 this introduces a dynamically generated mass for the quarks. When we have a $\langle\bar{q}q\rangle = c$ condensate we gain an effective mass term

$$m^2\bar{q}q, \tag{3.5.18}$$

where we identify

$$m = \frac{g^2 c}{\Lambda^2}. \tag{3.5.19}$$

To leading order we can approximate the NJL term as $\frac{m^2\Lambda^2}{g^2}$ [56]. We can see how to include this in a holographic model through Witten's proscription [57]. First we vary the action

$$\delta S = 0 = -\int \mathrm{d}\rho \left(\partial_\rho \frac{\partial \mathcal{L}}{\partial L'} - \frac{\partial \mathcal{L}}{\partial L}\right)\delta L + \frac{\partial \mathcal{L}}{\partial L'}\delta L\Big|_{UV,IR}. \tag{3.5.20}$$

Normally we would fix the mass at the UV and IR but instead here we will allow L to vary at the boundary and replace this constraint with a new one

$$0 = \frac{\partial \mathcal{L}}{\partial L'}\Big|_{\Lambda_{UV}} + \frac{2L(\Lambda_{UV})\Lambda_{UV}^2}{g^2}. \tag{3.5.21}$$

So the effect of including the NJL term is to shift the action by a surface term

$$S_{\mathrm{NJL}} = S_{\mathrm{DynamicAdS/QCD}} + \frac{L^2\rho^2}{g^2}\Big|_{\Lambda_{UV}} \tag{3.5.22}$$

This has no effect on the equations of motion but gives us an additional constraint on the asymptotic form of the solutions. As discussed above in the UV

$$L(\rho) = m + \frac{c}{\rho^2}. \tag{3.5.23}$$

So we now simply impose 3.5.19 as a condition on m and c.

Chapter 4

A Holographic Study of the Gauged NJL Model

4.1 Introduction

In this chapter we shall apply the dynamic AdS/QCD model described above to the observed QCD meson spectrum. In particular we shall study the model both with and without the inclusion of the NJL term.

Recall the foundations of the Dynamic AdS/QCD model. We have a $D7$ probe brane in a large N $D3$ brane background. The $D3$ branes are treated as fixed and we allow the $D7$ branes to relax to the, static, configuration which minimises their free energy. The $D7$ brane embeddings are given by

$$\partial_\rho \left[\rho^3 \partial_\rho L\right] - \rho \Delta m^2 L = 0 \tag{4.1.1}$$

where Δm^2 is a function that is chosen to encode the two loop QCD running which we have inserted by hand.

We can solve this differential equation numerically with the boundary conditions $L(m_{IR}) = m_{IR}$ to preserve the BF bound, and $L'(m_{IR}) = 0$, to ensure the brane closes off smoothly. Examples of these solutions are shown in 4.1.1.

The spectrum of the theory is then determined by looking at linearized fluctuations of the fields about the vacuum where fields generically take the form $f(\rho)e^{ip\cdot x}, p^2 = -M^2$. A Sturm-Louville equation results for $f(\rho)$ leading to a discrete spectrum. By substituting the wave functions back into the action and integrating over ρ the decay constants can also be determined. The normalizations of the fluctuations are determined by matching to the gauge theory expectations for the VV, AA and SS correlators in the UV limit of the theory. This full procedure is described in detail in [56].

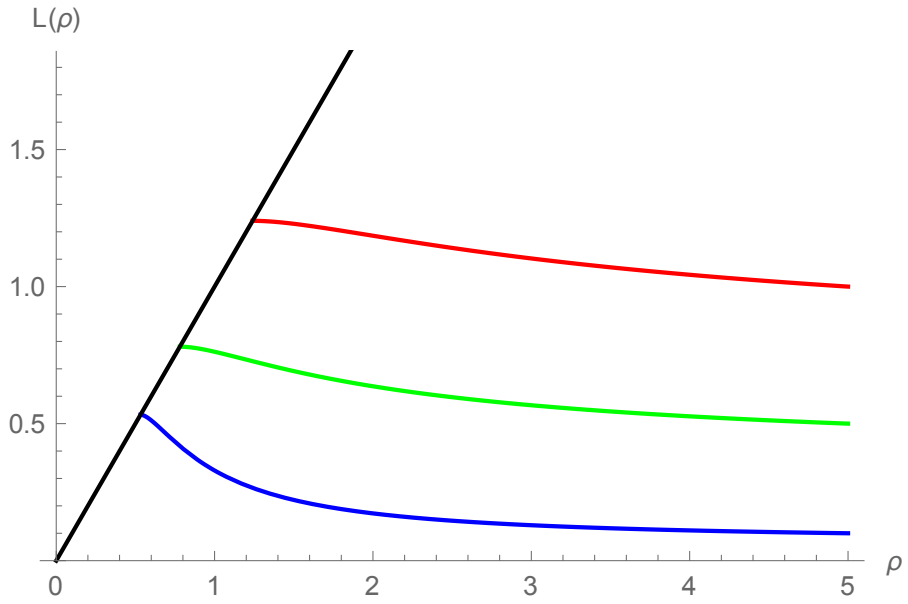

Figure 4.1.1: The embeddings for different IR choice L_0. Here the scale is set by the value of $\rho = m_{IR}$ at which the BF bound is violated (an approximation to Λ_{QCD} being set to 1).

4.2 QCD Spectrum

Now let us compare the results from our theory to QCD. With N_c and N_f fixed the free parameters in the theory are the overall scale which we shall fix by fixing m_{IR}, the UV quark mass and the 5d coupling κ. For example one can fix m_{IR} by scaling to give the correct m_ρ; the remaining parameters can then be fitted to the data. We choose to minimize the maximum deviation $|\delta O|/O$ in any observable O and find a good fit at $m_{UV} = 0.05 m_{IR}$ at a UV scale of $5m_{IR}$ and $\kappa = 76$:

	Model	QCD
m_ρ	775 MeV	775 MeV
m_{a_1}	1467 MeV	1230 MeV
m_σ	981 MeV	500 MeV & 980 MeV
F_ρ	311 MeV	345 MeV
F_{a_1}	390 MeV	433 MeV
f_π	77 MeV	92 MeV

All the mesonic variables lie within 20% of the experimental centrepoints shown except for the σ meson mass that lies very close to the first excited $f_0(980)$ state. The lighter $f_0(500)$ is thought to potentially be a mesonic molecule [58] which might explain the discrepancy. In anycase our model provides a sufficiently close spectrum match to begin an analysis of NJL dynamics in the model.

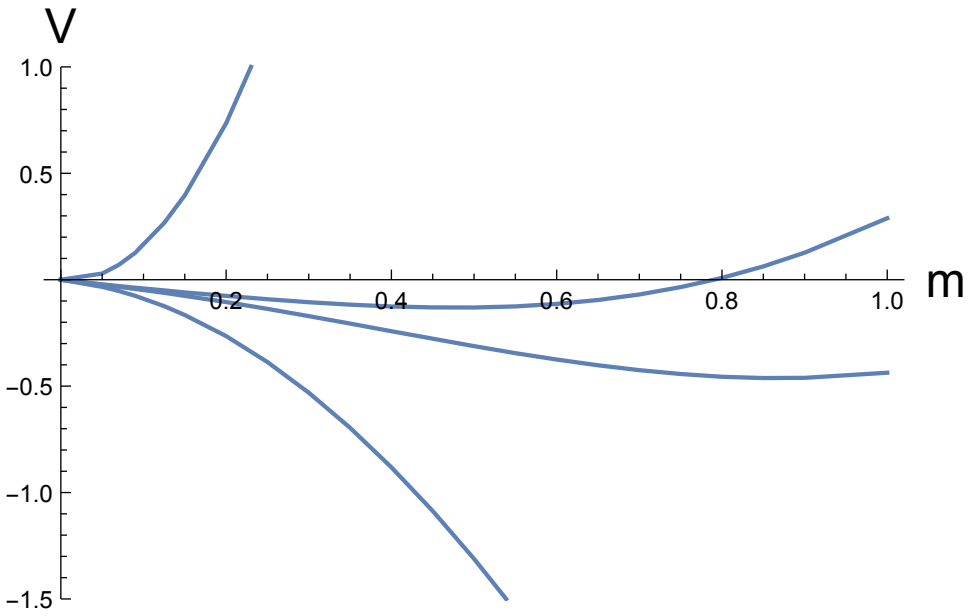

Figure 4.2.1: Plots of the potential against the UV quark mass: the lower curve is that of the underlying gauge theory without an NJL term and is unbounded. Moving up we have added the term $\Lambda^2 m^2/g^2$ with $g = 2.5, 2.3, 1$ from bottom to top. The addition of an NJL term generates a minimum of the potential that tracks to $m = 0$ at $g = 0$. All dimensionful objects are expressed in terms of m_{IR}.

4.3 Results for the Gauged NJL Model

Now let us turn on the quartic fermion interaction term. The effect of this on the quark masses can be seen in Figure 4.2.1. The minimum of the potential moves away from $m = 0$. How this impacts the meson spectrum will be explored in this section.

We can now study the mesonic variables of our holographic model in the presence of an NJL interaction. In Fig 4.2.2 and Fig 4.3.1 we display respectively the meson masses $(m_\rho, m_{a_1}, m_\sigma)$ and the decay constants (F_ρ, F_{a_1}, f_π) of the SU(3) gauge theory with $N_f = 2$. When the NJL coupling $g = 0$ the model generates the output of the table above and corresponds to our description of QCD. Results are shown in the figures for cut offs $\Lambda = 10, 15, 20, 50 m_{IR}$. As g grows at the cut off the NJL interaction enhances the mass gap of the theory. At larger g the NJL interaction dominates and generates a much larger gap that sharply grows to the cut off scale. This clearly shows the anticipated cross over behaviour. As the cut off is taken large relative to Λ_{QCD} the transition from constant to rapidly growing behaviour as a function of g becomes sharper and moves closer to the second order NJL only behaviour. The holographic model reproduces the expected physics well. Interestingly there is a small dip in the sigma meson mass before the NJL interaction dominates although it is not a large effect. In Fig 4.3.2 we show the full set of observables, normalized by their value at $g = 0$, against g for two different Λ to stress the sharpening of the transition with growing cut off and show the relative growth of the observables.

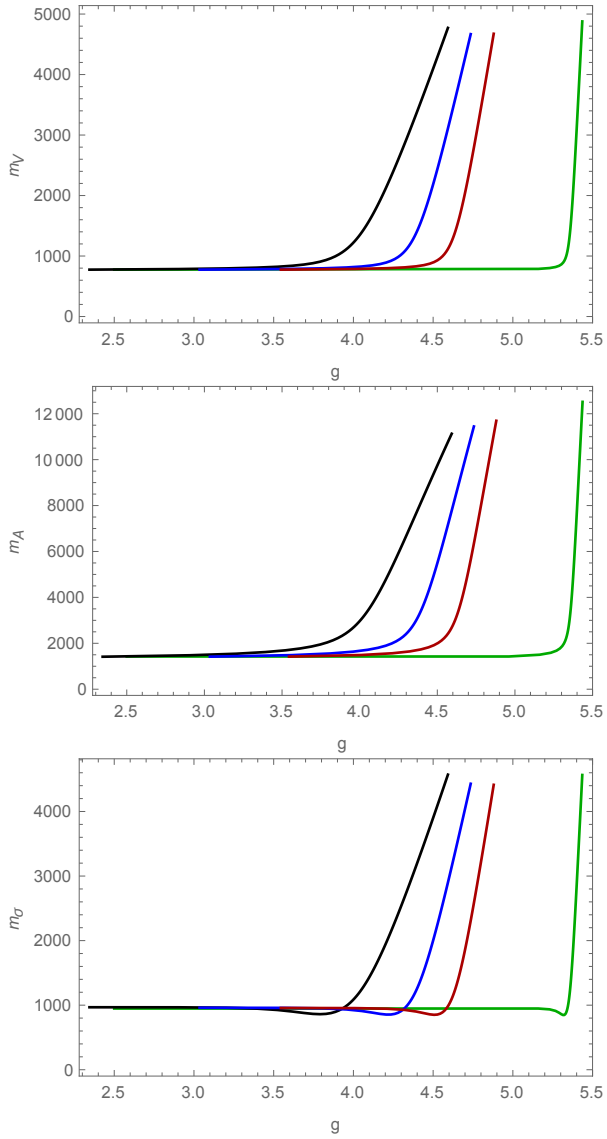

Figure 4.2.2: Plots showing the vector and axial vector meson (ρ and a_1) and σ meson (f_0) masses against the NJL coupling constant g for choices of UV cut off $\Lambda = 10, 15, 20, 50 m_{IR}$.

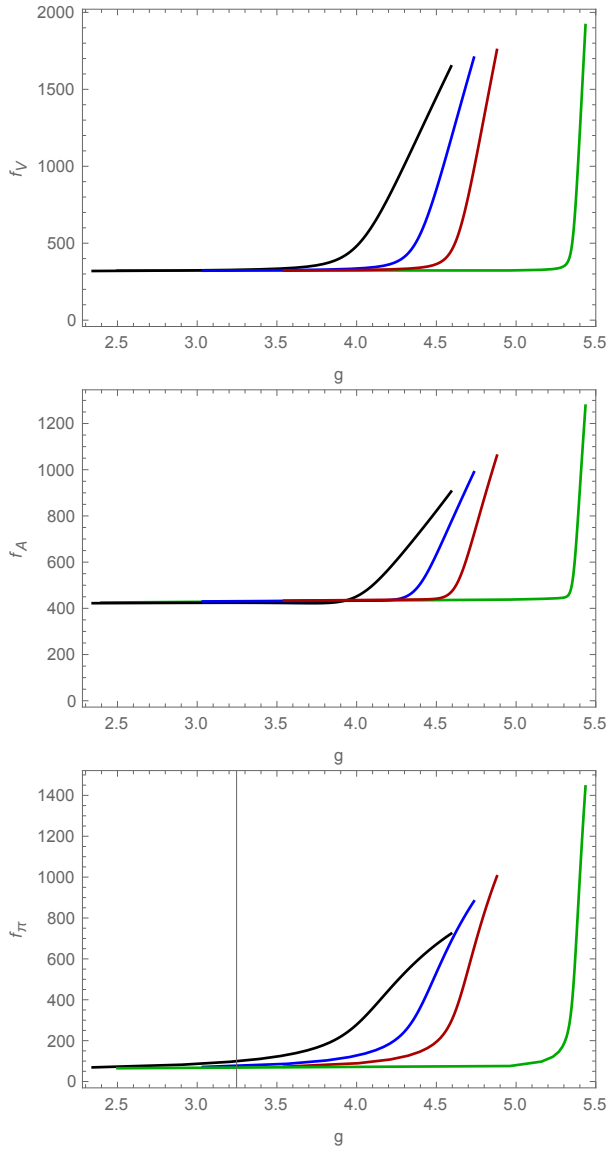

Figure 4.3.1: Plot showing the vector and axial vector meson and π meson decay constants against the NJL coupling constant g for choices of UV cut off $\Lambda = 10, 15, 20, 50 m_{IR}$.

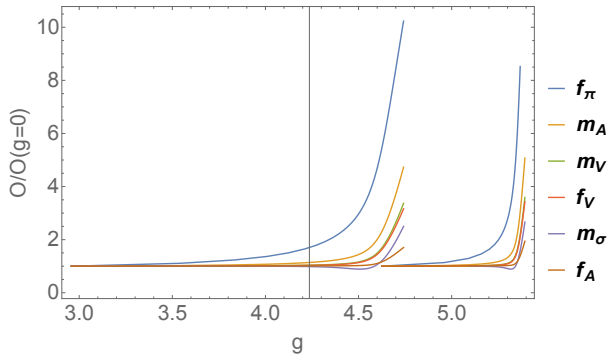

Figure 4.3.2: Plots showing the full set of observables against NJL coupling g for $\Lambda = 20$ and $50m_{IR}$.

The success in finding a holographic description of the gauged NJL model opens up the possibility of doing a range of beyond the standard model physics including extended techniolour [59] and top condensation [60] interactions. We explore this more thoroughly in the next chapter.

Chapter 5

Holograms of a Dynamical Top Quark

Now that we have a robust model of holographic QCD we will turn our attention to an application. Technicolour [61, 62, 60, 41] remains an appealing paradigm for breaking electroweak symmetry since it mirrors the symmetry breaking mechansim in QCD and superconductors. It has long faced a variety of attacks from flavour changing neutral current data [63, 64], precision electroweak data [65] and now the discovery of a very fundamental looking higgs state [66, 67]. There still perhaps seems a small hope that these issues can be dodged by suitable tuning in the parameter space of the collection of strongly coupled gauge theories. In particular walking theories [68], in which there is a large anomalous dimension for the quark bilinear over a large energy range, might raise the flavour scale, lower the electroweak S parameter [69], and even generate a light technidilaton type state [70, 71, 72, 73, 74, 75].

The discovery of the top quark 23 years ago [76] with its very large mass presented the toughest challenge. If one naively uses extended technicolour (ETC) [63, 64] interactions to generate the top mass then one expects

$$m_t \simeq \frac{g^2\langle\bar{Q}Q\rangle}{\Lambda^2} \simeq \frac{g^2(4\pi v^3)}{\Lambda^2} \tag{5.0.1}$$

where Q are techni-quark fields, v is the electroweak scale and Λ the mass scale of the new interactions generating the top mass.

Throughout this chapter we shall refer to three parameters of the electroweak interaction:

- $\delta\rho$ is the mass splitting between the two states in an isospin doublet [77].
- S is one of the Peskin–Takeuchi parameters [78]. Is the difference in the number of left and right handed fermions which carry isospin.
- T is another of the Peskin–Takeuchi which parametrises the contribution of new physics to the radiative corrections to electroweak diagrams.

Naturally, with the ETC coupling $g \simeq 1$, Λ should be at or below the 1 TeV scale. When one tried to include the isospin violating physics neeeded to generate the top bottom mass splitting at such a low scale deviations in the electroweak precision $\delta\rho$ or T parameter were of order 100 rather than 0.1 [79, 80]! This issue is so confounding that most more recent work on technicolour has concentrated on the core electroweak breaking dynamics and put aside completely the flavour generation mechanism - the top remains the elephant in the room!

Two possible resolutions of the top problem have been suggested. The first is that walking dynamics might enhance the techni-quark condensate and raise Λ. Twenty years ago gap equation [81, 82, 83, 84] and Pagel Stokar type formulae [85] were the state of the art for addressing this issue but it was hard to generate a sufficient rise in the tail of the techni-quark self energy to raise Λ sufficiantly [79, 80, 83]. The second idea was essentially top condensation [86, 87, 88, 59]; additional strong interactions of the top at high scale generated NJL operators that by themselves generated a top condensate and the top mass independently of the technicolour sector which still performed the majority of the work of breaking electroweak symmetry. A mix of these ideas and the possibility that the ETC interactions were also strongly interacting seemed possible but it was hard to construct a computational framework that seemed in anyway reliable.

Holography is particularly well suited to the study of walking dynamics because the running anomalous dimension is the key input. The expected increase in the quark condensate and a light higgs-like σ have been observed in the model in the walking regime [56] (the lightness of this state has been disputed in the alternative holographic model of [89, 90] where deep IR conformal symmetry breaking raises the state's mass but other states seem to behave similarly in the different models). One can hope as one moves towards theories with walking behaviour the model will continue to make sensible predictions of the spectrum.

We will present a hologram of a top condensation model. We show the critical behaviour for chiral symmetry breaking and the fine tuning needed to achieve $m_t \ll \Lambda$. Holography should be trusted where strong interactions are dominating the dynamics. In top condensation the NJL operator is strong in a regime where all other interactions are weak and the holographic description of the quarks is less secure. AdS/QCD models pass muster in the weakly coupled regime because they contain a memory of N=4 SYM theory which, like the perturbative gauge theory, is near conformal and protects the anomalous dimensions of the operators considered to their perturbative values. In fact the memory of supersymmetry means that the effective potential is flat with quark mass in the absence of running in our holographic model - the expected fermion loop contributions to the effective potential are absent (they have cancelled aginst the squark contribution in the origin theory). When running is introduced by the mechanism described in 3.5, supersymmetry is broken and an effective potential that falls to large quark mass develops allowing the behaviour we have described. The effective potential

is dominated by "cracked egg" diagrams where gluons are exchanged across the fermion loop. Given this distinction from the basic NJL description of top condensation one does not realize exactly the same critical coupling but all the characteristic behaviours are present. There is also a phenomenological parameter, κ (a 5d gauge coupling) which is unfixed in the model and determines f_π for a given m_t - for order one values of κ the top mass can not generate sufficient f_π to explain the electroweak symmetry breaking vev as one expects.

Our second model is a one electroweak doublet extended technicolour model. Dynamic AdS/QCD allows us to study an SU(N_{TC}) gauge group with varying number of flavours, N_f. Our input in each case is the running anomalous dimension of the quark bilinear, γ, taken from the two loop perturbative running of the technicolour coupling α_{TC}. The IR fixed point in this approximation crosses through the point $\gamma = 1$ where chiral symmetry breaking is triggered for $N_f \simeq 4N_c$ (the "edge" of the conformal window [91]). In the gravity dual this transition corresponds to where the BF bound is violated in the IR by the running mass of the scalar dual to the quark condensate. We will study the $N_{TC} = 3$ case and vary N_f. At higher N_{TC} one can sample very similar running profiles with less discrete jumps but the $N_{TC} = 3$ case suffices to show the main features. For higher N_{TC} similar examples can be found by appropriate choices of N_f.

Here we assume extra techni-quarks beyond the single electroweak doublet (contributing $N_f = 2$) are electroweak singlets which allows us to impose walking behaviours for the running on a minimal electroweak sector. These models are perhaps most likely to be compatible with the electroweak S parameter [65]. The S parameter essentially counts electroweak doublets and perturbatively a doublet contributes $1/6\pi \simeq 0.05$ to be compared with an experimental upper limit of 0.3. QCD-like strong dynamics are known to increase this contribution by a factor of 2 or more so with $N_{TC} = 3$ copies of a single doublet the bound is close to saturation. It is possible walking dynamics alleviates this isssue [69]. This drop in S as one approaches the edge of the conformal window can be modelled in the Dynamic AdS/QCD model by allowing the parameter κ of the model to fall to zero as $N_f \to 4N_c$ [56]. The contribution to S in Dynamic AdS/QCD can be found in Fig 10 of [56] - we will not address this issue further here. The need for a low S motivates our restriction to $N_{TC} = 3$ also though.

In this model, since technicolour is strong (even out to the ETC scale in the walking cases), the cracked egg diagram domination of the effective potential is more appropriate and the holographic description of the NJL interaction hopefully sensible. We put in the four fermion operators of a classic ETC unification to generate the top mass - they link the top to the tecnhi-U quark but not the techni-D quark. We begin by finding solutions for the NJL and TC couplings that generate some given top mass whilst correctly generating the electroweak scale $f_\pi = 246$ GeV. Generically there are two solutions. One matches to the usual weakly coupled ETC regime - for low top masses the technicolour dynamics dominates electroweak symmetry breaking and the ETC coupling is small. A second set

of solutions exist though in which technicolour plays a sub-dominant role to the ETC interactions which generate most of f_π by being super-critical and generating masses that strongly break isospin in the technidoublet. These latter solutions are strongly ruled out by the $\delta\rho/T$ parameter so we do not explore them in much detail. The more normal solutions can be followed to larger top masses where the NJL interaction is strong. We find there is a maximum top mass (here the two branches of solutions merge) that is compatible with the electroweak scale which is a little above 500 GeV for a QCD-like, low N_f model. For models with larger N_f the enhancement of the techniquark condensate by walking allows a given top mass to be generated with a weaker ETC coupling and significantly larger m_t can be achieved. These results confirm the ability to compute with both walking and strong NJL interactions present.

We then concentrate on models with $m_t = 175$ GeV. We track the growing strength of the NJL coupling with rising ETC scale. Walking's enhancement of the condensate allows solutions at lower ETC coupling for a given ETC scale. Phenomenologically the key question is whether these solutions are compatible with the tight $\delta\rho$ parameter constraint (it must be less than 0.4%). There are two contributions to $\delta\rho$ [79, 80]. The first is a direct contribution in which a single ETC gauge boson is exchanged across a techniquark loop contributing to the W and Z masses. The contribution to $\delta\rho$ is expected to be

$$\delta\rho = \frac{g^2 v^4}{\Lambda^2} \tag{5.0.2}$$

where here g also includes any group theory factors from the ETC model. This bound can be evaded by pushing the ETC mass scale up above 3 TeV or so although it is easier to avoid in walking (large N_f) models where the ETC interactions can be smaller. A second contribution is harder to avoid though [83]. The isospin breaking ETC interactions tend to generate mass splitting between the techni-U and techni-D quarks. This mass splitting gives $\delta\rho$ contributions. For a perturbative doublet, with N_{TC} degeneracy, this mass splitting gives

$$\delta\rho = 0.4\% N_{TC} \left(\frac{\Delta m^2}{(175 GeV)^2} \right) \tag{5.0.3}$$

The holographic model allows us to plot the self energy function of the quarks against RG scale. We find typical mass splittings between 20 and a few 100 GeV. Interestingly extreme walking models generate the largest IR mass splitting. When the technicolour interactions are strong at the ETC scale the dynamics are much more sensitive to the high scale NJL isospin violation. Models with N_f between 3 and 8 are compatible with both the $\delta\rho$ bounds as estimated so far for ETC scales out to 30TeV or above. One would hope that the holographic model would allow a non-perturbative estimate of $\delta\rho$ to move beyond (5.0.3). This is a little subtle because holographically mixed flavour states are described by strings. For very small splittings the non-abelian DBI action [92, 93] of a collection of branes would give a field theoretic computation for these states in which the background metric becomes some average over the two flavour embeddings. It is not

clear this is valid for the large isospin breaking that is needed for the top but we estimate $f_{\pi^\pm}$ in this fashion. The resulting computation shares much with Pagel Stokar type estimates [85] depending not just on the value of the self energy but also its derivatives. Here that enlarges the $\delta\rho$ estimates substantially (by as much as an order of magnitude) and the maximum ETC scale compatible with the constraints lies between 5 and 15TeV depending on N_f. A judicious choice of a low ETC scale (∼5 TeV), some walking ($N_f = 8$), and strong ETC does appear compatible. The tension with $\delta\rho$ has, of course, been previously observed (although we hope the holographic model provides a more robust framework for the observation) and was the motivation for top condensation assisted technicolour [86, 87, 88, 59]. Here a separate NJL interaction is introduced for the top quark to generate its mass independently of the electroweak breaking technicolour sector which removes the isospin breaking from the technicolour sector. We briefly show this mechanism at work in the holographic model where the ETC interaction can be switched off as the top condensation coupling grows whilst still achieving a fixed m_t.

Finally for completion we consider a one family ETC model with an SU(3) technicolour group, $N_f = 8$ (there are now 4 electroweak doublets so the strain on S would be high!). We compute the ETC coupling as a function of ETC scale. The model faces worse constraints on the mass splitting in the techni-doublet since there are three colours of techni-U quarks. The holographic description does though allow the model to evade these constraints for ETC scales between 3 and 7 TeV.

5.1 A Hologram of Top Condensation

The simplest model of NJL operators within Dynamic AdS/QCD is top condensation. We consider the case with the quark anomalous dimension running with $N_c = 3$ and $N_f = 6$ massless quarks to represent the six standard model quarks and their QCD interactions. This running breaks the conformal symmetry of the model and introduces a bulk contribution to the effective potential in analogy to (2.2.2). We set $\alpha_s(eGeV) = 0.39$ so the BF bound is violated at 1 GeV setting the scale Λ_{QCD}. Without an NJL operator the strong force becomes strong at the few hundred MeV scale where it breaks chiral symmetry and generates an IR quark mass for all six quarks of ~ 350MeV.

We will then include the four fermion interaction

$$\frac{g^2}{\Lambda^2}\left(\bar{\psi}_L t_R \bar{t}_R \psi_L \; + \; h.c.\right) \tag{5.1.1}$$

Which we shall now impose for one flavour, the top, only; ψ_L is the SU(2)$_L$ top-bottom multiplet but only the top quark mass is influenced since only t_R enters.

To impose the presence of the NJL operator in the holographic model we require that the embedding function for the top quark at the cut off Λ takes the form

$$L_t = m_t + \frac{c_t}{\rho^2}, \qquad m_t = \frac{g^2 c_t}{\Lambda^2} \tag{5.1.2}$$

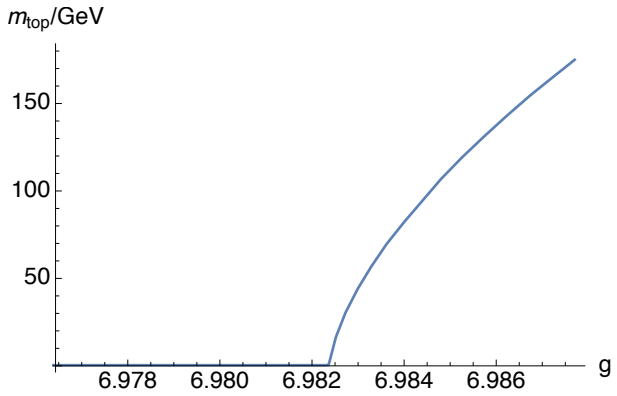

Figure 5.1.1: The top condensation model with $\Lambda = 10TeV$: the IR top mass against NJL coupling showing critical value of the coupling. Note below the critical value the mass rises from 365 MeV at $g = 0$ from the underlying QCD dynamics. Note that our numerical calculation takes $m_{\rm top}$ as an input and g is calculated from that so we should not be so concerned about numerical instability.

To numerically extract m_t and c_t we perform a numerical fit of this form to $L(\rho)$ in a small range in ρ just below Λ.

The 5 remaining quarks play only a spectator role contributing to the form of the running of γ. For these we require $L \to 0$ at the cut off so they are massless. They also make a negligible contribution to the electroweak f_π of order 100 MeV.

We proceed by picking the IR boundary value of L_t for the top, which we interpret as the IR value of the top mass, $m_t^{\rm phys}$. We then numerically evolve by shooting to the UV boundary Λ. There we can read off the UV values of m_t and c_t and impose the NJL condition (5.1.2) to extract g. In Fig 5.1.1 we show the resulting plot for $\Lambda = 10$TeV. It shows the classic NJL behaviour of the presence of a critical value of the coupling at which a second order transition occurs (in fact because of the underlying QCD dynamics the IR mass does not fully switch off below the critical coupling but it does fall to just 350MeV). To achieve $m_t^{\rm phys} \ll \Lambda$ requires one to live fine tuned to the critical coupling as one would expect. It's interesting that here, because we choose the IR top mass, numerically there is no difficult tuning to be done - it emerges once one computes g for those solutions.

In Fig 5.1.2 we show the resulting computation of f_π in this model. It again shows critical NJL behaviour. The precise value depends on the choice of the parameter κ. One might usually fix κ from the $\rho - a$ mass splitting in QCD but this is a low energy estimate of κ which could change by scales as enormous as 10 TeV. The usual expectation in top condensation models is that the observed top mass (which corresponds to the largest values of g shown in Figs 5.1.1 & 5.1.2) is insufficent to generate the electroweak f_π and this is bourne out here by choices of κ of order one as shown. Henceforth in describing the top sector we will take $\kappa = 1$. In Fig 5.1.3 we display the dependence of f_π on the cut off scale - here at each value of Λ we have arranged g to generate the physical top mass. The value asymptotes to fixed values with higher Λ. For $\kappa \simeq 1$ f_π can not achieve the

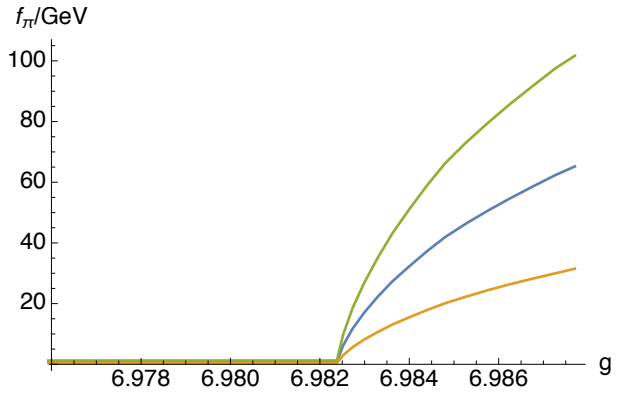

Figure 5.1.2: The top condensation model: $\Lambda = 10TeV$: top contribution to f_π against NJL coupling showing critical value of the coupling. Here for $\kappa = 1, 5, 15$ from bottom to top.

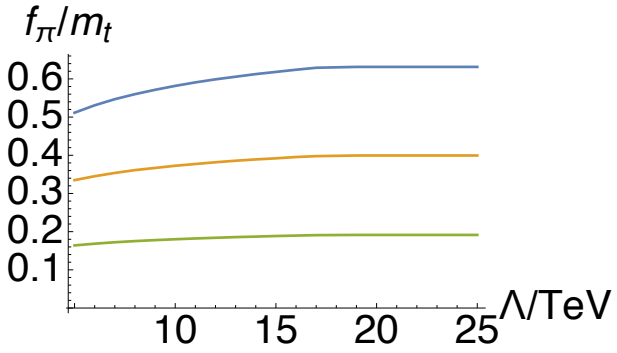

Figure 5.1.3: The top condensation model tuned to $m_t^{\rm phys} = 175$ GeV: $f_\pi/m_{\rm top}$ against Λ for $\kappa = 1, 5, 15$ from bottom to top.

electroweak scale, the usual failure of top condensation.

We can also compute the mass of the scalar bound state of the top quark, σ, and we find the value of its mass is very stable with Λ at $\simeq 590$GeV. This is the state which in a pure top condensation model would correspond to the higgs boson.

5.2 A Hologram of One Doublet ETC

We will next describe a "classic" dynamical model of the top mass - technicolour plus extended technicolour interactions to generate the top mass.

Consider a model with an SU(N_{TC}) gauge group under which a single electroweak doublet of techniquarks (U, D) transform in the fundamental representation. In addition there may be extra electroweak singlet techniquarks that allow us to dial $N_f^{\rm sing}$ and hence change the running. This sector is simply described by Dynamic AdS/QCD with the running fixed by N_{TC} and $N_f = 2 + N_f^{\rm sing}$. We now choose the value of κ to be

$$\kappa^2 = 7.6(N_f - N_f^c). \tag{5.2.1}$$

The only remaining free parameter then is the value of α_{TC} at some scale (we have found

it numerical useful to set this paramter at the scale e^2 TeV) which one dials to generate the correct f_π for electroweak symmetry breaking. A naive model such as this of the technicolour sector preserves custodial isospin - the ETC sector will break that.

A simple ETC model places the top quark (t_R and $\psi_L = (t,b)_L$) and the techni-quarks (U_R and $\Psi_L = (U,D)_R$) in the fundamental representation of an SU(6) ETC gauge group that is broken at some scale (by dynamics we don't specify) to SU(3)$_{TC}\otimes$ SU(3)$_{QCD}$ generating a mass, Λ, for the ETC gauge bosons associated with the broken generators. The ETC boson exchange associated with broken step up and down operators of the SU(6) ETC group form the four fermion operators

$$\frac{g^2}{2\Lambda^2_{ETC}}\bar{\Psi}^\alpha_L U^\alpha_R \bar{t}^i_R \psi^i_L \tag{5.2.2}$$

here α is a technicolour index and i is a QCD colour index each of which are summed over. There is also a broken diagonal generator

$$T_{\rm diag} = \tfrac{1}{\sqrt{12}}{\rm diag}(1,1,1,-1,-1,-1)$$

which gives us

$$\frac{g^2}{12\Lambda^2}\bar{\Psi}^\alpha_L U^\alpha_R \bar{U}^\beta_R \Psi^\beta_L + \frac{g^2}{12\Lambda^2}\bar{\psi}^i_L t^i_R \bar{t}^j_R \psi^j_L \tag{5.2.3}$$

Holographically we will describe the QCD quark sector including the top as in the top condensation model: we take a second Dynamic AdS/QCD sector with $N_c = 3$ to represent QCD and $N_f = 6$ to represent the six quarks. We set α so that the BF bound is violated at the 1 GeV scale to represent QCD becoming strongly coupled. In this model we solve numerically for the embedding function $L(\rho)$ for the top quark subject to $L_t^{IR} = m_t^{\rm phys}$. This function is now fixed and from it we can read off the UV embedding parameters m_t and c_t at any scale Λ by fitting to the form $L \sim (m_t + c_t/\rho^2)|_\Lambda$. The remaining quark masses are so small that we leave them as massless spectators at the electroweak scale.

In the Dynamic AdS/QCD description of the technicolour sector we now split the embedding functions for the U and D techniquarks. The D quark's embedding function, $L_D(\rho)$, must fall to zero at the UV cut off scale - we will find this unique function for each choice of $\alpha_{TC}(e^2 TeV)$ and Λ. The U techniquark embedding function L_U though will be allowed to have non-zero m_U at the UV scale and we will read off m_U and c_U in the same fashion as for the top. For each choice of the IR value of L_U, which leads to a UV pair (m_U, c_U), we must also pick $\alpha_{TC}(e^2 TeV)$ so that the sum of the U,D and top contributions to f_π match the electroweak scale (f_π=246 GeV). Alternatively one can chose a value of $\alpha_{TC}(e^2 TeV)$ and allow L_U^{IR} to vary to match f_π.

The job now is to find the choice of $\alpha_{TC}(e^2 TeV)$ and m_U at the UV scale that is consistent with the desired top mass given the ETC interactions we have chosen. Holographically

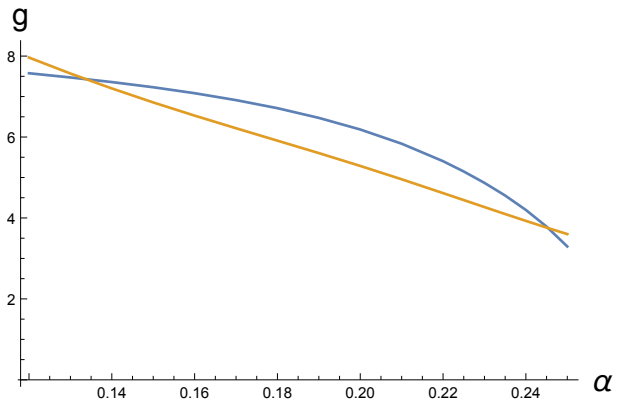

Figure 5.2.1: One doublet model ($N_{TC} = 3, N_f = 2$) with $\Lambda = 5TeV$. We use an embedding for the top quark with $L_t^{IR} = 175$ GeV. We vary $\alpha_{TC}(e^2$ TeV) and then determine $L_D(\rho)$ that vanishes at the cut off, and the value of L_U^{IR} that ensures the correct EW f_π. We then plot the value of g from each of (5.2.4) and (5.2.5). The crossing points mark a self consistent solution and determines g. The left point is an NJL dominated solution the right hand one TC dominated.

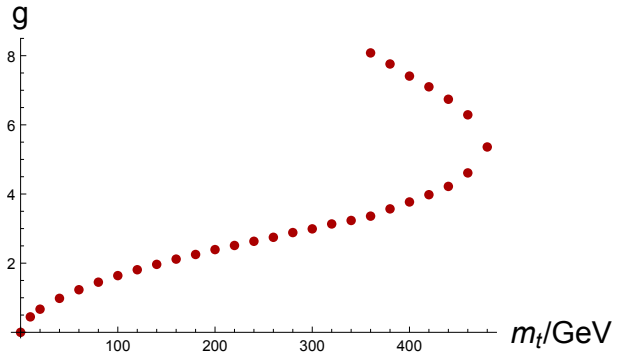

Figure 5.2.2: Plots of g vs $m_t^{\rm phys}$ for consistent solutions in the one doublet model with $N_c = 3$ and $N_f = 2$ at Λ =5 TeV showing both TC and NJL dominated branches.

the multi-trace prescription for our NJL operators are

$$m_U = \frac{g^2}{12\Lambda^2}c_U + \frac{g^2}{2\Lambda^2}c_t \tag{5.2.4}$$

and

$$m_t = \frac{g^2}{12\Lambda^2}c_t + \frac{g^2}{2\Lambda^2}c_U \tag{5.2.5}$$

Thus at each choice of Λ we must plot the value of g extracted from each of these equations as we vary the $L_U^{IR}/\alpha_{TC}(e^2 TeV)$ pair, each time getting different (m_U, c_U) pairs. We seek the point where both equations return the same value of g and are self consistent. An example of this fit is shown in Fig 5.2.1. Note that generically there are two solutions. The left hand cross point at higher g is an "NJL dominated" model of electroweak symmetry breaking - the technicolour interaction is rather weak and the technidown quark plays almost no role in generating the electroweak f_π. The top and techni-up quark are

both heavy and contribute dominantly to the electroweak scale. These solutions, whilst interesting, are at odds with experiment. They have very large isospin breaking between the U and D techniquarks which is certainly ruled out experimentally. The right hand solution at lower ETC coupling is a more technicolour dominated model. The techniquarks provide most of the electroweak scale and are, at least somewhat, degenerate. We will concentrate on these latter solutions below. Note that as the cut off is increased or the desired top mass raised the two curves in Fig 5.2.1 pass through each other - the two solutions move together and will eventually coalesce into a single solution before at higher m_t or Λ there is no physical solution. The critical solution is where both strong ETC and TC are working together hardest to generate the largest possible top mass whilst still maintaining the physical weak scale.

In Fig 5.2.2 we show an example of the evolution of the two solutions with varying $m_t^{\rm phys}$. Here the model has $N_{TC} = 3$ and $N_f^{\rm sing} = 0$ (thus a total $N_f = 2$ model) and we solve for g to generate different values of the top mass with an ETC scale of 5 TeV. We see that at generic $m_t^{\rm phys}$ there are two branches - the lower weakly coupled ETC branch merges to $g = 0$ at $m_t^{\rm phys} = 0$ and that is the standard weakly coupled ETC behaviour. For higher $m_t^{\rm phys}$ there are two solutions with one having a larger ETC coupling - these solutions are where the D's contribution to f_π is much smaller than the U's. At $m_t^{\rm phys} \simeq 500$ GeV the two branches merge and this is the maximum achievable top mass in the model with these parameters (higher $m_t^{\rm phys}$ could be achieved if f_π was raised above the physical value). Henceforth we will neglect the upper branch since it is phenomenologically unacceptable due to the huge isospin breaking in the techniquark sector. Note that here the experimental top mass is achievable.

5.2.1 Top Mass

We are now ready to explore how g must be chosen to generate the observed top mass for any given choice of Λ_{ETC} and $N_f^{\rm sing}$. Two mechanisms have been proposed for how to obtain the 175 GeV physical top mass with an ETC scale of a few TeV or above in this system. The first is to allow the ETC interactions to become strong. The second is to enhance the techniquark condensate by walking dynamics. We can see both mechanisms at work here.

Let's again consider the model with $N_{TC} = 3$ and $N_f^{\rm sing} = 0$ which has a very slow running gauge coupling and so we expect to need to depend on strong ETC to generate the 175 GeV top quark mass. For smaller top mass values naively one would consider ETC to be weakly coupled and just use the last term in (5.2.5) and it is interesting to see how badly that approximation fares at large ETC coupling. To test this we can study the theory at $\Lambda = 5$ TeV - again we fit for g as a function of the top quark masses, $m_t^{\rm phys}$, in our model (in each case requiring the 246 GeV value of f_π). The results are repeated as the top curve/points in Fig 5.2.3. The solid line is the prediction of g from just the final term in (5.2.5) - here we neglect the top mass in computing f_π and determine the condensate in a fully isospin symmetric TC model. The points are the full data from our model. In

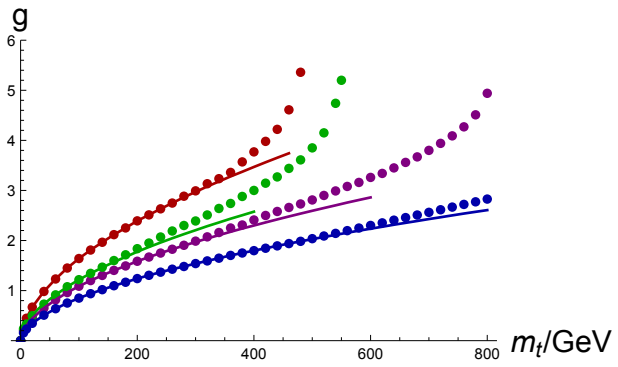

Figure 5.2.3: Plots of g vs $m_t^{\rm phys}$ in the one doublet model with $N_c = 3$ and $N_f = 2, 4, 8, 11$ (from the top down). The points are data from the holographic model. The curves are the result of computing just using the simple ETC formula from just the last term in (5.2.5). For the first three cases the final point is the largest value of m_t achievable.

fact they lie reasonably close except near the highest m_t value - that highest value is a non-perturbative prediction of the model. Note at least a part of the reason that the full model requires a larger ETC coupling for high top mass is that the top is contributing significantly to f_π which drives the TC scale and condensate down.

The walking argument [68] says that if we tune N_f to the critical number of flavours for chiral symmetry breaking then the running will leave the theory with an anomalous dimension for the quark condensate close to 1 up to large scales approaching the ETC cut off. The dimension 3 condensate will then be given by the enlarged $\langle \bar{q}q \rangle \simeq 4\pi v^2 \Lambda$. For $N_f = 3$ the edge of the conformal window is just below 12 in the approximations we make. In Fig 5.2.3 we repeat the above computation for $N_f = 4, 8$ and 11 ($N_f^{\rm sing} = 2, 6, 9$). These are, in order, the curves below the $N_f = 2$ case in the figure. The enhancement of the condensate is apparent with the ETC coupling values falling by 2 or more as N_f grows. If one allowed fractional N_f values above 11 the condensate can be driven arbitrarily higher yet which reflects the ability to tune further if one introduced higher N_c values. The model does therefore incorporate the walking solution for generating the top mass too.

We stress that independently of the phenomenology we will next discuss it is a success to be able to compute in a model that incorporates both strong NJL operators and the walking enhancement of the quark condensate.

Next we can study the ability of the theories to generate the experimental top mass at different ETC mass scales. Now fixing $m_t^{\rm phys} = 175$ GeV we search for the ETC coupling g in each of the theories at different cut offs. We display the results in Fig 5.2.4 - the curves are for $N_f = 2, 4, 8, 11$ coming down the plot. The plot again nicely illustrates the two mechanisms at work here. The curves bend down to the right from straight because the strong ETC dynamics is enhancing the top mass. As N_f increases the coupling needed to generate the phyiscal top mass falls because walking is enhancing the condensate.

Are these solutions phenomenologically acceptable though? The worry as we stressed

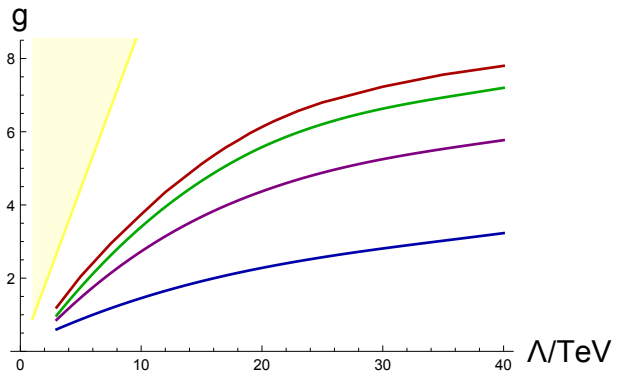

Figure 5.2.4: g vs UV cut off Λ for consistent solutions with the physical top mass on the TC dominated branch for $N_c = 3$, $N_f = 2, 4, 8, 11$ from the top down. The shaded region is excluded by the two loop $\delta\rho$ contribution.

in the introduction is the $\delta\rho$ parameter that must lie below 0.4%. The first concern is the two loop contribution to the W and Z masses from the exchange of a single diagonal ETC gauge boson across the techniquark loop contributing to M_Z [79, 80]. Naively this gives a contribution

$$\delta\rho = \frac{g^2 v^4}{12\Lambda^2} \tag{5.2.6}$$

We plot the excluded range from this estimate in Fig 5.2.4 as the shaded region. In fact the group theory coefficient of $1/12$ enables this bound to be evaded even for $\Lambda \simeq 3$TeV. The generic lesson though is that moving to larger cut off with a strengthening ETC coupling or moving to larger N_f to enhance walking both move the model away from the excluded region.

Even in these cases which escape the first contribution to $\delta\rho$ there is a secondary contribution that can dominate [83]. The ETC interaction that breaks isospin strongly to generate the top bottom mass splitting can also enter into the techni-U and techni-D masses generating a large splitting there also. This we can calculate here explicitly and compare to the result in (5.0.3). This equation places a bound of 100 GeV on the mass splitting. We will attempt a holographic non-perturbative computation to compare below.

Let us first plot a sample of the embedding functions $L(\rho)$ for the techniquarks, U and D - see Fig 6.1.1. It is good intuition, for comparison to gap equation analysis, to treat these as the self energy function $\Sigma(p)$ for the quark. Broadly the IR is dominated by the TC dynamics and the self energies of the U and D are degenerate there whilst in the UV the four fermion interaction generates a UV mass splitting. The scales of these are set by f_π and $m_t^{\rm phys}$ respectively. In Fig 6.1.1 we have shown examples for $N_f = 2$ and 11 to show there is some N_f dependence. In particular the walking theory where the TC coupling is stronger in the UV leads to the IR theory displaying more isospin breaking.

To study this further we plot the mass splitting between the U and D in the UV as a function of N_f and Λ in Fig 5.2.6. The $N_f = 2$ curve is at the top, $N_f = 4, 8$ central, and the $N_f = 11$ curve is lower. This ordering reflects the growth of the condensate due to walk-

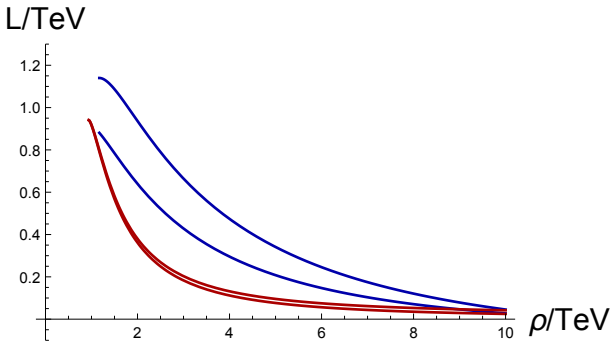

Figure 5.2.5: The self energy function $L(\rho)$ for the U (higher) and D (lower) techniquarks against RG scale ρ for solutions with the physical top mass, $N_c = 3$, $N_f = 2$ (lower two curves in the IR) and 11 (higher two curves in the IR). Here $\Lambda = 10$ TeV

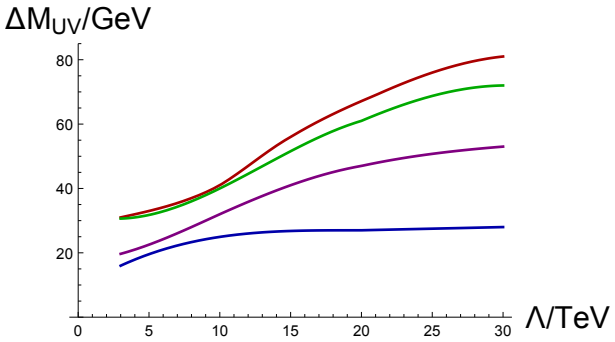

Figure 5.2.6: The UV cut off difference in the mass of the U and D techni-quarks for solutions with the physical top mass, $N_c = 3$, $N_f = 4, 8, 11$ from top to bottom.

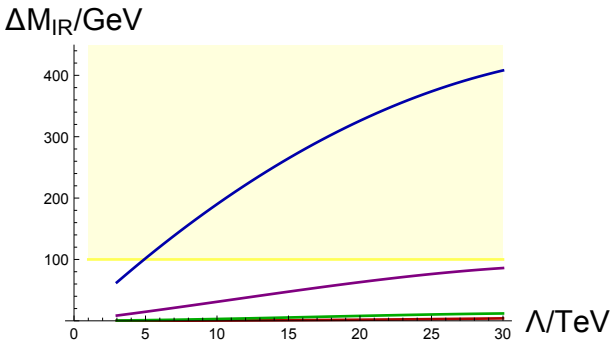

Figure 5.2.7: The difference in the mass of the U and D techni-quarks in the deep IR for solutions with the physical top mass, $N_c = 3$, $N_f = 4, 8, 11$ from bottom to top. The shaded region is excluded by the perturbative mass splitting computation of $\delta\rho$.

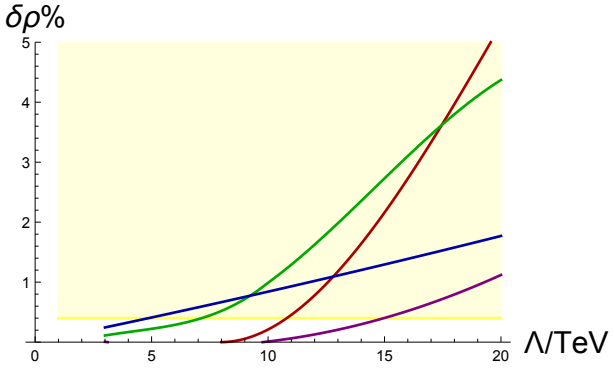

Figure 5.2.8: The holographic computation of $\delta\rho$ for solutions with the physical top mass, $N_c = 3$. Moving down the right hand side of the plot are the curves for $N_f = 2, 4, 11, 8$. The shaded region is experimentally excluded. Since mass is a derived parameter the depends only on Λ, for each value of N_c and N_f we can view Λ as a proxy for mass (at least at low energies until the mass saturates).

ing. The NJL interaction is weaker in walking theories to generate a given $m_t^{\rm phys}$. Note all of these values lie below the 100 GeV naive bound.

In Fig 5.2.7 we show the deep infra-red mass splitting between the U and D techniquarks for the solutions at each Λ_{ETC} and for $N_f = 2, 4, 8, 11$. Here $N_f = 2$ is the lower plot, $N_f = 11$ the higher curve (the reverse of the UV behaviour). In the strongly running theories at low N_f the symmetry breaking is dominated at low scales and the UV physics is suppressed since it lives in the asymptotically free regime of the theory - there is little IR mass splitting in the techni-sector. As we increase the anomalous dimension at the UV scale by walking we make the UV physics more important to the IR symmetry breaking and the NJL interaction plays a bigger role in enhancing the IR mass splitting. This model suggests that the gain of less splitting in the UV with walking is more than compensated by extra splitting in the IR. By $N_f = 11$ the mass splitting in the techni-quark sector is greater than the 100 GeV perturbative bound (shown as the shaded area in the plot).

Naively at this stage the $N_f \leq 8$ theories at a cut off scale up to 30 TeV appears to avoid all the $\delta\rho$ bounds: both that in Fig 5.2.4 and with the mass splitting in the technisector being below 100 GeV at all scales as shown Fig 5.2.6 and Fig 5.2.7.

Ideally one would like to compute the $\delta\rho$ contribution directly in our holographic model. Technically it is hard to compute $f_{\pi^\pm}$ holographically because in full string models $\bar{U}D$ states are described by true strings stretching between the U and D flavour branes. The spirit, as can be seen from the non-abelian Dirac Born Infeld action (which is only known for very small mass splittings) [92, 93], would be that the $f_{\pi^\pm}$ calculation would be some smearing over the two brane geometries. A reasonable proposal for this computation at the field theory level would be to replace equation 3.5.16 (for the pion) with

$$\partial_\rho \left[\rho^3 \partial_\rho A\right] - \kappa^2 \frac{\frac{1}{4}(L_U + L_D)^2 \rho^3}{(L_U^2 + \rho^2)(L_D^2 + \rho^2)} A = 0\,. \tag{5.2.7}$$

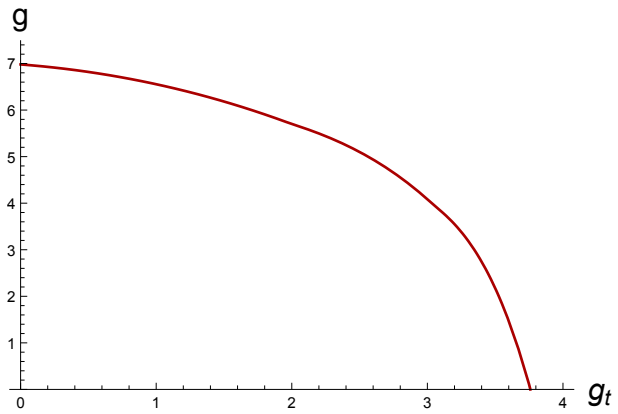

Figure 5.3.1: The top condensate coupling against the ETC coupling for solutions with the physical top mass, $N_c = 3$, $N_f = 2$ $\Lambda = 5$ TeV.

We then have

$$\delta\rho = \frac{f_{\pi 0}^2 - f_{\pi_\pm}^2}{f_{\pi 0}^2} \tag{5.2.8}$$

We can compute this for the cases we have considered - the results for $N_f = 2, 4, 8, 11$ as a function of Λ are shown in Fig 5.2.8 where it can be seen that the result is considerably larger than the perturbative estimate in (5.0.3) suggests. The holographic computation of f_π depends on more than just the magnitude of the self energy functions but also on derivatives etc (in this sense it is like the Pagel Stoker formula [85] used with gap equations) and so can reasonably produce a larger result. There is also no clear pattern of behaviour with N_f which is directly attributable to the fact that the IR mass splitting grows with N_f whilst the UV splitting falls. Nevertheless the $N_f = 8$ theory with a judicious amount of walking and moderately strong ETC appears able to survive constraints until a cut off of 15 TeV.

5.3 Top Condensation Assisted Technicolour

The difficulties of hiding the top mass generation mechanism from the $\delta\rho$ parameter are not new although our computational framework clearly presents them. Previously it has been suggested that the problem can be alleviated by an additional top self interaction as in top condensation models [86, 87, 88, 59]. Clearly if a separate NJL model does the work of generating the top quark mass then the ETC interactions that feed that mass back into the techniquark masses will be reduced. Top colour [94] is an example of a model underlying such a mechanism.

In the one doublet models we can just include a top self interation with coupling g_t in (5.2.5)

$$m_t = \frac{g^2}{12\Lambda_{ETC}^2} c_t + \frac{g^2}{2\Lambda_{ETC}^2} c_U + \frac{g_t^2}{\Lambda_{ETC}^2} c_t \tag{5.3.1}$$

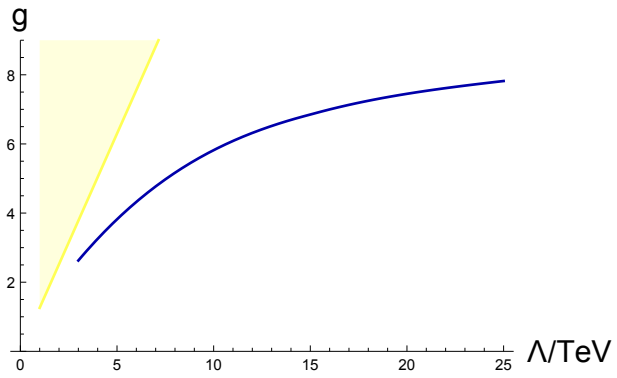

Figure 5.4.1: The ETC coupling against ETC scale in the one family TC model.

For example we can compute with $N_f = 2$ at $\Lambda = 5$TeV, setting $m_t^{\rm phys} = 175$ GeV in the IR. At each value of α_{TC} we tune the UV mass of the U embedding to give the physical f_π and then read off g from (5.2.4). g_t then follows from (5.3.1). In Fig 5.3.1 we plot the g vs g_t line that achieves the physical top mass and electroweak scale. As advertised one can trade the strength of the ETC interactions for a stronger top NJL coupling. In principle this can be used in any case to solve the $\delta\rho$ problem from the techni-sector.

5.4 A Hologram of One Family Technicolour

Another classic ETC configuration is to have a full family of techni-fermions (U^i, D^i, E, N, ie $N_f = 8$) each in the fundamental representation of SU(N_{TC}). The minimal ETC group to generate just the top mass is to place $\Psi_L^i = (U^i, D^i)_L$ and $\psi_L^i = (t^i, b^i)_L$ and t_R^i in the fundamental representation of an SU($N_{TC}+1$) ETC group that is then broken at the scale Λ to the technicolour group. The broken step generators lead to the four fermion operators

$$\frac{g^2}{2}\bar{\Psi}_L^i t_R^i \bar{U}_R^i \psi_L^i \tag{5.4.1}$$

and the diagonal generator for N_{TC}=3 ($1/\sqrt{24}$ diag(1,1,1,-3)) gives

$$\frac{g^2}{24}\bar{\Psi}_L^i U_R^i \bar{U}_R^i \Psi_L^i + \frac{9g^2}{24}\bar{\psi}_L^i t_R^i \bar{t}_R^i \psi_L^i \tag{5.4.2}$$

where here the colour index i is not summed over.

The holographic description is as follows. The QCD sector is described by Dynamic AdS/QCD with $N_c = 3$ and $N_f = 6$ - the model predicts the quark condensate at the ETC scale which we must divide by 3 to get the condensate contribution from a single QCD colour of quark. In principle one ought to adjust the QCD running above the techni-quark mass, however, since this is in the slow running perturbative regime for the QCD coupling where the top quark mass runs very slowly we neglect this complication.

The technicolour sector is described by a Dynamic AdS/QCD model with $N_{TC} = 3$ and $N_f = 8$. As before we require the $m_D = m_E = m_N = 0$ at the ETC scale. These five

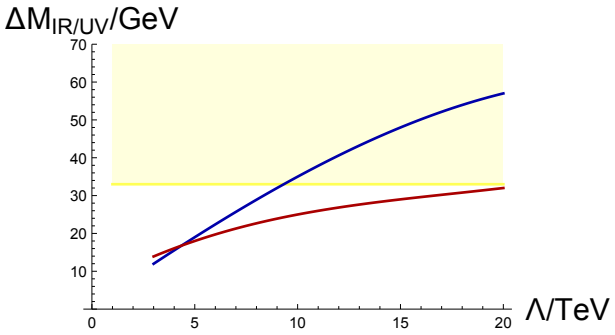

Figure 5.4.2: U-D mass splittings in the one family TC model against Λ. On the right of the plot, the top line is the IR mass splitting, the lower line the UV splitting.

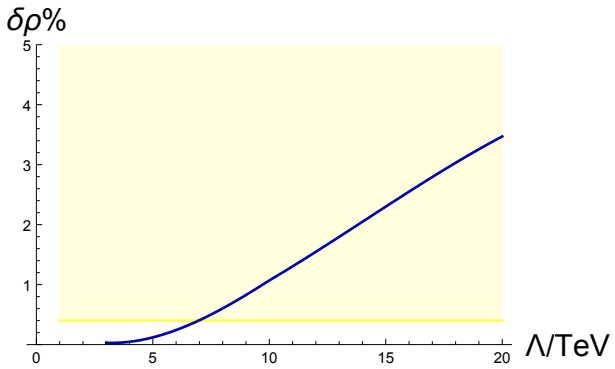

Figure 5.4.3: $\delta\rho$ in the one family model as a function of ETC scale. The yellow region is excluded by the experimental bound.

fermions contribute degenerately to f_π. We can then dial $\alpha_{TC}(e^2\text{TeV})$ and m_U^{IR} to generate configurations with the correct electroweak $f_\pi = 246\text{GeV}$ - the three colours of techni-Us and the top also contribute here. To determine the correct combination of top and techni-up embeddings we now require at the UV scale that

$$m_U = \frac{g^2}{24\Lambda^2}c_U + \frac{g^2}{2\Lambda^2}\frac{c_t}{N_c} \tag{5.4.3}$$

and

$$m_t = \frac{9g^2}{24\Lambda^2}\frac{c_t}{N_c} + \frac{g^2}{2\Lambda^2}c_U \tag{5.4.4}$$

We again plot g vs Λ for the model in Fig 5.4.1 where we see that strong ETC values of g are required to generate $m_t^{\text{phys}} = 175$ GeV. There is again a second NJL dominated branch of solutions which we don't show - as in the one doublet model these have very large isospin breaking in the techni-quark doublet. We plot the mass splittings in the techni-quark doublets Δm_{IR} (evaluated in the IR) and Δm_{UV} (evaluated at the ETC scale) against Λ for the technicolour dominated solutions in Fig 5.4.2. The splittings are between 10 and 70 GeV. Remember here that there are 3 electroweak doublets with this splitting contributing to $\delta\rho$ so much of the range is excluded again even by the pertubative estimate of $\delta\rho$ - the excluded region is shaded in the plot. Finally we plot the values of $\delta\rho$ from the

holographic computation of $f_{\pi^\pm}$ which are considerably larger and exclude the model for ETC scales above 7 TeV.

In conclusion the one family model struggles more on all phenomenological fronts from S to $\delta\rho = \alpha T$! Of course a direct top condensation NJL interaction could again be used to decouple the techniquark sector from the isospin breaking of the top mass.

Holographic models provide a calculationally efficient tool to study the broad behaviours of strongly coupled gauge theories. They incorporate the ideas of walking dynamics very directly since the AdS mass of states translates to the running anomalous dimension of the quark condensate, γ. The Dynamic AdS/QCD model we have used here is a very simple crystallization of these ideas inspired by top-down string models. It allows the study of the mesonic sector of any theory if a sensible guess is made for the running of γ - here we have used the two loop running of the gauge coupling which incorporate the physics of the conformal window, chiral symmetry breaking when $\gamma = 1$, walking for theories just above that point in N_f and then QCD-like dynamics for smaller N_f.

Four fermion NJL operators can be included using Witten's multi-trace prescription and the critical behaviour of the NJL model can be realized. Here we have included NJL operators in Dynamic AdS/QCD and again shown traditionally NJL like behaviour (see also [1]). We have designed descriptions of dynamical symmetry breaking models of the electroweak sector. A pure NJL model can be used to generate a top quark condensate - in Fig 5.1.1 we show the rise of the top mass above some critical NJL coupling (close to the perturbative 2π value for the coupling).

We have then studied the interplay between a strongly coupled technicolour gauge theory and the top quark, linking the two sectors by extended technicolour NJL operators. In our first model we used NJL operators inspired by a one doublet technicolour model (with $N_c = 3$) and the simplest extended technicolour unification of the top quark. We allowed for possible electroweak singlet techniquarks to vary the total N_f of the gauge theory. We studied solutions where the electroweak f_π is achieved and various values of the top mass. There are two possible solutions. One is an NJL dominated solution where the four fermion operators drive the majority of the electroweak breaking and technicolour is relatively weak; these models have large isospin breaking in the technicolour sector and are ruled out by precision data for $\delta\rho$. The second set of solutions match to traditional technicolour dominated electroweak symmetry breaking and weak ETC for small top masses. The dynamics can be followed here to strong ETC couplings and large top masses. A maximum top mass is possible without creating too large an f_π. For theories at low N_f this top mass value is close to 500 GeV but it increases significantly as N_f approaches the edge of the conformal window and walking enhances the techniquark condensate. When we studied solutions with the physical value of the top mass the holographic model allows us to study the IR and UV mass splittings in the techniquark sector induced by the isospin violating ETC interactions. These splittings lie between 20 and a few hundred GeV and taken naively with the perturbative expression for $\delta\rho$ (5.0.3)

suggest models may be compatible with electroweak data. However, we also used the holographic model to estimate $f_{\pi^\pm}$ and directly determine $\delta\rho$ and these estimates were up to an order of magnitude larger (due to isospin violating structure in the derivatives of the techniquark self energy) ruling out larger ETC scales. A judicious choice of ETC scale near 3-15 TeV, a modicum of walking (too much enhances the isospin breaking effects of the UV ETC interactions) and strong ETC should pass the experimental bounds though. In conclusion the holographic model provides a clean computational framework that emphasises the roles of walking dynamics and strong ETC interactions in the top mass ETC generation mechanism. A separate NJL interaction to generate the top mass can be used (as in top colour models) to isolate the isospin breaking of the top mass from the technicolour sector.

Finally we studied a one family technicolour model with $N_c = 3$ and $N_f = 8$ and observed the same structure of solutions. Here because of the three QCD colours of techniquarks the isospin splitting in the techniquark sector makes a larger contribution to $\delta\rho$ and these models are harder to reconcile with experiment although an ETC scale between 3-7 TeV seems possible.

Whilst many of the phenomenological conclusions of this analysis have been previously intuited in other ways we believe that the holographic approach to the problem provides a simple and revealing computational tool that has made it worth studying independently of the precise phenomenology. We hope that holographic models can play an important part in understanding strongly coupled sectors of beyond the standard model sectors in the future.

In the next chapter we shall discuss ideal walking, an intriguing form of walking technicolour which features a large conformal window in it's running.

Chapter 6

The Conformal Window and Ideal Walking

In chapter 4 a holographic [18] description of the gauged Nambu-Jona-Lasino (NJL) model [95, 96] was developed. The gauge theory action is

$$\mathcal{L} = \frac{1}{4g_{YM}^2} F^{\mu\nu}F_{\mu\nu} + i\bar{q}\not{D}q + \frac{g^2}{\Lambda^2}(\bar{q}_L q_R \bar{q}_R q_L + h.c.), \tag{6.0.1}$$

where g_{YM} is the Yang-Mills coupling, g the NJL coupling at the UV scale Λ, and the numbers of colours and flavours, N_f and N_c, can take any values. Here we study theories for different regimes of N_f in particular we loop for theories with a UV fixed point in γ. We find two cases: above a critical value for N_f we obtain enhanced chiral symmetry breaking through the NJL interaction while below that we do not. We study both cases.

In this chapter we will look at a very large range of energy scales as such, when we calculate the running of the anomalous dimension we will set $\alpha(1) = \frac{2}{3}\alpha^*$ where α^* is the value of α in the far IR. This method for setting the boundary condition is used in order to make the technique robust when automatically scanning over different values of N_f and N_c, if we chose $\alpha(1)$ to be a fixed value a solution would not always exist.

First let us review walking technicolour. For $N_f < 2.6N_c$ the two loop running has an IR pole and these are the QCD-like theories we have explored in 4. As N_f grows above $2.6N_c$ though an IR fixed point develops with the fixed point value of $\gamma = \gamma_*$ falling from infinity. When the fixed point value of γ_* lies above one there is still chiral symmetry breaking. Here there is interesting structure in the mass versus quark condensate plane - a spiral structure indicating the presence of excited states of the vacuum. These structures have previously been observed in D3/D7 models of magnetic field induced chiral symmetry breaking [97], the alternative dual of the conformal window of [89, 90], in the condensed matter models of [98] and more recently in holographic superconductor models [99]. Analysis of the effective potential shows these states are higher energy excitations of the true vacuum and indeed the σ meson is tachyonic in all but the low-

est energy vacuum. They correspond to condensation of radially excited states of the σ. These excited states have also been observed to play a role in BKT transitions where the instability to chiral symmetry breaking occurs due to tuning the AdS scalar mass through the BF bound, when the tachyons for each of these vacua become degenerate so the phase transition is not mean field [98, 89]. Their appearance in so many models, including those with symmetry breaking but no BKT transition, suggests they are a robust prediction of holographic models of symmetry breaking. Here for us they play a small role in understanding the vacua of the theory with a repulsive NJL term. In the presence of an attractive NJL operator the condensation in the true vacuum is enhanced. We explore whether the excited states of the theory give rise to meta-stable vacua in the presence of the NJL term although we do not find such states. A repulsive NJL term in the true vacuum reduces the gap but only an infinitely repulsive term completely switches condensation off - we discuss this physics also at the level of the effective potential. A brief analysis of similar ideas in the alternative holographic model of gauge dynamics in [89] can be found in [90].

As N_f approaches $\sim 4N_c$ from below the fixed point value falls very close to $\gamma_* = 1$ and we enter the so called "walking" gauge theory regime [68]. As one reduces N_f (which it is helpful to think of as a continuous parameter, as it is at large N_c) the scale at which $\gamma = 1$ is crossed falls sharply relative to some UV scale where the coupling is fixed across comparator theories. Formally there is a BKT transition as γ_* falls to precisely one and we see the spiral in the mass-condensate plane contract into the origin of the plot. Here at the low chiral symmetry breaking scale the quark condensate which has dimension close to two goes as $\langle \bar{q}q \rangle \sim f_\pi^2$, on dimensional grounds, where we use the pion decay constant, f_π, to set the scale of the chiral symmetry breaking dynamics. As one runs to the UV, the dimension of the condensate transitions at some intermediate scale, given by approximately the one loop pole scale Λ_1, and the condensate transforms to the dimension 3 $\langle \bar{q}q \rangle \sim f_\pi^2 \Lambda_1$. By arbitrarily tuning N_f one can arbitrarily separate the scales f_π and Λ_1 so that in the UV $\langle \bar{q}q \rangle / f_\pi^3 \to \infty$. This behaviour was first studied because of a possible role in suppressing flavour changing neutral currents in technicolour dynamics - increasing the condensate moves extended technicolour dynamics off to a higher scale. It is though also an interesting behaviour to study in the space of non-abelian gauge theories on its own.

In these walking theories it has been argued that the effective potential may be very flat as a result of the near conformality of the gauge theory and thus the mass of the higgs-like σ particle may be parametrically light relative to f_π. Again there is a motivation in describing the observed visible higgs but also an intrinsic field theory property of interest here. Both the growth of the quark condensate and the light σ have been observed for the walking case in the holographic model we will study here [56]. We will build on this study here with the properties of a slightly different scenario - "ideal walking" [100, 101].

A problem with walking is that N_f actually takes integer values and so, without going to

the extremes of theories with a very large number of colours, N_c, it is unlikely any real theory is sufficiently fine tuned to give exactly $\gamma_* = 1$. Ideal walking theories have been proposed as an alternative set up with some of the same gains. Here one studies a gauge theory, at larger N_f that lives in the so called conformal window [91] (ie $N_f \geq 4N_c$ and less than $N_f = 11N_c/2$ where the fixed point γ_* falls to zero and asymptotic freedom is lost) and has a true IR conformal fixed point. It never becomes strong enough to trigger chiral symmetry breaking itself. Instead a strongly coupled NJL interaction at a scale greater than Λ_1 is used to trigger chiral symmetry breaking. Here the fine tuning to set f_π below Λ_1 is provided by the NJL coupling rather than N_f. Now, if at the IR fixed point the anomalous dimension is $0 < \gamma_* < 1$, then $\langle \bar{q}q \rangle \sim f_\pi^{3-\gamma_*}$. In the UV it becomes the dimension 3 object $\langle \bar{q}q \rangle \sim f_\pi^{3-\gamma_*} \Lambda_1^{\gamma_*}$. Note here that as one tunes $f_\pi \ll \Lambda_1$ again we have $\langle \bar{q}q \rangle / f_\pi^3 \to \infty$. This will be the case for any theory in the conformal window no matter the size of γ_*. This is almost certainly achievable with discrete N_f at small N_c.

We begin study of this regime by determining the phase structure of the model at fixed N_c in the N_f against NJL coupling, g^2, plane. For $N_f < 4N_c$ there is always chiral symmetry breaking driven by the gauge theory. Above this value of N_f, where a BKT transition occurs in the massless theory with changing N_f, our analysis suggests there is a numerical discontinuity in the plane with chiral symmetry breaking then only occurring for g^2 greater than a finite critical coupling, rather than a smooth transition with the critical g^2 value growing from zero. There may be an exponential dependence of the condensate against NJL coupling but we have not seen numerical evidence for that.

Next we explore the enhancement of the UV condensate (or equally the suppression of any UV mass relative to its IR value which is also expected). First we study an idealized running where γ transitions from zero to a fixed point value at a sharp scale, Λ_1. We simply match the form of the solution on the two sides of the discontinuity analytically and show that the expected increase in the condensate (decrease in the mass) is realized. We then demonstrate the same phenomena occurring numerically with the two loop gauge theory running (where the intermediate scale is less clearly defined) - here it is easiest to follow the leading term in the holographic solution (the mass) but the behaviour is clearly reproduced.

Finally one might again wonder whether a light σ particle could emerge in this ideal walking setting to provide a different possibility for electroweak physics and its light higgs. Here again in our model we can produce an analytic result, showing that when the running of γ is slow the mass of the σ indeed falls towards zero. If one places the scale at which the NJL model causes symmetry breaking in the very conformal IR regime then its mass can be very small (below that needed to describe the higgs). We show that for $N_f = 12$ choices of the IR symmetry breaking scale and the UV cut off scale exist for which $m_\sigma / f_\pi \simeq 0.5$ and hence might form the basis of an electroweak model.

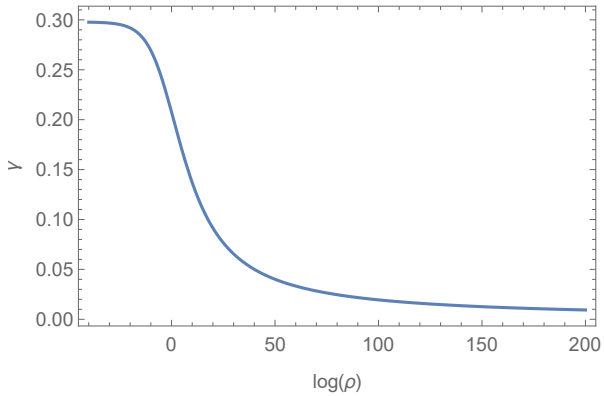

Figure 6.0.1: An example plot of the running of γ, calculated from two loops, from the IR fixed point to the asymptotically free UV. γ_* is the value in the IR. Here we have $N_c = 3$ and $N_f = 13$

6.1 Chirally Broken Phase: $2.6N_c < N_f < 4N_c$

In this range of N_f the IR fixed point value of γ is greater than one and the gauge theory generates chiral symmetry breaking on its own. To study this we seek solutions of (3.5.10) with the IR boundary conditions described. All the dynamical scales are set in terms of the scale at which $\gamma = 1$ (which here we set to be at r=11)) and the UV value of L which is the quark mass. From the UV form of the solution (3.5.11) we extract m_{UV} and c_{UV}. In Figure 6.1.1 we plot the solutions for $N_f = 9$ with $m_{UV} = 0$ in the UV.

Note there are an infinite set of such solutions - as the IR boundary value of L shrinks solutions with more oscillations can be found. The solutions with more oscillations are excited states of the vacuum - these are states where radially excited states of the σ meson are condensed, which since they are all described by a single holographic field are mixed together. In Figure 6.1.2 we plot the position of the solutions in the $m_{UV} - c_{UV}$ plane for two representative values of N_f - to compare theories we have chosen to fix the UV scale in both where $\gamma = 0.3$. As can be seen at $N_f = 9$ (the top plot) there is a spiral structure. The spiral makes an infinite number of loops before ending at the origin. This structure has been previously observed in the D3/probe-D7 model with a magnetic field [97], the alternative dual of the conformal window of [89, 90], in the condensed matter models of [98] and more recently in holographic superconductors [99] so it appears very generic to holographic symmetry breaking descriptions.

The solutions of the Euler Lagrange equation represent turning points of the action and hence the effective potential ($V_{eff} = -S$ evaluated on the vacuum solutions). It is a simple matter to evaluate the vacuum energy on the solutions and show that they monotonically increase in energy with the number of axis crossings. The flat embedding $L = 0$ has the highest energy. This means these turning points must be points of inflection of the effective potential since there are no interchanging maxima and minima. The interpretation is that the chirally symmetric phase $L = 0$ is unstable to condensation of the σ excitation but also all its radially excited states σ^*, σ^{**}... We envisage a four dimensional

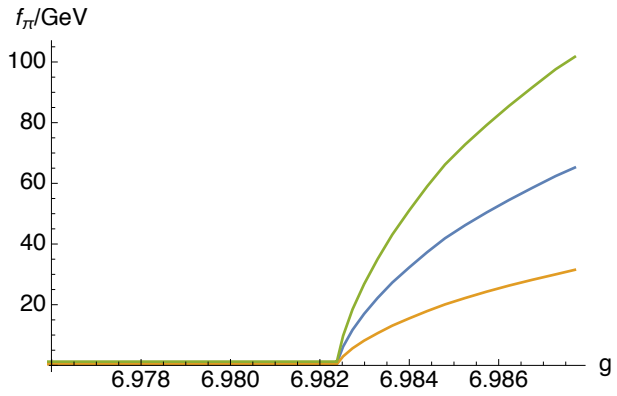

Figure 6.1.1: The functions $L(\rho)$ with $m = 0$ in the far UV for $N_f = 9$. In the IR we cut off scales below where the quarks become on mass shell when $L(\rho = m_{IR}) = m_{IR}$. Here the BF bound is violated at $r = 11$.

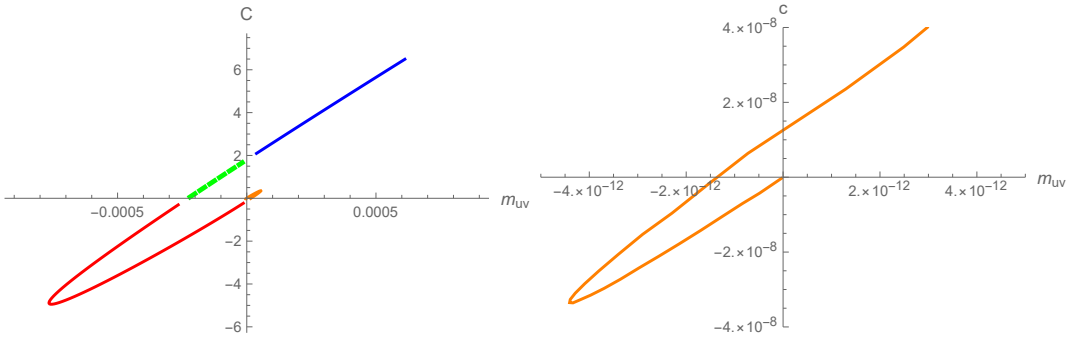

Figure 6.1.2: The regular embeddings $L(\rho)$ plotted in the $m_{UV} - c_{UV}$ plane for $N_f = 9$ (left) and $N_f = 11$ (right) showing the spiral structure and how the scale of chiral symmetry breaking shrinks as one approaches the BKT transition at $N_f \simeq 12$. Here both theories have $\gamma = 0.3$ at the same UV scale.

low energy potential for these states of the form

$$V_{eff} = -m_1^2|\sigma|^2 - m_2^2|\sigma_*|^2 + \lambda(|\sigma|^2 + |\sigma_*|^2)^2 + ... \tag{6.1.1}$$

This has minima of different depths on the σ and σ_* axes but the minima are smoothly connected in the full space with only one true local minimum where σ alone has a vev (see the top part in Figure 6.1.3 for a sketch of this form).

A simple way to test this hypothesis is to compute the σ meson mass in each of the vacua. In the lower part of Figure 6.1.3 we plot the σ's mass against the UV quark mass as we move along the spiral of Figure 6.1.2 and it is worth considering the physics here in detail. First note that at $m_{UV} = 0$ only the L profile that does not cross the ρ axis (the top curve in Fig 6.1.1) has a stable σ. This is the true vacuum of the theory. There is another U(1)$_A$ rotated equivalent version of the vacua where the curve lies entirely below the axis (this is the opposite side of the wine bottle shaped potential one expects). Now as we switch on a positive m_{UV} as expected the σ mass rises. When we add in a negative mass there is a period when the σ mass remains positive - here we are describing the fate of the U(1)$_A$ rotated vacua in the presence of a mass. The vacuum manifold is tilted and this state is the unstable side of the potential (the pion is tachyonic). For sufficiently large negative mass the wine-bottle shaped form of the effective potential is lost and the non-true vacuum side of that potential becomes unstable for the σ also. Beyond this point though the solution remains as a turning point of the potential - to understand its evolution we can follow it back to the $m_{UV} = 0$ point where it is the second curve down in Fig 6.1.1. This is the vacuum where the σ^* has condensed (although it is unstable to a roll to the true vacuum since the σ is tachyonic). Tracking back along negative m_{UV} tells us we are seeing this state in the presence of the negative mass. Continuing on one moves smoothly to the even less stable vacua with condensation of higher excitations of the σ.

These spirals have also been previously seen in the alternative model of the N_f dependence of gauge theories in [89, 90] and in the condensed matter models of [98]. There the authors stressed the role of these extra vacua as one approaches a BKT phase transition. If the AdS scalar mass can be tuned to the BF bound (as here by tuning N_f) then a non-mean field transition occurs because a set of Efimov states emerge - these correspond to an infinite number of tachyonic states whose masses pile up at zero and play a role in the transition. Here as N_f approaches the chiral transition it is these tachyons, for rolls to each of the vacua for the excited states of the σ, that are these Efimov states. Here, the existence of these states will play a role in understanding the response of the theory to NJL interactions.

We can now consider what happens when we switch on an NJL term in this theory. The easiest method is to use the boundary condition in (3.5.19) and convert the $m_{UV} - c_{UV}$ spiral to results in the $c_{UV} - g^2$ plane which we have done for $N_f = 9$ in Figure 6.1.4. The upper branch of the plot is the most important since these are the stable vacua. Positive

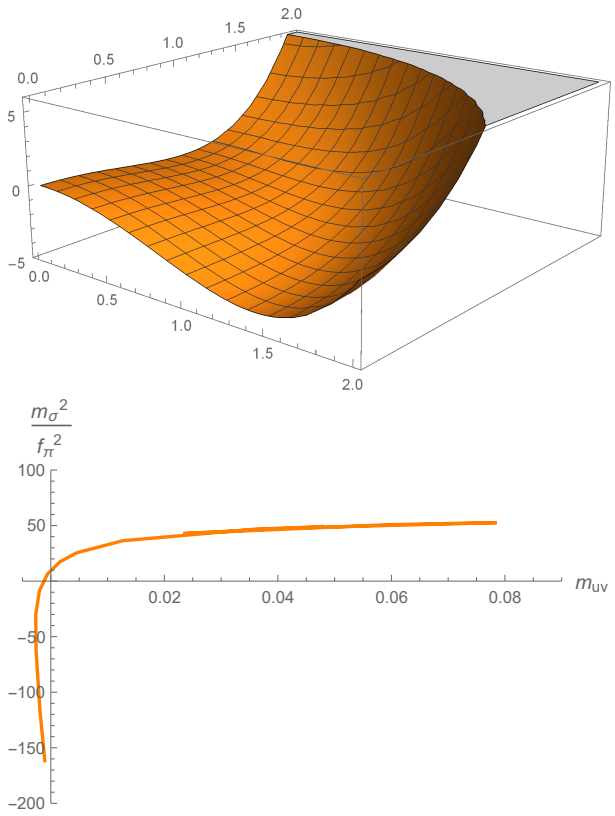

Figure 6.1.3: Above - a sketch of the low energy potential against the σ and σ_* fields showing mimina on each axis but only a single true minima on the σ axis. Below - the σ's mass against the UV quark mass as we move along the spiral of Figure 6.1.2 with $N_f = 9$ showing the instability of the excited states at $m_{UV} = 0$.

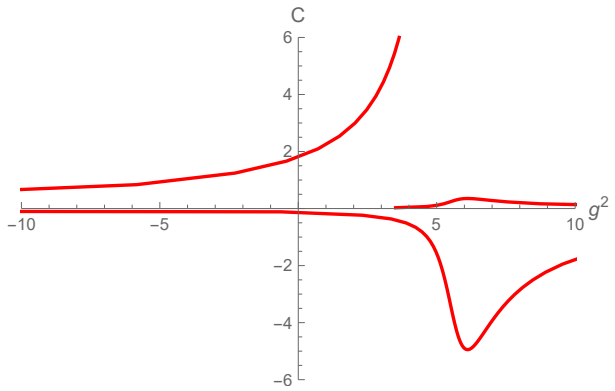

Figure 6.1.4: Plot of c_{UV} against g^2 for the $N_f = 9$ theory.

g^2 enhances c_{UV} from the bare gauge theory values at $g^2 = 0$.

To understand the role of the other "arms" of the spiral it is helpful to plot the effective potential against m_{UV} and c_{UV} which we do in Figure 6.1.5. We use the same shading as in the $m_{UV} - c_{UV}$ spiral for $N_f = 9$ in Figure 6.1.2. We plot the effective potential against m_{UV} and c_{UV} in the absence of an NJL interaction. Now adding an attractive NJL term corresponds to adding a positive term to the potential $m_{UV}^2\Lambda^2/g^2$ which we show in the lower plot of Figure 6.1.5. The solid curves show the potential with an attractive NJL coupling and the extra term produces a minimum that grows to larger $m_{UV}(c_{UV})$ as g^2 grows.

The case of repulsive NJL interactions is also interesting. The $c_{UV} - g^2$ plot in Figure 6.1.4 shows that a negative g^2 decreases the size of the quark condensate as one might expect, although surprisingly the condensation only fully switches off at infinite repulsive g^2. There is a more involved story if we look at these solutions at the level of the effective potential - see the dashed curves in the lower plot of Figure 6.1.5. As one begins to add a $-m^2\Lambda^2/g^2$ term to the potential at small g^2 the potential is highly unbounded with a single local maximum at $m = 0$. The theory has an instability which could presumably be cured by higher dimension operators near the cut off. If we ignore that instability (since an infintessimal repulsion at a very high scale presumably shouldn't totally change the theory), the local maximum matches to the $g^2 = 0$ vacua of the gauge theory and this presumably represents the impact of the NJL repulsion on the physics of that vacua. As g^2 grows the maximum tracks along the curve following the behaviour in the $c_{UV} - g^2$ plot until we arrive at $c_{UV} = 0$ but note here that $m_{UV} \neq 0$ and so g^2 has diverged. This is related to the existence of the spiral - if the $c_{UV} - m_{UV}$ curve in Figure 6.1.2 at negative m_{UV} simply returned to $m_{UV} = c_{UV} = 0$ directly then a finite g^2 would switch off the condensate. The conclusion is that the more complicated dynamics of the gauge theory (which one could think of as a tower of higher dimension operators) is sufficient to oppose even a very strong repulsive four fermion interaction.

The remaining lower structure in Fig 6.1.4 reflects the effect of the NJL term on the unstable vacuum states of the theory. One is tempted to see in Figure 6.1.5 metastable vacua but in all cases these states, with higher states of the σ condensed, are unstable (the true potential is higher dimensional in the spirit of Fig 6.1.3)- they have a tachyonic σ or π and are smoothly connected to the fully unstable vacuum at infinite positive m.

As one increases N_f, keeping γ fixed at some UV scale across all theories, the spiral rapidly contracts into the origin of the $m_{UV} - c_{UV}$ plane as can be seen from the rapidly sinking axes range in the plots of Figure 6.1.2 - this represents the expected reduction in the scale of chiral symmetry breaking as one approaches the BKT transition [89, 56] at the edge of the conformal window.

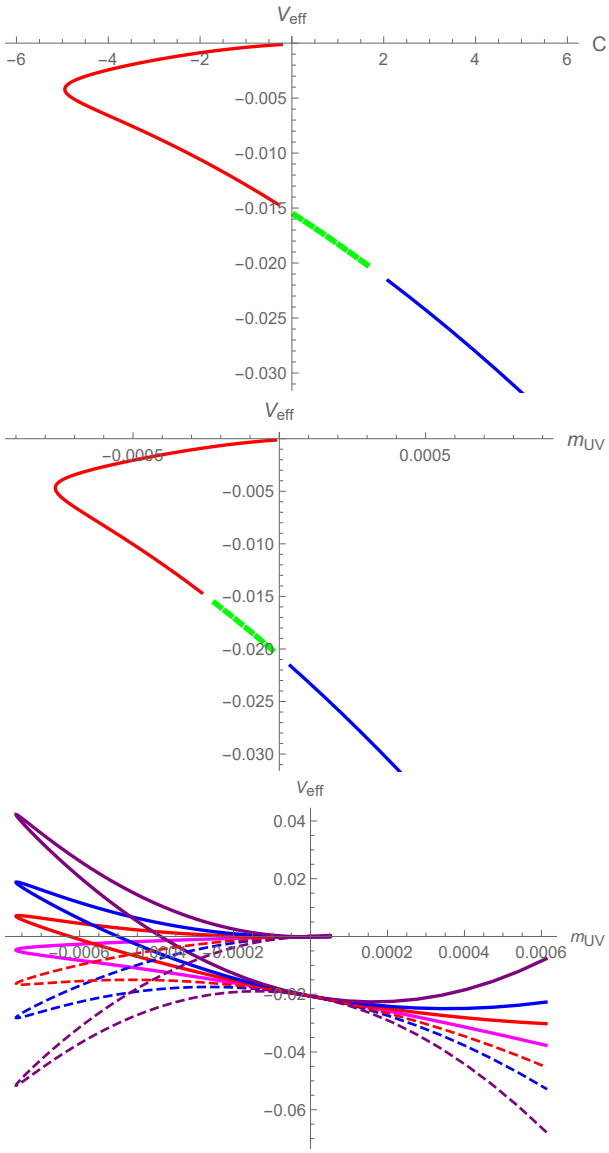

Figure 6.1.5: The top two plots show the effective action (-S evaluated on the vacuum solutions) for the solutions from Fig 6.1.2 for the $N_f = 9$ theory as a function of each of m_{UV} and c_{UV}. The lower plot shows the same potential against m_{UV} but including the NJL interaction term. The solid lines are for attractive NJL interactions, dashed lines for repulsive NJL interactions.

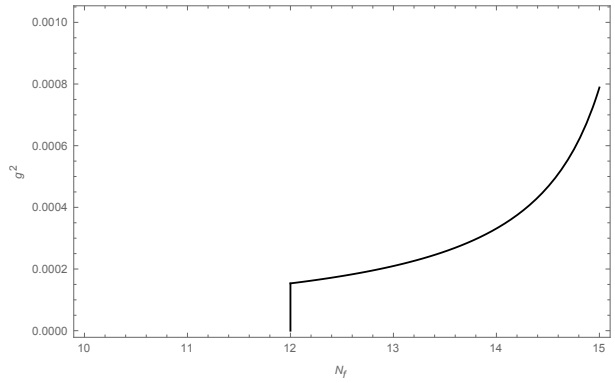

Figure 6.2.1: The $N_f - g^2$ Phase Diagram for $N_c = 3$ - the left hand region has chiral symmetry breaking, the right hand has restored chiral symmetry. Our numerics suggest that g^2 approaches zero extremely rapidly at $N_f = 0$. It is possible that with a smaller step size one could resolve an exponential approach but we did not investigate this.

6.2 $N_f - g^2$ Phase Diagram

Let us next study the phase structure of the $N_c = 3$ theory with N_f. Here as we vary N_f we set $\gamma(e) = 2/3\gamma_*$ so that the step scale Λ_1 is somewhat comparable in each theory and use a very high UV cut off $\Lambda = e^{20}$ so that all theories have $\gamma \simeq 0$ there. For $N_f < 12$ there is always chiral symmetry breaking triggered by the gauge theory alone. For larger N_f, in each case we look at embeddings $L(\rho)$ that correspond to small IR masses (remember we call the IR value of L as m_{IR}). We extract in the UV m_{UV} and c_{UV} from (3.5.11) and then find the NJL coupling by using (3.5.19). Varying the IR mass allows us to plot m_{IR} vs g and extrapolate to the point of the second order transition to find g_c where m_{IR} falls to zero. In this way we can plot the transition in the $g^2 - N_f$ plane between theories with conformal IRs and and those with a finite mass gap. We show this phase boundary in Figure 6.2.1.

The form of the phase diagram is straightforward - below $N_f = 12$ the gauge theory running (in the approximations we use) violates the BF bound and chiral symmetry breaking results. Above $N_f = 12$, the gauge theory alone lies in the conformal window and is ungapped. An NJL term is needed to generate chiral symmetry breaking. Naively one might think the NJL critical coupling would grow from zero as one moves upwards from $N_f = 12$ but in fact our numerical investigations suggest there is a finite critical coupling immediately above the transition leading to a discontinuity in the plane. It is possible there is an exponential approach to the BKT point at $g^2 = 0$ but we have not found numerical evidence for it. Note this phase diagram can be compared to the sketch of the similar physics described in [90] where the NJL like behaviour we have found when $N_f > 4N_c$ is not shown.

6.3 $N_f > 4N_c$ and Ideal Walking Behaviour

In the range $4N_c < N_f < 11N_c/2$ the pure gauge theory lives in the conformal window with an IR interacting fixed point but no chiral symmetry breaking. Here we can trigger chiral symmetry breaking by an NJL interaction term. If the interaction term is tuned so that the mass gap occurs in the IR where there is a large value for γ_* then in the UV the condensate is expected to be enhanced by "walking" like dynamics as explained in the introduction. We will explore these models in this section.

6.3.1 A Simplified Analysis

Let us first understand how the holographic model rather simply encodes the idea of Ideal Walking. Consider an idealized model with two regimes divided by a sharp scale Λ_1. At low energies below Λ_1 the theory has an anomalous dimension γ whilst above Λ_1 $\gamma = 0$. The Dynamic AdS/QCD description has $\Delta m^2 = 0$ in the high energy regime and the constant value $\Delta m^2 = \gamma(\gamma - 2)$ in the low energy regime. Now assume a UV NJL interaction triggers chiral symmetry breaking at an energy scale m_{IR} (this in the full model would be the choice of IR boundary condition on the field L). If m_{IR} lies above Λ_1 then the solution for the holographic field L is

$$L = m + \frac{c}{\rho^2}, \qquad m \sim m_{IR},\ c \sim m_{IR}^3 \tag{6.3.1}$$

where m, c are just fixed by dimensional grounds in terms of the only scale m_{IR} - this a normal "natural"' theory.

Now imagine moving m_{IR} into the IR regime below Λ_1. Here the solution looks like

$$L_{IR} = \frac{\hat{m}}{\rho^\gamma} + \frac{\hat{c}}{\rho^{2-\gamma}}, \qquad \hat{m} \sim m_{IR}^{1+\gamma},\ \hat{c} \sim m_{IR}^{3-\gamma} \tag{6.3.2}$$

with dimensional analysis again being used to fix the parameters. Now one should evolve this solution to Λ_1 and match to the UV form of the solutions. In the UV we will have

$$L_{UV} = m_{UV} + \frac{c_{UV}}{\rho^2}, \qquad m_{UV} \sim \frac{m_{IR}^{1+\gamma}}{\Lambda_1^\gamma},\ c_{UV} \sim m_{IR}^{3-\gamma}\Lambda_1^\gamma \tag{6.3.3}$$

IR quantities such as f_π will be determined simply by dimensional analysis in terms of the IR scale m_{IR} and the UV condensate is relatively enhanced by the presence of Λ_1 (whilst the UV mass is suppressed).

This is the origin of the effect in the full model we will discuss. A more complete setting is needed to set the UV and IR boundary conditions on the solution and ensure the effective potential from the bulk flows allows the NJL mechanism to operate. However, if one naively computes the NJL coupling in this approximation one finds $g^2/\Lambda_{UV}^2 = m_{UV}/c_{UV} = m_{IR}^{-2}(m_{IR}/\Lambda)^{2\gamma}$ which is a constant at $\gamma = 1$ and then for fixed m_{IR} rises as γ falls. This gives some support to the form of the phase diagram in 6.2.1.

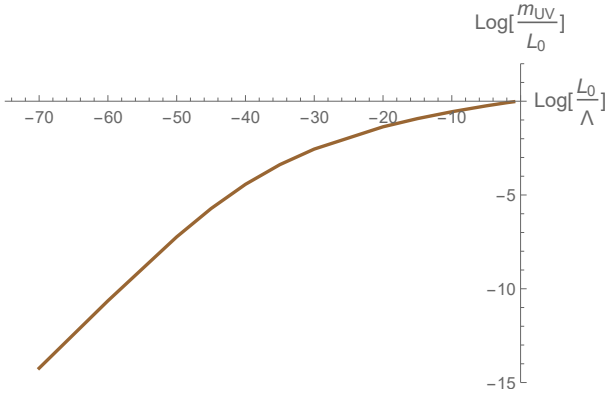

Figure 6.3.1: Plot of Log m_{UV}/m_{IR} against Log m_{IR}/λ_{UV} for $N_f = 13$, $\gamma(\Lambda_{UV}) = 0.05$

6.3.2 Two Loop Runnings

We can now numerically study the more complete theory with the two loop runnings for the $4N_c < N_f < 11N_c/2$ theories. For $N_c = 3$ the conformal window lives in the range $12 \leq N_f \leq 15.5$ which corresponds to the fixed point value of γ_* changing from 1 to 0 as one increases N_f. In [102] the hyper-scaling relations in the holographic model in the absence of NJL terms were studied. Essentially that paper confirmed that the form of the solutions and naive dimensional analysis used in the previous section apply at the level of a percent or better along the flows (because the flows are rather slow and locally taking γ to be a constant is a good approximation).

Here we provide a further piece of evidence of the scaling behaviour we expect. Consider the $N_f = 13$ theory for which the running of γ is plotted in Figure 6.0.1. We fix a UV cut off at the scale where $\gamma(\Lambda_{UV}) = 0.05$ and then choose a variety of IR initial condition values of $L = m_{IR}$. Solving for $L(\rho)$ we can then extract m_{UV} at the cut off scale from the value of $L(\Lambda_{UV})$. In Figure 6.3.1 we plot Log(m_{UV}/m_{IR}) against Log L_0/Λ_{UV}. If the scaling were the canonical UV scaling then $m_{UV} \simeq m_{IR}$ and the line would be flat at zero. However, we see that as m_{IR} is reduced m_{UV} decreases relative to the canonical scaling expectation and eventually after moving through the running regime of Fig 6.0.1 enters a regime where m_{UV} is decreasing with a fixed power as the naive analysis above predicts.

In principle one could perform the same analysis for the condensate but since it is the sub-leading term in the behaviour of L it quite hard to precisely numerically follow it over decades of evolution so we have not produced such clean figures. The naive analysis of the previous section though is clearly appropriate, confirmed for m, and the expected growth in the condensate is certainly described in the model.

6.3.3 A Light σ

The Ideal Walking systems become an interesting possibility for replacements for a normal technicolour description of electroweak symmetry breaking since they enhance the UV condensate which would help to push flavour physics to high scales. A key question

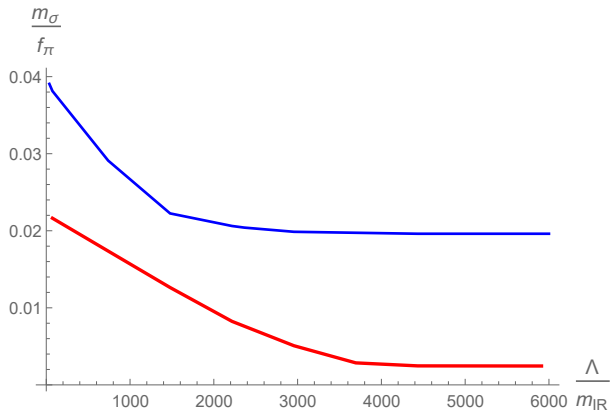

Figure 6.3.2: The $N_f = 13$ theory with m_{IR} lying in the fixed point regime. The σ's mass is plotted against Log Λ/m_{IR} for different separations between the IR and UV cut offs.

though is whether they can describe a light higgs like state (one would need $m_\sigma \simeq f_\pi/2$).

Here again we can provide an analytic answer before we proceed to numerics. The σ meson spectrum is found by solving (3.5.12) although we must be careful with boundary conditions in the prescence of an NJL term. When we find the vacuum form of $L(\rho)$ we interpret the UV boundary constants of the solution as $m_{UV}/c_{UV} = g^2/\Lambda^2$. When we vary by the field S about that background we must maintain the same value of g^2/Λ^2 rather than the usual $S \to 0$ UV boundary behaviour of the NJL free theory. Numerically this is straightforward.

Now consider (3.5.12) in the near conformal limit where Δm^2 varies only very slowly - we may neglect the third term in the equation. Now is there an $M^2 = 0$ solution? We set the final term to zero also. (3.5.12) is now precisely (3.5.10) which we solved for the background L_0. We already know a solution, the background L_0 itself, that satisfies the relevant NJL boundary condition. So such a massless state is present. Note that the c parameter in the solution to this equation will, in general, differ from the c parameter in the embedding we are expanding around so this is not simply a trivial redefinition of the vacuum. This argument shows that if we place the IR mass scale and the UV cut off, separated, but both deep in the IR fixed point regime of the gauge theory we would expect to get an arbitrarily small σ mass.

The set up with both the dynamical scale and the cut off in the deep IR regime generates too small a σ mass for an electroweak theory higgs and would also not generate an enhanced condensate because the running does not see a transition in γ. In fact the runnings in the conformal window are rather slow generically, as can be seen in Figure 6.0.1 so Δm^2 is generically quite flat and the challenge is to make the σ as heavy as $f_\pi/2$.

We show some numerical results with the two loop runnings in Figures 6.3.2 and 6.3.3. In Figure 6.3.2 for $N_f = 13$ we have fixed the IR mass scale (m_{IR}) at a scale in the IR fixed point regime and then varied Λ to compute the σ mass. The result is small because the coupling is running so slowly.

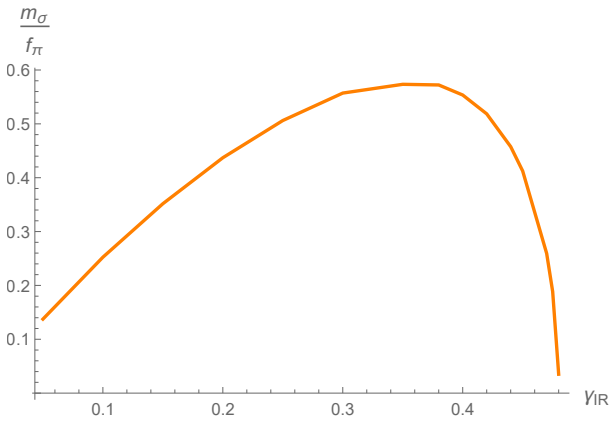

Figure 6.3.3: This is a plot in the $N_f = 12$ theory where the IR fixed point is $\gamma_{IR} = 0.48$. Here we have a separation of 7.5 between the m_{IR} and Λ. We vary m_{IR} to scales with different values of γ_{IR} and compute the σ mass in units of f_π.

In Figure 6.3.3 we show an example of a theory that achieves a large enough m_σ for an electroweak model. Here $N_f = 12$ where the IR fixed point is $\gamma_{IR} = 0.48$. We have a separation of 7.5 between the scales m_{IR} and Λ. We vary m_{IR} to scales with different values of γ_{IR} and compute the σ mass in units of f_π. To achieve a larger m_σ one needs to sandwich the strongest running between the IR and UV scales.

We conclude that Ideal Walking could, dependent on the precise running at intermediate strength couplings beyond perturbation theory, generate a light σ as well as playing the role of enhancing the quark condensate. In this sense it looks an attractive set up although it relies on NJL terms whose origin is unspecified.

6.4 Summary

We have used a holographic model to study the gauged NJL model with different runnings for the gauge theory in or near the conformal window. We have used the two loop computations of the running of the gauge coupling at $N_c = 3$ and varying N_f to represent these runnings from asymptotic freedom to different IR fixed points.

For theories in which N_f lies below $4N_c$ the runnings for the anomalous dimension of the quark bilinear pass through $\gamma = 1$ and chiral symmetry is triggered when the NJL coupling g^2 is zero. Adding an attractive NJL interaction reinforces condensation leading to a bigger mass gap. The basic gauge theories display a spiral pattern in the mass vs condensate plane - at zero quark mass there are vacuum states in which the σ, σ^*.. etc condense although we show only the one with the σ alone condensed is stable. This structure is now clearly a prediction of holographic models with symmetry breaking because it has been seen in many models [97, 89, 90, 98, 99]. Here this structure in the mass-condensate plane impacts when a repulsive NJL term is added, with the surprising result that condensation is only switched off by an infinite NJL coupling.

For $4N_c < N_f < 11N_c/2$ the pure gauge theory lies in an IR conformal regime with non-

zero γ. An additional attractive NJL term generates chiral symmetry breaking above a critical NJl coupling value - we have displayed the phase structure. These theories have an intermediate running regime between the $\gamma = 0$ UV and the IR fixed point. The values of the UV quark mass and condensate are decreased and increased respectively as the theory runs through this regime. This is the mechanism of Ideal Walking models in which $\langle \bar{q}q \rangle / f_\pi^3$ can be very much enhanced relative to that in theories with fast running and no IR fixed point. We have also shown that our model predicts a light σ particle when the running in these theories is slow which might be helpful in constructing a dynamical model of the electroweak scale.

Chapter 7

Conclusion

After introducing the basic foundations needed to understand this area of research, on both the field theory side and on the gravity and string theory side, we described the dynamic AdS/QCD model which will make up the bulk of this work.

Dynamic AdS/QCD is a bottom up holographic theory of QCD that breaks supersymmetry and conformal invariance by two artificial additions.

- Supersymmetry is broken by adding a phenomenological parameter to the coefficient of the kinetic terms for the vector and axial vectors, κ in 3.5.8.
- Conformal invariance is broken by including a "dilaton", inspired by the technique of adding an external magnetic field to introduce a mass scale, who's functional form is chosen to match the two loop running for QCD. Since we do not have access to the full nonperturbative QCD running we must treat these results as approximate, although we expect the full theory to exhibit the same qualitative behaviour.

The model also incorporates four fermion interaction NJL interactions. When a $\langle \overline{q}q \rangle$ condensate forms this quartic term dynamically generates our quark masses. The gravity dual of this model is an $AdS_5 \times S^5$ spacetime generated by a stack of N_c D3 "colour" branes with another stack of N_f D7 "flavour" probe branes extending into the spacetime from the boundary.

We can then calculate the running of the quark masses with the renormalisation scale by finding the embeddings of the D7 branes into the bulk. It is also possible to find the masses and decay rates of bound states by looking at the excitations around the ground state embeddings of the probe branes.

7.1 NJL Interactions in Dynamic AdS/QCD and Observed Mesons

The natural first application of this model is to study the QCD meson spectrum and their decay rates. This was conducted in chapter 4. We found plausible results for the

observed mesons and showed that the NJL term has it's expected effect, to enhance the masses of these bound states.

In particular it was found that the behaviour of the meson masses and decay constants moves from a regime in which the chiral condensate is well described by the QCD vacuum to one dominated by the quartic term as the NJL coupling is increased.

Our success in this initial exploration motivated the application of this model to the more complex case of technicolour in the following chapters.

7.2 Holographic Technicolour and the Top Quark

We then moved on to study beyond the standard model phenomena in chapter 5. First we explored a model which aims to explain the very large observed top mass called top condensation where the NJL term goes as $\equiv \overline{\psi}_L t_R \bar{t}_R \psi_L + h.c.$. The effect of this is that only the top quark gains a mass through this mechanism. There are a further 5 "spectator" quarks which we take to be massless in the UV. We are able to show that such a model can produce the necessary large top mass.

Next we studied one doublet extended technicolour. We use a model consisting of an electroweak doublet of techniquarks and a set of N_f^{sing} singlets which couple to each other through an $SU(N_{TC})$ technicolour gauge interaction and with a top quark through an NJL term. We found two solutions which agree with the observed f_π, Higgs mass, and top mass:

- An NJL dominated solution where electroweak symmetry breaking is dominated by the quartic fermion term and technicolour is weak. These models are ruled out by the observed electroweak parameter, $\delta\rho$.
- A technicolour dominated phase where the NJL term is small. This is closer to being valid but is still ruled out by precision electroweak data.

The second solution comes close to being experimentally permitted. In fact we are able to squeeze into the allowed region by moving into the so called "walking" limit close to $N_f = 12$ where the coupling remains strong much further into the UV than would other wise be the case.

Finally in this chapter we looked at a one family technicolour model with 3 colours and 8 flavours which seems to be less phenomenological desirable.

7.3 Spirals and Ideal Walking

In chapter 6 we investigated including NJL interactions to gauge theories in two regimes. First we looked at the region $N_f < 4N_c$. These theories feature an intriguing spiral patten when one plots the mass against the condensate. We found that an attractive four fermion interaction leads to the expected enhanced condensate and mass while we found, unexpectedly, that an infinite repulsive coupling would be required to eliminate the condensate.

In the second part we studied the region with $4N_c < N_f < \frac{11}{2}N_c$ which feature a conformal window, where the coupling remains approximately constant for an extended region of the running in the IR. This causes the condensate to be enhanced further. We show that these models contain a light scalar which could be phenomenologically interesting as an explanation for the observed "Higgs" state.

7.4 Closing Remarks

We have used the Dynamic AdS/QCD model to study "vanilla" QCD as well as a menageré of beyond the standard model technicolour theories. In these studies the model has proved it's value as a model of strongly coupled gauge theories. Physics has an abundance of these and so there is no shortage of potential extensions to this work. In particular Dynamic AdS/QCD has already been applied to study the speculated colour superconductor phase of QCD [99]. There are also a class of theories called "Composite Higgs" where the lightest scalar bound state is used for the standard model Higgs but the chiral symmetry breaking mechanism is not exploited [103] which would be well suited to study in this way.

Bibliography

[1] W. Clemens and N. Evans, *A Holographic Study of the Gauged NJL Model*, *Phys. Lett.* **B771** (2017) 1–4, [arXiv:1702.0869]. xiii, 74

[2] W. Clemens, N. Evans, and M. Scott, *Holograms of a Dynamical Top Quark*, *Phys. Rev.* **D96** (2017), no. 5 055016, [arXiv:1703.0833]. xiii

[3] K. Bitaghsir Fadafan, W. Clemens, and N. Evans, *Holographic Gauged NJL Model: the Conformal Window and Ideal Walking*, arXiv:1807.0454. xiii

[4] A. Einstein, *On the Electrodynamics of Moving Bodies*, *Annalen der Physik* **17** (1905). 1

[5] A. Einstein, *Die Feldgleichungen der Gravitation. (German) [The field equations of gravitation]*, *j-S-B-PREUSS-AKAD-WISS-2* **??** (1915), no. ?? 844–847. 1

[6] L. D. Landau and E. M. Lifshitz, *Mechanics, Third Edition: Volume 1 (Course of Theoretical Physics)*. 1976. 1

[7] L. D. Landau and E. M. Lifshitz, *The Classical Theory of Fields*. Butterworth-Heinemann, 4 ed., 1980. 2

[8] M. E. Peskin and D. V. Schroeder, *An Introduction to quantum field theory*. Addison-Wesley, Reading, USA, 1995. 2, 5, 9

[9] A. Shomer, *A Pedagogical explanation for the non-renormalizability of gravity*, arXiv:0709.3555. 3

[10] G. 't Hooft and M. J. G. Veltman, *One loop divergencies in the theory of gravitation*, *Ann. Inst. H. Poincare Phys. Theor.* **A20** (1974) 69–94. 3

[11] S. Weinberg, *ULTRAVIOLET DIVERGENCES IN QUANTUM THEORIES OF GRAVITATION*, in *General Relativity: An Einstein Centenary Survey*, pp. 790–831. 1980. 3

[12] Z. Koba and H. Nielsen, *Reaction amplitude for n-mesons a generalization of the veneziano-bardakçi-ruegg-virasoro model*, *Nuclear Physics B* **10** (1969), no. 4 633 – 655. 3

[13] J. Scherk and J. H. Schwarz, *Dual models for non-hadrons*, *Nuclear Physics B* **81** (1974), no. 1 118 – 144. 3

[14] T. Yoneya, *Connection of Dual Models to Electrodynamics and Gravidynamics*, *Prog. Theor. Phys.* **51** (1974) 1907–1920. 3

[15] M. B. Green and J. H. Schwarz, *Supersymmetrical string theories*, *Physics Letters B* **109** (1982), no. 6 444 – 448. 3

[16] D. J. Gross, J. A. Harvey, E. Martinec, and R. Rohm, *Heterotic string*, *Phys. Rev. Lett.* **54** (Feb, 1985) 502–505. 3

[17] P. Horava and E. Witten, *Heterotic and type I string dynamics from eleven-dimensions*, *Nucl. Phys.* **B460** (1996) 506–524, [hep-th/9510209]. [,397(1995)]. 3

[18] J. M. Maldacena, *The large n limit of superconformal field theories and supergravity*, . 3, 40, 77

[19] S. Sachdev, *Condensed Matter and AdS/CFT*, arXiv:1002.2947. [Lect. Notes Phys.828,273(2011)]. 3

[20] D. Anninos, T. Hartman, and A. Strominger, *Higher Spin Realization of the dS/CFT Correspondence*, *Class. Quant. Grav.* **34** (2017), no. 1 015009, [arXiv:1108.5735]. 3

[21] L. Fidkowski, V. Hubeny, M. Kleban, and S. Shenker, *The Black hole singularity in AdS / CFT*, *JHEP* **02** (2004) 014, [hep-th/0306170]. 3

[22] J. Erdmenger, N. Evans, I. Kirsch, and E. Threlfall, *Mesons in Gauge/Gravity Duals - A Review*, *Eur. Phys. J.* **A35** (2008) 81–133, [arXiv:0711.4467]. 3

[23] P. K. Kovtun, D. T. Son, and A. O. Starinets, *Viscosity in strongly interacting quantum field theories from black hole physics*, *Phys. Rev. Lett.* **94** (Mar, 2005) 111601. 3

[24] L. H. Ryder, *Quantum field theory*. Cambridge university press, 1996. 5, 6, 8, 13

[25] H. Fritzsch, M. Gell-Mann, and H. Leutwyler, *Advantages of the Color Octet Gluon Picture*, *Phys. Lett.* **47B** (1973) 365–368. 5, 12

[26] C. N. Yang and R. L. Mills, *Conservation of isotopic spin and isotopic gauge invariance*, *Phys. Rev.* **96** (Oct, 1954) 191–195. 5, 12

[27] L. D. Faddeev and V. N. Popov, *Feynman diagrams for the Yang-Mills field*, *Physics Letters B* **25** (July, 1967) 29–30. 6

[28] R. P. Feynman, *Space-time approach to quantum electrodynamics*, *Phys. Rev.* **76** (Sep, 1949) 769–789. 12

[29] M. Göckeler, R. Horsley, V. Linke, P. Rakow, G. Schierholz, and H. Stüben, *Is there a landau pole problem in qed?*, *Phys. Rev. Lett.* **80** (May, 1998) 4119–4122. 12

[30] B. R. Holstein, *Anomalies for pedestrians*, *American Journal of Physics* **61** (1993), no. 2 142–147, [https://doi.org/10.1119/1.17328]. 13

[31] J. Bardeen, L. N. Cooper, and J. R. Schrieffer, *Theory of superconductivity*, *Phys. Rev.* **108** (Dec, 1957) 1175–1204. 13

[32] J. Goldstone, A. Salam, and S. Weinberg, *Broken symmetries*, *Phys. Rev.* **127** (Aug, 1962) 965–970. 13

[33] M. Gell-Mann, *The Eightfold Way: A Theory of strong interaction symmetry*, . 14

[34] J. Greensite, *The Confinement problem in lattice gauge theory*, *Prog. Part. Nucl. Phys.* **51** (2003) 1, [hep-lat/0301023]. 15

[35] B. Lucini, M. Teper, and U. Wenger, *Glueballs and k-strings in SU(N) gauge theories: calculations with improved operators*, *Journal of High Energy Physics* **6** (June, 2004) 012, [hep-lat/0404008]. 15

[36] G. Hooft, *A planar diagram theory for strong interactions*, *Nuclear Physics B* **72** (1974), no. 3 461 – 473. 15

[37] G. Jona-Lasinio, *Relativistic field theories with symmetry breaking solutions*, . 16

[38] M. Herrero, *The Standard model*, *NATO Sci. Ser. C* **534** (1999) 1–59, [hep-ph/9812242]. 17

[39] **Particle Data Group** Collaboration, J. e. a. Beringer, *Review of particle physics*, *Phys. Rev. D* **86** (Jul, 2012) 010001. 18

[40] R. K. Kaul, *Technicolor*, *Rev. Mod. Phys.* **55** (Apr, 1983) 449–475. 20, 21

[41] C. T. Hill and E. H. Simmons, *Strong dynamics and electroweak symmetry breaking*, *Phys. Rept.* **381** (2003) 235–402, [hep-ph/0203079]. [Erratum: Phys. Rept.390,553(2004)]. 21, 57

[42] A. Belyaev, M. S. Brown, R. Foadi, and M. T. Frandsen, *The Technicolor Higgs in the Light of LHC Data*, *Phys. Rev.* **D90** (2014) 035012, [arXiv:1309.2097]. 21

[43] A. Bilal, *Introduction to supersymmetry*, hep-th/0101055. 23

[44] E. D'Hoker and D. Z. Freedman, *Supersymmetric gauge theories and the AdS / CFT correspondence*, in *Strings, Branes and Extra Dimensions: TASI 2001: Proceedings*, pp. 3–158, 2002. hep-th/0201253. 23, 40, 41

[45] **CMS** Collaboration, A. M. Sirunyan *et. al.*, *Constraints on models of scalar and vector leptoquarks decaying to a quark and a neutrino at $\sqrt{s} = 13$ TeV*, *Phys. Rev.* **D98** (2018), no. 3 032005, [arXiv:1805.1022]. 23

[46] S. R. Coleman and J. Mandula, *All Possible Symmetries of the S Matrix*, *Phys. Rev.* **159** (1967) 1251–1256. 23

[47] G. Bossard, P. S. Howe, K. S. Stelle, and P. Vanhove, *The vanishing volume of D=4 superspace*, *Class. Quant. Grav.* **28** (2011) 215005, [arXiv:1105.6087]. 32

[48] D. Tong, *String Theory*, arXiv:0908.0333. 32

[49] K. Becker, M. Becker, and J. H. Schwarz, *String theory and M-theory: A modern introduction*. Cambridge University Press, 2006. 37

[50] F. Gliozzi, J. Scherk, and D. I. Olive, *Supersymmetry, Supergravity Theories and the Dual Spinor Model*, *Nucl. Phys.* **B122** (1977) 253–290. 37

[51] M. Ammon and J. Erdmenger, *Gauge/gravity duality*. Cambridge University Press, Cambridge, 2015. 39, 41

[52] S. Moroz, *Below the Breitenlohner-Freedman bound in the nonrelativistic AdS/CFT correspondence*, *Phys. Rev.* **D81** (2010) 066002, [arXiv:0911.4060]. 41

[53] A. Zaffaroni, *Introduction to the ads-cft correspondence*, *Classical and Quantum Gravity* **17** (2000), no. 17 3571. 43

[54] A. Karch and E. Katz, *Adding flavor to ads / cft*, . 44

[55] D. K. Hong, T. Inami, and H.-U. Yee, *Baryons in ads/qcd*, *Physics Letters B* **646** (2007), no. 4 165 – 171. 44

[56] N. E. T. Alho and K. Tuominen, *Dynamic ads/qcd and the spectrum of walking gauge theories*, . 49, 50, 51, 58, 59, 78, 84

[57] E. Witten, *Multitrace operators, boundary conditions, and ads / cft correspondence*, 0112258. 50

[58] J. R. P. J. T. Londergan, J. Nebreda and A. Szczepaniak, *Identification of non-ordinary mesons from the dispersive connection between their poles and their regge trajectories: The $f_0(500)$ resonance*, . 52

[59] C. T. H. W. A. Bardeen and M. Lindner, *Minimal dynamical symmetry breaking of the standard model*, . 56, 58, 61, 71

[60] E. Farhi and L. Susskind, *Technicolour*, *Physics Reports* **74** (1981), no. 3 277 – 321. 56, 57

[61] S. Weinberg, *Implications of Dynamical Symmetry Breaking*, *Phys. Rev.* **D13** (1976) 974–996. [Addendum: Phys. Rev.D19,1277(1979)]. 57

[62] L. Susskind, *Dynamics of Spontaneous Symmetry Breaking in the Weinberg-Salam Theory*, *Phys. Rev.* **D20** (1979) 2619–2625. 57

[63] E. Eichten and K. D. Lane, *Dynamical Breaking of Weak Interaction Symmetries*, *Phys. Lett.* **90B** (1980) 125–130. 57

[64] S. Dimopoulos and L. Susskind, *Mass Without Scalars*, *Nucl. Phys.* **B155** (1979) 237–252. [2,930(1979)]. 57

[65] M. E. Peskin and T. Takeuchi, *A New constraint on a strongly interacting Higgs sector*, *Phys. Rev. Lett.* **65** (1990) 964–967. 57, 59

[66] **ATLAS** Collaboration, G. Aad *et. al.*, *Observation of a new particle in the search for the Standard Model Higgs boson with the ATLAS detector at the LHC*, *Phys. Lett.* **B716** (2012) 1–29, [arXiv:1207.7214]. 57

[67] **CMS** Collaboration, S. Chatrchyan *et. al.*, *Observation of a new boson at a mass of 125 GeV with the CMS experiment at the LHC*, *Phys. Lett.* **B716** (2012) 30–61, [arXiv:1207.7235]. 57

[68] B. Holdom, *Raising the Sideways Scale*, *Phys. Rev.* **D24** (1981) 1441. 57, 67, 78

[69] R. Sundrum and S. D. H. Hsu, *Walking technicolor and electroweak radiative corrections*, *Nucl. Phys.* **B391** (1993) 127–146, [hep-ph/9206225]. 57, 59

[70] K. Yamawaki, M. Bando, and K.-i. Matumoto, *Scale Invariant Technicolor Model and a Technidilaton*, *Phys. Rev. Lett.* **56** (1986) 1335. 57

[71] M. Bando, K. iti Matumoto, and K. Yamawaki, *Technidilaton*, *Physics Letters B* **178** (1986), no. 2 308 – 312. 57

[72] V. A. Miransky and K. Yamawaki, *Conformal phase transition in gauge theories*, *Phys. Rev.* **D55** (1997) 5051–5066, [hep-th/9611142]. [Erratum: Phys. Rev.D56,3768(1997)]. 57

[73] T. Appelquist and F. Sannino, *The Physical spectrum of conformal SU(N) gauge theories*, *Phys. Rev.* **D59** (1999) 067702, [hep-ph/9806409]. 57

[74] D. K. Hong, S. D. H. Hsu, and F. Sannino, *Composite Higgs from higher representations*, *Phys. Lett.* **B597** (2004) 89–93, [hep-ph/0406200]. 57

[75] D. D. Dietrich, F. Sannino, and K. Tuominen, *Light composite Higgs from higher representations versus electroweak precision measurements: Predictions for CERN LHC*, *Phys. Rev.* **D72** (2005) 055001, [hep-ph/0505059]. 57

[76] **CDF** Collaboration, F. Abe *et. al.*, *Observation of top quark production in $\bar{p}p$ collisions*, *Phys. Rev. Lett.* **74** (1995) 2626–2631, [hep-ex/9503002]. 57

[77] M. Veltman, *Limit on mass differences in the weinberg model*, *Nuclear Physics B* **123** (1977), no. 1 89 – 99. 57

[78] M. E. Peskin and T. Takeuchi, *New constraint on a strongly interacting higgs sector*, *Phys. Rev. Lett.* **65** (Aug, 1990) 964–967. 57

[79] R. Chivukula, B. Dobrescu, and J. Terning, *Isospin breaking and fine-tuning in top-color assisted technicolor*, *Physics Letters B* **353** (1995), no. 2 289 – 294. 58, 60, 68

[80] T. Appelquist, N. J. Evans, and S. B. Selipsky, *Phenomenology of the top mass in realistic extended technicolor models*, *Phys. Lett.* **B374** (1996) 145–151, [hep-ph/9601305]. 58, 60, 68

[81] T. W. Appelquist, D. Karabali, and L. C. R. Wijewardhana, *Chiral Hierarchies and the Flavor Changing Neutral Current Problem in Technicolor*, *Phys. Rev. Lett.* **57** (1986) 957. 58

[82] T. Appelquist and L. C. R. Wijewardhana, *Chiral Hierarchies from Slowly Running Couplings in Technicolor Theories*, *Phys. Rev.* **D36** (1987) 568. 58

[83] T. Appelquist, T. Takeuchi, M. B. Einhorn, and L. C. R. Wijewardhana, *High-energy Isospin Breaking in Technicolor Theories*, *Phys. Lett.* **B232** (1989) 211–216. 58, 60, 68

[84] S. F. King and D. A. Ross, *Numerical studies of walking technicolor theories*, *Physics Letters B* **228** (1989), no. 3 363 – 369. 58

[85] H. Pagels and S. Stokar, *The Pion Decay Constant, Electromagnetic Form-Factor and Quark Electromagnetic Selfenergy in QCD*, *Phys. Rev.* **D20** (1979) 2947. 58, 61, 71

[86] V. A. Miransky, M. Tanabashi, and K. Yamawaki, *Dynamical Electroweak Symmetry Breaking with Large Anomalous Dimension and t Quark Condensate*, *Phys. Lett.* **B221** (1989) 177–183. 58, 61, 71

[87] V. A. Miransky, M. Tanabashi, and K. Yamawaki, *Is the t Quark Responsible for the Mass of W and Z Bosons?*, *Mod. Phys. Lett.* **A4** (1989) 1043. 58, 61, 71

[88] Y. Nambu, *BOOTSTRAP SYMMETRY BREAKING IN ELECTROWEAK UNIFICATION*, . 58, 61, 71

[89] M. Jarvinen and E. Kiritsis, *Holographic models for qcd in the veneziano limit*, . 58, 77, 78, 80, 82, 84, 90

[90] M. Jarvinen and F. Sannino, *Holographic conformal window - a bottom up approach*, . 58, 77, 78, 80, 82, 86, 90

[91] D. D. Dietrich and F. Sannino, *Conformal window of SU(N) gauge theories with fermions in higher dimensional representations*, *Phys. Rev. D* **75** (Apr., 2007) 085018, [hep-ph/0611341]. 59, 79

[92] R. C. Myers, *Dielectric branes*, *JHEP* **12** (1999) 022, [hep-th/9910053]. 60, 70

[93] J. Erdmenger, K. Ghoroku, and I. Kirsch, *Holographic heavy-light mesons from non-Abelian DBI*, *JHEP* **09** (2007) 111, [arXiv:0706.3978]. 60, 70

[94] C. T. Hill, *Topcolor assisted technicolor*, *Phys. Lett.* **B345** (1995) 483–489, [hep-ph/9411426]. 71

[95] K. Yamawaki, *Dynamical symmetry breaking with large anomalous dimension*, 9603293. 77

[96] Y. Nambu and G. Jona-Lasinio, *Dynamical model of elementary particles based on an analogy with superconductivity*, . 77

[97] R. C. R. V. G. Filev, C. V. Johnson and K. S. Viswanathan, *Flavoured large n gauge theory in an external magnetic field*, . 77, 80, 90

[98] N. Iqbal, H. Liu, and M. Mezei, *Quantum phase transitions in semilocal quantum liquids*, *Phys. Rev.* **D91** (2015), no. 2 025024, [arXiv:1108.0425]. 77, 78, 80, 82, 90

[99] K. Bitaghsir Fadafan, J. Cruz Rojas, and N. Evans, *A Holographic Description of Colour Superconductivity*, arXiv:1803.0310. 77, 80, 90, 95

[100] H. S. Fukano and F. Sannino, *Conformal Window of Gauge Theories with Four-Fermion Interactions and Ideal Walking*, *Phys. Rev.* **D82** (2010) 035021, [arXiv:1005.3340]. 78

[101] J. Rantaharju, C. Pica, and F. Sannino, *Ideal Walking Dynamics via a Gauged NJL Model*, *Phys. Rev.* **D96** (2017), no. 1 014512, [arXiv:1704.0397]. 78

[102] N. Evans and M. Scott, *Hyper-Scaling Relations in the Conformal Window from Dynamic AdS/QCD*, *Phys. Rev.* **D90** (2014), no. 6 065025, [arXiv:1405.5373]. 88

[103] G. Panico and A. Wulzer, *The Composite Nambu-Goldstone Higgs*, *Lect. Notes Phys.* **913** (2016) pp.1–316, [arXiv:1506.0196]. 95